G-QUADRUPLEXES: TARGETING WITH AZACYANINES AND APPLICATION TO HYDROXYCHLOROQUINE DETECTION

A THESIS SUBMITTED TO
THE GRADUATE SCHOOL OF NATURAL AND APPLIED SCIENCES
OF
MIDDLE EAST TECHNICAL UNIVERSITY

BY

KÜBRA DOĞAN

IN PARTIAL FULFILLMENT OF THE REQUIREMENTS
FOR
THE DEGREE OF MASTER OF SCIENCE
IN
CHEMISTRY

JANUARY 2022

Approval of the thesis:

G-QUADRUPLEXES: TARGETING WITH AZACYANINES AND APPLICATION TO HYDROXYCHLOROQUINE DETECTION

submitted by **KÜBRA DOĞAN** in partial fulfillment of the requirements for the degree of **Master of Science** i**n Chemistry, Middle East Technical University** by,

Prof. Dr. Halil Kalıpçılar
Dean, Graduate School of **Natural and Applied Sciences** _____

Prof. Dr. Özdemir Doğan
Head of the Department, **Chemistry** _____

Assoc. Prof. Dr. Özgül Persil Çetinkol
Supervisor, **Chemistry, METU** _____

Examining Committee Members:

Prof. Dr. Levent Toppare
Chemistry, METU _____

Assoc. Prof. Dr. Özgül Persil Çetinkol
Chemistry, METU _____

Assist. Prof. Dr. Şebnem Eşsiz
Molecular Biology and Genetics, Kadir Has University _____

Assist. Prof. Dr. Çağatay Dengiz
Chemistry, METU _____

Assist. Prof. Dr. Süreyya Özcan Kabasakal
Chemistry, METU _____

Date: 24.01.2022

I hereby declare that all information in this document has been obtained and presented in accordance with academic rules and ethical conduct. I also declare that, as required by these rules and conduct, I have fully cited and referenced all material and results that are not original to this work.

Name Last name : Kübra Doğan

Signature :

ABSTRACT

G-QUADRUPLEXES: TARGETING WITH AZACYANINES AND APPLICATION TO HYDROXYCHLOROQUINE DETECTION

Doğan, Kübra
Master of Science, Chemistry
Supervisor: Assoc. Prof. Dr. Özgül Persil Çetinkol

January 2022, 89 pages

The use of small molecules as therapeutic agents opens up new possibilities for treating a variety of diseases, including cancer. A major class of chemotherapy agents act on cancer cells by altering or damaging the cell's DNA structure. G-quadruplexes (G4s) are a type of non-canonical DNA secondary structures that forms in guanine-rich regions. They are essential in regulation of transcription and translation, as well as telomere maintenance. Targeting G4s with small molecules has been a promising strategy in cancer research. Even though many small molecules are used in the treatment of different cancer types, there is still a need for the discovery of new ones that are more selective and less toxic to the cells. Within the scope of this thesis, in the first part, three new Azacyanine derivatives that might potentially be chemotherapeutic agents as DNA binding small molecules were synthesized and characterized. Nuclear Magnetic Resonance spectroscopy, UV-vis spectroscopy, Mass spectroscopy and Elemental Analysis were used for characterization. The extinction coefficients and quantum yields were calculated. After that, their interactions with different DNA structures were investigated using competition dialysis assay, UV-vis absorption and Circular Dichroism (CD) spectroscopy. Our investigations demonstrated that the synthesized Azacyanine

derivatives have an affinity towards G4 structures, especially to Pu22, BCL-2, C-myc and VEGF.

In the second part of this thesis, a fluorescent detection method for Hydroxychloroquine (HCQ) based on the interactions between Tel24 G4 structure and Thioflavin T was developed. HCQ, a medication used primarily to prevent and treat malaria, has many side effects including, cardiomyopathy and retinopathy. Accordingly, the development of simple, fast, and effective sensors is required for HCQ containing pharmaceuticals and biological samples. G4 based biosensors have received great attention in recent years due to their low detection limit, easy operation, rapid detection ability and high sensitivity. Here, a G4 based fluorescent sensor for HCQ detection was developed with the limit of detection (LOD) of 0.116 μM under the optimized conditions. The applicability of the developed method in real samples was assessed using human serum and urine samples. The average recoveries (%) were found to be in the range of 75-110% for human urine samples and 62-83% for human serum samples, which demonstrate the suitability of the proposed fluorometric method in detecting HCQ in different matrices.

Keywords: G-quadruplex, Azacyanine, Hydroxychloroquine, Fluorometric Detection

ÖZ

G- DÖRT YAPILARI: AZASİYANİNLER İLE HEDEFLENMELERİ VE HİDROKSİKLOROKİN TESPİTİNDE KULLANIMLARI

Doğan, Kübra
Yüksek Lisans, Kimya
Tez Yöneticisi: Doç. Dr. Özgül Persil Çetinkol

Ocak 2022, 89 sayfa

Küçük moleküllerin terapötik ajanlar olarak kullanılması, kanser de dahil olmak üzere çeşitli hastalıkların tedavisi için yeni olanaklar sunmaktadır. Kemoterapi ajanlarının birçoğu, hücrenin DNA yapısını değiştirerek veya zarar vererek kanser hücreleri üzerinde etki etmektedir. G-dörtlüleri (G4'leri), guanin açısından zengin bölgelerde oluşan kanonik olmayan DNA ikincil yapılarının bir türüdür. Telomer yapısını stabilize etmenin yanı sıra transkripsiyon ve translasyonun düzenlenmesinde de rol oynarlar. G4'lerini küçük moleküllerle hedeflemek, kanser araştırmalarında umut verici bir strateji olmuştur. Farklı kanser türlerinin tedavisinde birçok küçük molekül kullanılmasına rağmen, hücreler için daha seçici ve daha az toksik olan yeni moleküllerin keşfedilmesine halen ihtiyaç duyulmaktadır. Bu tez kapsamında, ilk bölümde, DNA'ya bağlanma ve kemoterapötik ajan olabilme potansiyeli olan üç yeni Azasiyanin türevi sentezlenmiş ve karakterize edilmiştir. Nükleer Manyetik Rezonans spektroskopisi, UV-vis spektroskopisi, Kütle spektroskopisi ve Elemental Analiz metotları karakterizasyon için kullanılmıştır. Daha sonra, sentezlenen Azasiyaninlerin farklı DNA yapıları ile etkileşimleri rekabetçi diyaliz deneyleri, UV-vis absorbsiyon ve Circular Dichroism (CD)

spektroskopisi kullanılarak incelenmiştir. Elde edilen sonuçlara göre, sentezlenen Azasiyanin türevlerinin G4 yapılarına, özellikle Pu22, BCL-2, C-myc ve VEGF'ye afinitesi olduğunu belirlenmiştir.

Bu tezin ikinci bölümünde, Hidroksiklorokin (HCQ) için Tel24 G4 yapısı ile Thioflavin T arasındaki etkileşimlere dayalı bir floresan tespit yöntemi geliştirilmiştir. Özellikle sıtmayı önlemek ve tedavi etmek için kullanılan bir ilaç olan HCQ, kardiyomiyopati ve retinopati gibi birçok yan etkiye sahiptir. Bu nedenle, HCQ içeren farmasötik ve biyolojik numunelerin analizi için basit, hızlı ve etkili sensörlerin geliştirilmesi gerekmektedir. G4 tabanlı biyosensörler, düşük tespit limitleri, kolay kullanımları, hızlı tespit kabiliyetleri ve yüksek hassasiyetleri nedeniyle son yıllarda büyük ilgi görmektedir. Bu çalışmada HCQ tespiti için G4 tabanlı bir floresan sensör geliştirilmiş ve optimize edilmiş koşullar altında saptama limiti (LOD) 0.116 μM olarak hesaplanmıştır. Geliştirilen yöntemin gerçek örneklerde uygulanabilirliği, insan serumu ve idrar örnekleri kullanılarak değerlendirilmiştir. Ortalama geri kazanımların, insan idrar numuneleri için %75-110 ve insan serum numuneleri için %62-83 aralığında olduğu belirlenmiştir. Elde edilen bu sonuçlar önerilen florometrik yöntemin farklı matrislerde HCQ'yu tespit etmek için uygun olduğunu göstermektedir.

Anahtar Kelimeler: G-dörtlüsü, Azasiyanin, Hidroksiklorokin, Florometrik Tespit

To my family…

ACKNOWLEDGMENTS

I would like to thank my supervisor, Assoc. Prof. Dr. Özgül Persil Çetinkol, for her support, guidance and valuable advices. Being a member of her research group has been a great honor for me.

I would like to thank to my committee members Prof. Dr. Levent Toppare, Assist. Prof. Dr. Şebnem Eşsiz, Assist. Prof. Dr. Çağatay Dengiz and Assist. Prof. Dr. Süreyya Özcan Kabasakal for their time and effort.

I would like to thank Prof. Dr. Ahmet M. Önal and his reserch group for their help with the fluorescence experiments.

I also would like to thank all the members of Özgül Persil Çetinkol Research Group. Especially, Ecenaz Bilgen and Müge Usta for their friendship. Also, I would like to thank Dr. Mehrdad Forough for his support and knowledge throughout the research.

I also would like to express my greatest gratitude to Zeynep Suvacı for her friendship and every moment we share. She offered me a shoulder to cry on whenever I needed.

I also would like to dedicate my huge appreciation to my best friend, Furkan Demirbilek. Words alone will not be enough to express my love to him. You and Hera are my whole world. Thanks for always being with me.

I would like to appreciate my family for their endless love and always believing in me. I could not succeed without them.

I would like to thank METU Chemistry Department for giving the opportunity to conduct research.The first part of this work has been supported by Middle East Technical University Scientific Research Projects Coordination Unit under grant number TEZ-YL-103-2021-10697.

TABLE OF CONTENTS

LIST OF TABLES

TABLES

LIST OF FIGURES

FIGURES

LIST OF ABBREVIATIONS

ABBREVIATIONS

BCL-2	B-cell lymphoma-2
BPES	Buffered phosphate EDTA with sodium chloride
CD	Circular dichroism
C-myc	Cellular MYC (Myelocytomatosis)
DDD	Dickerson–Drew dodecamer
DMSO	Dimethyl sulphoxide
DNA	Deoxyribonucleic acid
HCQ	Hydroxychloroquine
Her-2	Human epidermal growth factor receptor-2
Kras	Kirsten rat sarcoma
NMR	Nuclear magnetic resonance
RB	Retinoblastoma
RNA	Ribonucleic acid
ThT	Thioflavin T
T_C	Cooling temperature
T_H	Heating temperature
UV-vis	Ultraviolet-visible

CHAPTER 1

INTRODUCTION

1.1 Nucleic acids

Nucleic acids are biopolymers made up of nucleotide units. Nucleotide units contain a nitrogen-containing base, a ribose sugar and a phosphate group. Based on their structural differences, nucleic acids are separated into two main groups, ribonucleic acid (RNA) and deoxyribonucleic acid (DNA). RNA contains the ribose sugar, which has a hydroxyl group at the 2' position of the sugar unit, whereas DNA contains a deoxyribose unit with a hydrogen at the 2' position. DNA contains four nitrogenous bases that are adenine (A), guanine (G), cytosine (C) and thymine (T). RNA has the same bases except has uracil (U) instead of T. The phosphate group serves as structural support in both DNA and RNA [1]. Nucleic acids are essential biological macromolecules for the continuity of life since they store and express genetic information.

1.2 Structure of DNA

Watson-Crick DNA consists of two polynucleotide chains wound around the same axis to form a right-handed double helix. The hydrophilic backbone of the DNA molecule is located on the outside, and the hydrophobic part of the double helix mainly due to stacked bases is located in the interior of the double helix. Each nucleotide base in one strand pairs in the same plane with the base on the other strand. Purine bases, G and A, pair up with pyrimidine bases, C and T, respectively via hydrogen bonding. In genomic DNA, mainly Watson-Crick base pairing governs interactions between purine and pyrimidine bases with three hydrogen bonds within

each G:C pairing and two hydrogen bonds within each A:T pairing. As shown in Figure 1, Watson- Crick pairing occurs at the O6, N1 and N2 atoms of G and N1 and N6 atoms of A. In contrast, Hoogsteen hydrogen bonding, occurs at the other hydrogen bonding face in a given DNA base pair, at the N7 and O6 atoms of G and N6 and N7 atoms of A (Figure 1) [2]. Since the environmental condition can alter the pKa of ionizable groups, changes in environmental conditions such as pH can alter the base pairing interactions. Furthermore, environmental changes can induce changes in sugar conformation, that will lead to conformational changes in DNA structures. Sugar groups, unlike base pairs, lack protonation sites, yet oxygen atoms can build enormous hydrogen-bonding networks that support and sustain DNA's structure. The nucleotides are joined to one another via a phosphodiester bond between the sugar of one nucleotide and the phosphate of the next nucleotide, resulting in the formation of the sugar-phosphate backbone [3]. The phosphate backbone of the DNA strand is the most exposed and vulnerable to solvent effects. As a result, salt concentrations and moisture levels can alter the DNA structure easily also via alternations in the backbone structure [4].

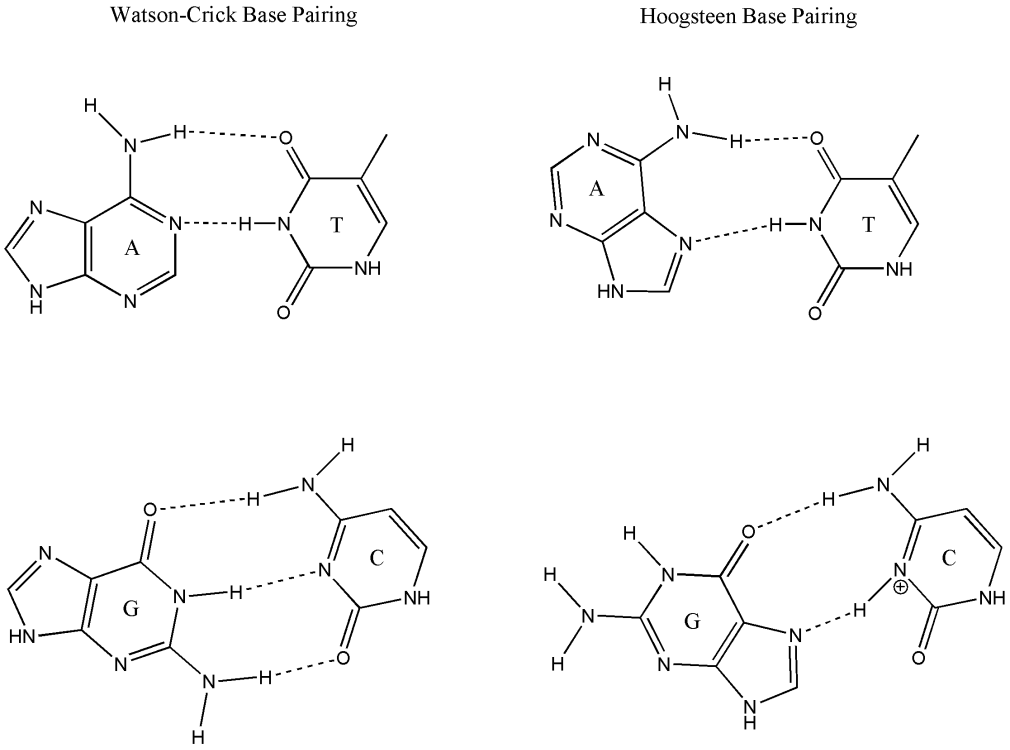

Figure 1. Schematic representations of Watson-Crick and Hoogsteen base pairings.

Although genomic DNA is mostly a double helix, various conformations also exist. One of the secondary structures of DNA is hairpins formed at the single-stranded ends of DNA, where complementary bases assemble to form pin-like conformations [5]. Hairpin DNA is involved in cellular activities like transcription, replication, and gene expression [6]. Another secondary structure is triplexes. They are formed via association of a single strand DNA with double-stranded DNA [7]. Triplex DNA structures are observed to be located in mirror repeat and long polypurine-polypyrimidine stretches regions and interferes with gene expression [8]. In recent years, G-quadruplexes, form in the G-rich areas in DNA, have been one of the most studied DNA secondary structures [9]. Because they are involved in gene regulation and have structural specificity, these secondary DNA structures have a lot of promise as therapeutic targets [10].

1.3 G-quadruplexes

G-quadruplexes (G4s) which are a non-canonical secondary DNA structure, are formed in guanine-rich sequences [11]. In G4s, four guanine bases are held together with Hoogsteen hydrogen bonds and form G-tetrads. Each G-tetrad is stacked on another G-tetrad, stabilized by a cation such as Na^+ or K^+ at the center [4].

Sequences rich in guanine are known to play a crucial role in the regulation of telomere maintenance, transcription and translation regulation [12]. Promoter regions are transcription initiation sites and are located on the same sequence as the gene to be transcribed [13]. Any mutation in promoter regions has the potential to lead to cancer or cell death. The most commonly investigated proto-oncogenes with mutations in their promoter regions are C-myc, BCL-2, VEGF, Her-2, RB and Kras. And the promoter regions of all these genes are known to have guanine-rich sequences that are prone to form G-quadruplex structures [14,15]. In recent years, the idea of targeting these guanine-rich sequences in promoter sequences become a widespread strategy in cancer treatment. For instance, Vascular Endothelial Growth Factor (VEGF) induces proliferation and migration of vascular endothelial cells [16]. VEGF is one of the most important angiogenesis factors and triggers the movement of vascular endothelial cells and their vascular permeability [17]. It has been proven that VEGF protein levels are higher in breast, ovarian and lung cancer patients compared to healthy individuals [18,19]. The formation of stable G-quadruplex structures in VEGF sequences was proven and, accordingly, the interactions of VEGF G4s with various drugs and small molecules have been studied [20,21]. Another proto-oncogene, MYC proto-oncogene bHLH transcription factor (C-myc), is an important gene involved in cell division, growth control and programmed cell death. C-myc protein is a multifunctional protein and takes part in the regulation of many other genes. If the cell is damaged during the cycle or a fault is found in one of the stages, C-myc expression drops, and the cell cycle stops. In addition, interruption of any mitogenic signal coming from inside or outside can lead to cell death with the help of C-myc [22]. Mutations of this gene are observed at a high rate

in many types of cancer [23].The BCL-2 proto-oncogene also has an essential role in controlling cell death mechanisms directly involved in apoptosis, necrosis and autophagy [24]. Therefore, it is one of the targets in cancer research.

1.4 Targeting DNA with small molecules

In drug design, especially in design of anti-cancer agents, DNA targeting has long been an active area of research [25]. Nucleic acid-binding ligands can easily interfere with transcription and DNA replication and, therefore, control and even inhibit gene expression. There are two broad types of interactions between ligands and DNA: covalent and non-covalent interactions. Covalent interactions are irreversible [26] whereas the non-covalent interactions are reversible and depend on the principle of recognition [27]. Non-covalent DNA binding ligands are classified into two main categories: intercalators and groove binders.

1.4.1 Intercalators

Intercalators, which mostly have aromatic core in their structure, can intercalate in between the bases of DNA. When an intercalator molecule stacks between base pairs, DNA structure, stability and function are perturbed [28]. One of the modes of intercalation is called the “classical” intercalation. In classical intercalation, the aromatic structure of the intercalator is stacked between the base pairs of double-stranded DNA. The other mode of intercalation is called the “threading intercalation”. In threading intercalation, the intercalator stacked between the base pairs is also able to interact with DNA in the minor or the major groove via its bulky substituents positioned in the groove [29]. One of the threading intercalator ligands is Doxorubicin, an effective chemotherapeutic ligand that has been in clinical use [30].

1.4.2 Groove binders

Groove binders are classified according to their interaction sites. They can interact with either the major or minor groove sites of DNA. Groove binders alter and/or block the binding of enzymes, such as polymerases, helicases and topoisomerases to DNA, by blocking the grooves DNA [31]. Some widely studied minor groove binders are Netropsin, Hoechst and DAPI. Minor groove binders mostly target A and T-rich regions of nucleic acids [32,33]. On the other hand, structural features of major groove binders have not been studied as extensively as the minor groove binders.

1.5 Targeting G-quadruplexes with small molecules

All cells in our body contain canonical DNA. For this reason, chemotherapy agents that bind to double-stranded DNA have more side effects. In other words, these drugs cause target the DNA of both healthy and cancer cells, and trigger apoptosis in both. Therefore, drug development studies in recent years have focused on drugs targeting non-canonical DNA sequences such as the G-quadruplexes.

G-quadruplex structures have proven to be a promising target for cancer treatment due to their roles in gene regulation and expression [34]. It is reported that in guanine-rich oncogenes, formation and stabilization of G-quadruplex structures could terminate the overexpression of genes [35]. One of the first explored promoter regions in breast cancer was Her-2 and the G4 structure formed by Her-2 promoter region held a regulatory role in the transcription of the gene [36,37]. It is found to that, BCL-2 promoter regions are also over expressed in cancer cells and they are able to form G4s [24,38]. In addition, Kras promoter region shows mutation in tumor cells and also found to be forming G4 structures [39]. Another G4 promotor gene is C-myc which is overexpressed in leukemia, prosthetic and breast cancer [40]. Additionally, VEGF promoter region become a potential target for anti-cancer therapies due to its upregulation in tumor cells [41].

In recent years, many small molecules targeting G-quadruplexes were discovered. Telomestatin, Quindoline, BRACO-19, RHPS4, Quarfloxin, and TMPyP4 are some of them.

Quarfloxin is the first G4 interacting drug that has entered the phase II clinical trials to treat neuroendocrine tumors [42]. Although it was showing promising pharmaceutical activity, due to the lack of bioavailability, it was unable to continue beyond phase II clinical trials [21]. TMPyP4 is another G4 interacting molecule that has a high binding affinity to G4s [43]. However, its selectivity towards G4s is low compared to double-stranded DNA, mainly due to its high positive charge [44]. On the other hand, Quindoline has high selectivity and binding affinity towards G4 structures compared to other DNA structures [45]. It was reported that quindoline derivatives downregulate MYC expression and have antiproliferative activity in cancer cells [46]. Telomestatin is a natural molecule which interacts specifically with human telomeric G4 [47]. It was found that telomestatin has antiproliferative effects in leukemia and myeloma [48]. BRACO-19 and RHPS4 are also targeting G4s in promoter regions and they can stabilize telomeric G4s [4]. BRACO-19 has high selectivity and binding affinity to G4s and prevents cell growth of tumor cells, including breast cancer, melanoma and retinoblastoma [49,50]. Studies showed that RHPS4 induces apoptosis and telomere injury in breast cancer cells in mice and also inhibits cell growth in brain tumor cells [51].

In brief, today using small molecules tageting G4s for the treatment of cancer is an accepted effective alternative. Although, G4 interacting small molecules provide alternatives to overcome current challenges in cancer treatment there is still a need for more selective and less toxic small molecules for cancer therapy.

1.5.1 Azacyanines

Azacyanines are benzimidazole and benzothiazole derivatives, first synthesized as possible chloride ion channel inhibitors [52,53]. Azacyanines have positively

charged heterocyclic structures with one or more nitrogen atoms. Based on their spectral characteristic, they have recently emerged in a variety of fields, including coloring agents in the textile industry [54], surface treatment of optical recording media [55], molecular recognition [56], biological applications, and biomedical imaging [20,57].

Interactions of Azacyanines with different DNA structures have been investigated, and it has been determined that these molecules are more selective against non-canonical DNA structures, including human telomeric DNA (Tel24) and polyd(A).polyd(T).polyd(T) triplex DNA structure [57–59]. Due to the strong affinity towards G4s, Azacyanines are also used in sensor applications. Recently Bilgen et al. developed a sensor using Azacyanine 5 molecule for the detection of VEGF promoter region [60]. In this context, Azacyanines, which are determined to be selective against non-canonical sequences, are thought to be promising G4 targeting drug candidates.

1.6 G-quadruplex based detection platforms

G-quadruplex-based biosensors also have received considerable attention in recent years. Low detection limit, cheap and easy operation, rapid detection ability, and high sensitivity are advantageous features of G-quadruplex based biosensors. G-quadruplexes are commonly employed as biosensors to detect metal ions [61], organic molecules [62] and nucleic acids [63].

Different metal ions have different abilities to stabilize the structure of G4. Due to the binding ability of metal ions, biosensors based on G4s have been developed. Li et al. developed a Hg^{2+} detection probe by altering the proper folding of the G-quadruplex structure with a detection limit of 50 nM [64]. In another study, based on the inhibition of G-quadruplex structure formation by Ag^{+}, a detection method for Ag^{+} was developed with a 64 nM detection limit [65]. Also, Qin et al. developed a

chemosensor to detect Cu^{2+} ions, which depends on fluorescence enhancement of N-methyl mesoporphyrin IX (NMM) by G-quadruplex [66].

G-quadruplex-based probes are also used for the detection of nucleic acids. Cheng and his group developed a calorimetric biosensing system for microRNA detection [67]. Another research group developed a single-stranded DNA sensing system based on a G-quadruplex integrated hybridization chain reaction system and this system has a detection limit of 7.5 nM and 4 nM by colorimetric and fluorometric methods, respectively [68].

In addition to nucleic acid and metal ions, G-quadruplex-based fluorescent probes are used to detect organic molecules. Based on NMM/G-quadruplex structure, Yang and coworkers developed an antibiotic kanamycin detection probe with a 0.5 nM detection limit [69]. Another research group developed a G-quadruplex-based fluorescent probe for cisplatin with 750 nM detection limit [70]. In another study, G-quadruplex/ThT fluorescence aptasensor was developed to detect tetracycline and the limit of detection of the sensor was 0.001 μmol/L [71].

1.7 Thioflavin T

Thioflavin T is a benzothiazole dye that produces enhanced fluorescence when bound to amyloid fibrils and is extensively used to identify amyloid fibrils both in vivo and in vitro [72,73]. ThT also binds to human telomeric G-quadruplexes, generating a fluorescent light-up signal change, and has a strong specificity towards G4s among other DNA structures [74]. It has recently been employed as a fluorescent probe for RNA G-quadruplex identification and targeting G-quadruplex structures [75–78]. G-quadruplex - ThT fluorescence platforms are easy to use, sensitive, and cost-effective sensors.

1.8 Hydroxychloroquine

Hydroxychloroquine is a member of the 4- aminoquinoline class of medicines and was firstly synthesized to reduce the toxicity of chloroquine that is used to treat malaria, by adding a hydroxyl group to chloroquine [79,80]. Due to its antimalarial properties, HCQ was initially used also to treat malaria [81]. Later, HCQ is started to get used to treat rheumatoid arthritis and systemic lupus erythematosus due to its anti-inflammatory and immunomodulatory properties [82–85]. It was also the first line of medication used in the treatment of COVID-19 at the beginning of the pandemic [86,87]. However, due to its inefficacy and adverse effects in treating COVID-19, the US Food and Drug Administration (FDA) has revoked HCQ's emergency use authorization [88]. Still, the potential benefits of HCQ and possible application areas are still being investigated. For instance, Lie et al. indicated that HCQ inhibited cell growth in human bladder cancer cells in vitro [89].

Hydroxychloroquine is easily absorbed by the intestines, that results in its accumulation in the liver, spleen, lungs, and kidneys [90]. Its t toxic dosage is 6.5 mg/kg body weight [91], and an overdose can result in retinopathy and cardiomyopathy [92,93]. Also, due to its use in many different diseases, large amounts of HCQ is consumed worldwide that results in discharge of hight amounts of HCQ into waste waters [94]. As a result, due to its toxic effects in human body and contamination of the environment, HCQ-containing drugs must undergo strict quality control and development of simple, fast, and effective methods for identifying HCQ in pharmaceutical and biological samples is required.

1.8.1 Hydroxychloroquine detection methods

In the literature, electrochemical, spectrophotometric and chromatographic techniques are used to detect HCQ in different matrices. Arguelho et. al. determined HCQ in pharmaceutical tablets using differential pulse voltammetry method with a limit of detection of 11.2 μg ml^{-1} [95]. Another electrochemical detection method

for HCQ was developed by Deroco et.al. They developed the method by using square wave voltammetry and determined HCQ in synthetic urine samples and pharmaceutical tablets [96]. Also, a simplistic method using UV-vis spectroscopy in pharmaceutical tablets was developed with an LOD of 0.38 μgmL^{-1} [97]. Liquid chromatography (LC) is another method used in the detection of HCQ. Wang et al. developed LC-tandem mass assay for the determination of HCQ in human blood samples [98]. Loe et al. developed a ultra-high performance liquid chromatography – fluorescent method for determination of HCQ in whole blood samples with a lower limit of quantitation of 10 ng/mL [99].

Direct fluorometric detection of HCQ was not investigated previosly even though it is considered advantageous compared to other methods reported due to its high sensitivity and ease of use.

1.9 Thesis focus

In this study, we aim to synthesize novel Azacyanines, investigate their interactions with G4s, and develop a new, sensitive and selective detection platform for HCQ based on G4 structure.

Using small molecules as therapeutic agents opens up new opportunities to treat many diseases, including cancer. Although many small molecules are used in the treatment of different types of cancer, new ones that are more selective and less toxic to cells still need to be discovered. Due to the high affinity to G4s instead of genomic DNA, Azacyanines might be good alternatives to anticancer therapy. Within the scope of this thesis, three new Azacyanines including Azacyanine-6-methyl, azacyanine-6-fluoro and Azacyanine-6-chloro were synthesized, characterized, and their interactions with different G4 structures were investigated using competition dialysis, UV-vis and CD spectroscopy.

In the second part of the studies, G4 based novel fluorescent probe was developed to detect HCQ. The designed probe takes advantage of Tel24 G4-ThT interactions. The

probe was developed based on the fluorescent enhancement due to Tel24-ThT complex, and the subsequent fluorescence decrease upon addition of HCQ. The detection platform developed in here is the first G4 based fluorometric detection method for HCQ detection.

Overall, this study provides the synthesis and characterization of new G4 binding Azacyanines molecules and their interactions with Pu22 G4 DNA. In addition, this thesis provides a novel G4 based fluorometric detection platform for HCQ in various matrices.

CHAPTER 2

SYNTHESIS OF AZACYANINES AND ASSESTMENT OF THEIR SELECTIVITY TOWARDS DIFFERENT NUCLEIC ACID STRUCTURES

2.1 Materials and methods

2.1.1 Chemicals and instrumentation

The starting materials for the synthesis of Azacyanines; 2-Amino-6-methylbenzothiazole, and 2-amino-6-fluorobenzothiazole were obtained from Alfa Aesar (Kandel, Germany). 2-Amino-6- chlorobenzothiazole was purchased from TCI (Tokyo Chemical Industry, Tokyo, Japan). 2-(2-ethoxyethoxy) ethanol (99.0%), perylene (≥99%), dichloromethane (≥99%), sodium chloride (NaCl), sodium phosphate monobasic (NaH_2PO_4), sodium phosphate dibasic (Na_2HPO_4), ethylenediaminetetraacetic acid disodium salt dihydrate (Na_2EDTA) and sodium dodecyl sulfate (SDS), poly(A), poly(U), and poly(dA):poly(dT) were purchased from Sigma-Aldrich (St. Louis, USA). Dimethylsulfoxide (DMSO, 99.8%) and cyclohexane (99.5%) were purchased from AppliChem GmbH (Darmstadt, Germany). Deuterated dimethyl sulfoxide (DMSO-d_6) for NMR spectroscopy, pyridine (spectroscopic grade; 99.0%), acetone, methanol (≥99.8%), dichloromethane, glacial acetic acid (≥99%), and all other organic solvents were obtained from Merck (Darmstadt, Germany). Diiodomethane (CH_2I_2, 99.0%) was obtained from abcr GmbH (Karlsruhe, Germany). All oligonucleotides were purchased from Integrated DNA Technologies (IDT) (Leuven, Belgium). All the starting materials, solvents and oligonucleotides were used without further purification.

All NMR (^{1}H and ^{13}C) spectra were obtained using a 400 MHz Bruker AVANCE III NMR spectrometer (Bruker, Karlsruhe, Germany). High-resolution mass spectra (HRMS) were obtained using electrospray ionization and time-of-flight (ToF) detection via Waters SYNAPT G1 MS spectrometer (Waters, Milford, MA., USA). Elemental analyses (C, H, N, and S) were performed on a Leco analyzer (CHNS-932, USA). An Agilent Cary UV−vis photodiode array spectrophotometer (Santa Clara, CA, USA) was used for absorption measurements, and an Agilent Cary Eclipse spectrofluorometer (Agilent Technologies, USA) was used for the fluorescence intensity measurements. Jasco J-1500 spectropolarimeter (Easton, USA) equipped with a Peltier-type temperature control system was used for circular dichroism (CD) studies. A Mettler Toledo Seven CompactS210 pH meter (Greifensee, Switzerland) was used for pH measurements.

2.1.2 Synthesis of Azacyanines

Briefly, 1.0 g of the starting material was taken in a round-bottom flask with a magnetic stirrer. The mixture of 20.0 mL of 2-(2-ethoxyethoxy) ethanol and 5.0 mL of pyridine was added to the flask and stirred at room temperature to get a clear solution. Afterwards, 600.0 µL of glacial acetic acid was added to the reaction mixture, and the mixture was heated to 200 °C. Next, 7.5 mmol diiodomethane was immediately injected into the reaction mixture, and the reaction mixture was refluxed at 200 °C for 15 minutes under nitrogen flow. Subsequently, the heater was turned off, and the mixture was allowed to cool down to room temperature. Once it was cooled down, the precipitate was filtered and washed several times with pure acetone and dichloromethane and dried at 65 °C overnight. The final product was recrystallized with a 20% (v/v) methanol-water mixture and characterized via ^{1}H and ^{13}C NMR, HRMS and elemental analysis. For further experiments, the stock solutions of the synthesized Azacyanines were prepared in DMSO.

2.1.3 Molar extinction coefficient and fluorescence quantum yield calculations

The molar extinction coefficients of Azacyanines were calculated by measuring the maximum absorbance of stock solutions, varying in concentration. For this purpose, for each synthesized Azacyanine derivative, five stock solutions at different concentrations were prepared in DMSO. To prepare the stock solutions, 5.0, 10.0, 15.0, 20.0 and 25.0 mg of the Azacyanine derivatives were carefully weighed and individually dissolved in 50.0 mL DMSO. Six different dilutions were prepared from each of the stock solutions to obtain UV-vis spectra with an absorbance scale between 0.3-0.8. The extinction coefficients of the synthesized Azacyanine derivatives were calculated using the absorption vs. concentration plots using the Beer-Lambert law. The slope of Absorbance (A) versus Molar Concentration (c) divided by b (cell length; 1cm) gives the molar absorption coefficient value. For each Azacyanine derivative, the values obtained for five different stock solutions were averaged out.

Fluorescence quantum yields (ΦF) of the synthesized Azacyanines were calculated using the comparative method suggested by Williams et al. [100], which involves the use of well-characterized standard samples with known ΦF values. Briefly, solutions of the standard and test samples (synthesized Azacyanines) with identical absorbance at the same excitation wavelength (at their maximum absorbance wavelength; 410 nm) were prepared. For each Azacyanine derivative, five solutions with increasing concentrations were prepared in DMSO. The quantum yield was calculated using the integrated emission intensities from the sample and reference pairs at identical concentrations. It should be noted that to minimize re-absorption effects, absorbances in the 10 mm fluorescence cuvette were never let to exceed 0.1 at the excitation wavelength. Accordingly, solutions that have absorbance values between 0.02 to 0.1 were tested. Excitation wavelength of 410 nm was used, and

emission spectra were collected from 411 to 675 nm. Excitation slit was set to 2.5 nm, and emission slit was set to 5.0 nm. The fluorescence QYs were determined using the following equation:

$$\Phi_x = \Phi_{ST}\left(\frac{Grad_x}{Grad_{ST}}\right)\left(\frac{\eta_x}{\eta_{ST}}\right)^2$$

Where the Φx and Φ_{ST} are the quantum yields of the Azacyanine derivatives and the reference sample, respectively. Gradx and $Grad_{ST}$ are the intensities of the emission spectra of the Azacyanine derivatives and that of the reference sample, respectively, and η is the refractive index of the solvent used.

2.1.4 Competition dialysis

Competition dialysis experiments were performed according to the previously reported procedure by Chaires et al. [101]. Preparation of 1X BPES buffer is described in Appendix C, and nucleic acid sequences are given in Appendix B. The concentration of the oligonucleotides was calculated using their extinction coefficients listed in Appendix B. poly(A):poly(U) was prepared by mixing 1:1 equimolar ratio of poly(A) and poly(U).

All the oligonucleotides were prepared in 1X BPES buffer (1.0 mM Na_2EDTA, 6.0 mM Na_2HPO_4, 2.0 mM NaH_2PO_4 and 185 mM NaCl), pH 7.0. Prepared samples were annealed by heating at 95 °C for 5 min in a water bath followed by cooling down to room temperature overnight.

For the competition dialysis assay, 600.0 µL 60.0 µM oligonucleotide was put into Pierce (Thermo Fischer Scientific, USA) 7000 Da molecular cut-off dialysis cassettes. After that, the dialysis cassettes were dialyzed for 24 hours against 750 mL of 1.0 µM of Azacyanine solution. After the dialysis was completed, oligonucleotide

solutions were taken from the dialysis cassettes, and 1%(w/v) SDS was added to release the bound Azacyanine from the nucleic acids. After that, by using Fluorescence spectroscopy, Azacyanine concentration in each cassette was determined using the calibration curves constructed. Excitation and emission slits were both 5.0 nm. Azacyanine-6-methyl, Azacyanine-6-fluoro and Azacyanine-6-chloro were excited at 387nm, 390nm and 392 nm, respectively.

The calibration curve for each Azacyanine derivative was constructed by measuring the fluorescence intensity of a series of solutions with varying concentrations using the parameters given above. A calibration curve is constructed using the maximum fluorescence intensity at a specified wavelength vs. the concentration for each derivative. Using the linear equation from the calibration curve, the bound Azacyanine to each oligonucleotide was determined. For each Azacyanine derivative, two independent dialysis experiments were performed. The ratio of bound ligand to free ligand was determined using the equation: $C_b = C_t - C_f$ where C_b is the bound ligand concentration, C_f is the Azacyanine concentration in the positive control dialysis cassette and C_t total Azacyanine concentration in each dialysis cassette.

2.1.5 Determining nucleic acid-Azacyanine interactions via UV-vis and Circular Dichroism Spectroscopy

In line with the data, we obtained from the competition dialysis, the interactions of the synthesized molecules with the nucleic acid sequence to which they bind selectively and strongly were examined using UV-vis spectroscopy. For this purpose, 0:1,1:0 and 1:1 (DNA: Azacyanine) equimolar ratio samples were prepared in 1X BPES. The nucleic acid containing samples, 10.0 μM in concentration, were annealed as described previously before the addition of the corresponding Azacyanine. The UV-vis absorption spectra of the samples were collected using an Agilent Cary spectrophotometer at room temperature. The same samples were used

in CD spectroscopy studies. CD spectra of the samples collected between 200-550 nm at 15 ºC with 100 nm/min scanning speed and 1.00 nm bandwidth.

2.2 Results and discussions

"Synthesis and characterization of Azacyanines" and "Optical and photophysical properties of synthesized Azacyanines" parts of this thesis was published as "Novel Fluorescent Azacyanine Compounds: Improved Synthesis and Optical Properties" by K. Doğan, A. Gülkaya, M. Forough and O. Persil Çetinkol in *ACS Omega*, 5(36), 22874-22882,2020 [102].

2.2.1 Synthesis and characterization of Azacyanines

The synthesis procedure of Azacyanine-6-methyl, Azacyanine-6-fluoro, and Azacyanine-6-chloro is presented in Figure 2. The effect of the solvents used on the synthesis was tested using 1-butanol, 2-butanone, chloroform, isoamyl alcohol, toluene, dimethylformamide, tetrahydrofuran, acetonitrile, dimethylacetamide, pyridine and mixtures of these solvents with 2-(2-ethoxyethoxy) ethanol at different ratios. However, the syntheses of the Azacyanines with the electron-withdrawing substituents in pure solvents were not successful. The use of solvent mixtures increased the success of syntheses, and the best results were achieved in 2-(2-ethoxyethoxy) ethanol/pyridine (4:1 v/v). However, the Azacyanines with the electron-withdrawing substituents were not stable and they decomposed within days. To promote the stable synthesis of all Azacyanines, the syntheses were repeated under an acidic medium using glacial acetic acid. Finally, the binary solvent mixture [2-(2-ethoxyethoxy) ethanol/pyridine: 4:1 v/v] under acidic conditions was selected as the optimum system for the syntheses.

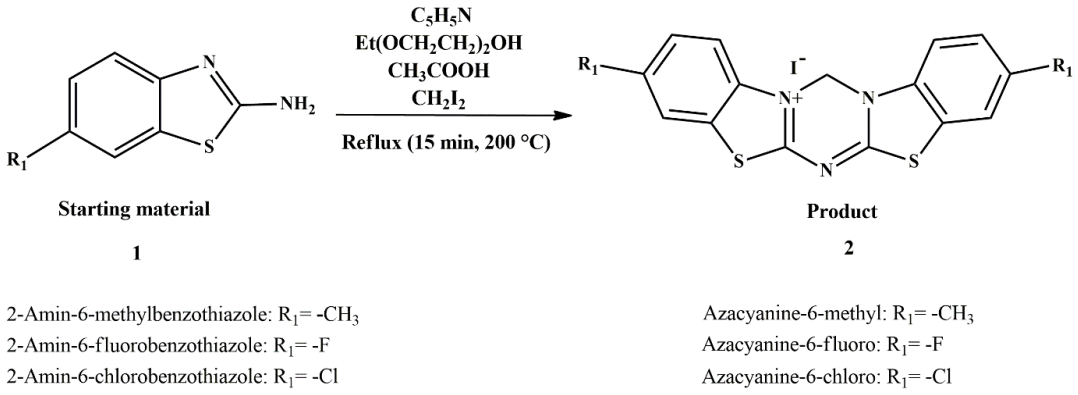

Figure 2. Synthetic scheme for Azacyanine synthesis.

The proposed reaction mechanism for the synthesis of Azacyanines is given in Figure 3. The mechanism is proposed based on the similar reaction of benzimidazoles with CH_2I_2 [59]. Here, the stoichiometry between the starting materials and products is 2:1. Firstly, the lone pair of the amine group induces lone pairs of nitrogen (numbered as 3) to facilitate its attack to diiodomethane. Between nitrogen and diiodomethane, an SN_2 reaction takes place. One of the iodine atoms leaves, and a covalent bond forms between the carbon and the nitrogen. Then, the lone pair of the nitrogen of the other starting benzothiazole attacks to the carbon and the second iodine atom leaves, while forming a new bridge between the two benzothiazoles. After that, the free iodine atom takes hydrogen from the nitrogen, and the formal charge of the nitrogen becomes zero. The lone pairs of nitrogen attack to the carbon atom in the thiazole ring, resulting in the movement of double bond electrons to the nitrogen. At the end of this step, a six-membered ring between two starting materials is formed. After taking a proton from the reaction medium, lone pair of the upper nitrogen joins the ring system, resulting in the loss of ammonia. Finally, the positively charged product and the negatively charged iodine form the salt.

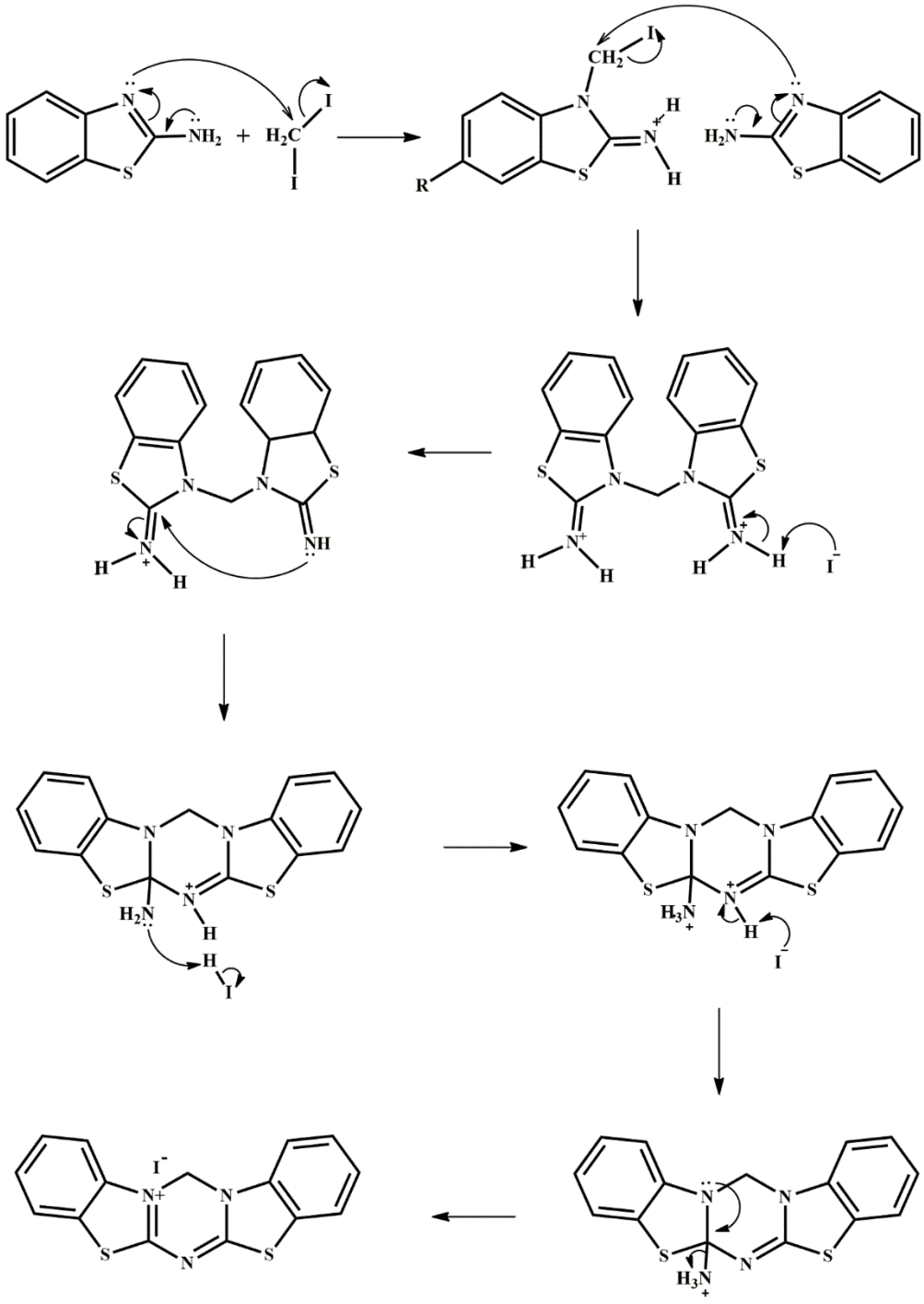

Figure 3. Reaction mechanism proposed for Azacyanine synthesis.

Azacyanine-6-methyl, Azacyanine-6-fluoro and Azacyanine-6-chloro were synthesized through a simple one-step method, as depicted in Figure 2. Structures of the newly prepared compounds were confirmed by ^{1}H and ^{13}C NMR, UV-vis

spectroscopy, HRMS and Elemental Analysis techniques. ^{1}H NMR and ^{13}C NMR results of Azacyanine-6-fluoro, Azacyanine-6-chloro and Azacyanine-6-methyl, are given in Appendix A. HRMS, and Elemental Analysis results are also presented in Appendix A.

The yields of the synthesis, the maximum absorption wavelengths in addition to the calculated molar extinction coefficients are given in Table 1. The synthesis yields for Azacyanine-6-methyl, Azacyanine-6-fluoro and Azacyanine-6-chloro were 45%, 34% and 60%, respectively. It is known that the electron donating groups substituted to Azacyanines can contribute electron density to the π system and stabilize the positive charge on the nitrogen atom, leading to a more stable state [103]. However, alkyl substituent bound to position 6 inAzacyanine-6-methyl, cannot donate lone pair electrons to the π system, but it could still increase the electron density of the ring system which is evident from the 45% yield of Azacyanine-6-methyl.

On the other hand, electron-withdrawing substituents create a less stable structure because they decrease the electron density on the aromatic ring [104]. They cannot stabilize the positive charge on the nitrogen and cannot contribute to the conjugation of the π system. However, Azacyanine-6-fluoro and Azacyanine-6-chloro can donate their lone pairs to the π system of the aromatic rings [105]. Chlorine and fluorine enhance the reactivity and induce electron density. The product yield of Azacyanine-6-fluoro and Azacyanine-6-chloro presented in Table 1 is in an acceptable range (34 and 60%, respectively). Because of the greater electronegativity of fluorine, as expected the product yield of fluorine was lower than chlorine.

Table 1.Spectral data and yield of synthesized Azacyanines.

	R_1	Yield (%)	λ_{max} (nm)	$\varepsilon(M^{-1} cm^{-1})^a \pm SD^b$
Azacyanine-6-methyl	$-CH_3$	45	392	31,000 ± 1100
Azacyanine-6-fluoro	-F	34	387	29,500 ± 1700
Azacyanine-6-chloro	-Cl	60	390	31,600 ± 2500

[a]Measured in DMSO.

[b]SD: standard deviation.

2.2.2 Optical properties of synthesized Azacyanines

Optical properties of Azacyanine-6-methyl, Azacyanine-6-fluoro and Azacyanine-6-chloro were investigated by using UV-vis absorption and fluorescence spectroscopy. All the synthesized Azacyanines were displaying intense and broad absorptions (ε> 20,000 M^{-1} cm^{-1}) in the UV region (λ_{max} (nm) = 387-392). As can be seen in Table 1, maximum absorbance wavelengths increase in order of Azacyanine-6-fluoro < Azacyanine-6-chloro <Azacyanine-6-methyl.

In Figure 4, normalized UV-vis absorption, fluorescence emission and excitation spectra obtained at room temperature were shown. All the synthesized Azacyanines exhibit a similar spectral region, and they have two observed vibronic bands. Azacyanine-6-methyl, has an electron-donating methyl group that has no lone pair electrons to contribute to the resonance structure. Only by the inductive effect, the methyl group can activate the ring and increase the electron density. By stabilizing the positive charge and favoring the conjugation, electron-donating groups result in a decrease in the π–π* or n–π* energy gap. On the other hand, Azacyanine-6-fluoro and Azacyanine-6-chloro have electron-withdrawing groups that can decrease the

electron density and deactivate the ring [106]. Electron withdrawing groups do not have such effects; they don't change the energy gap. Possibly because of these reasons, the maxima absorption wavelength differs between the three compounds.

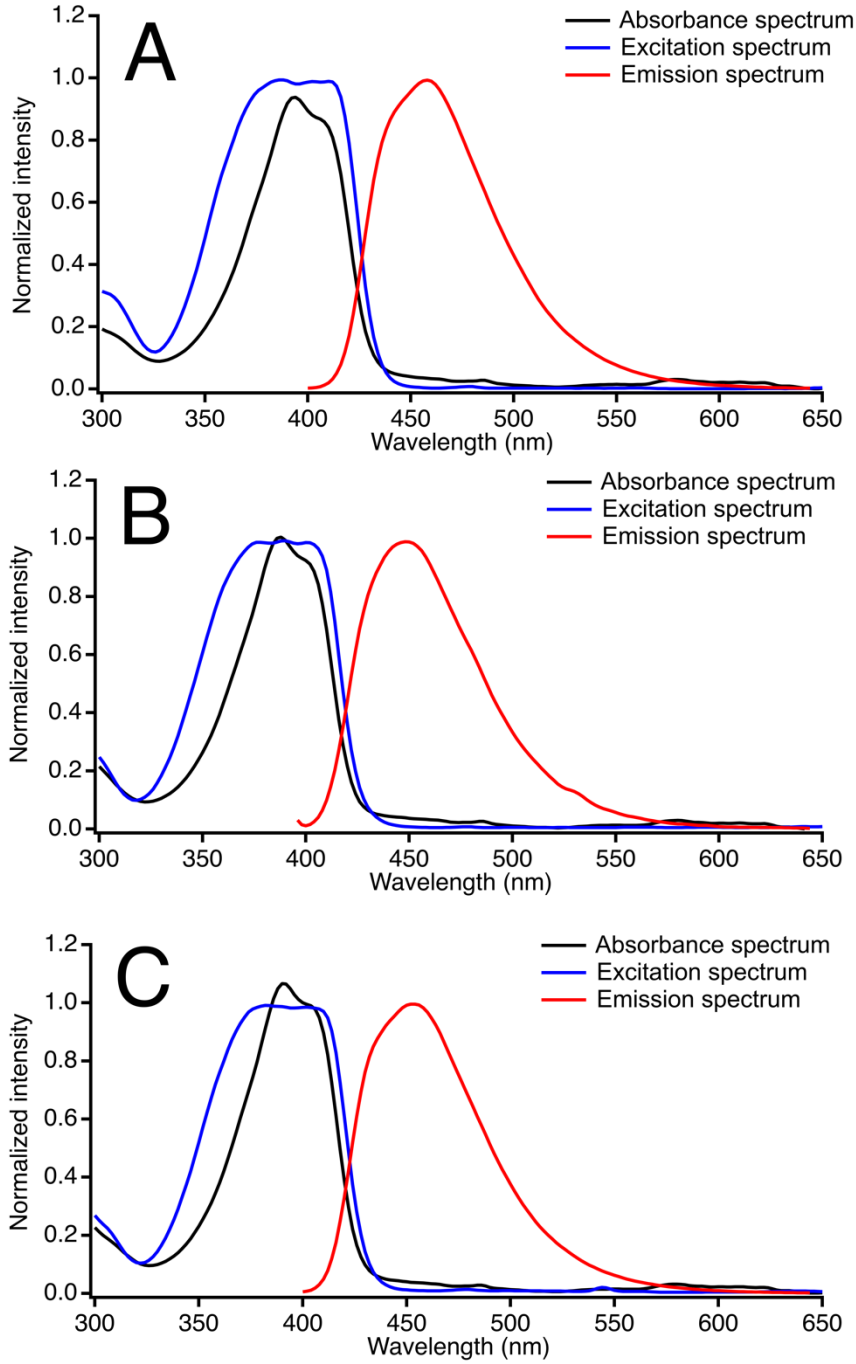

Figure 4. UV-vis absorption, fluorescence emission and excitation spectra of synthesized Azacyanines (30.0 μM) in DMSO at room temperature; (A) Azacyanine-6-methyl; (B) Azacyanine-6-fluoro; (C) Azacyanine-6-chloro.

For comparison, the fluorescence emission spectra of the synthesized Azacyanines are given in Figure 5. Azacyanine-6-methyl, Azacyanine-6-fluoro and Azacyanine-6-choloro have all the maximum emissions between 447 nm and 458 nm.

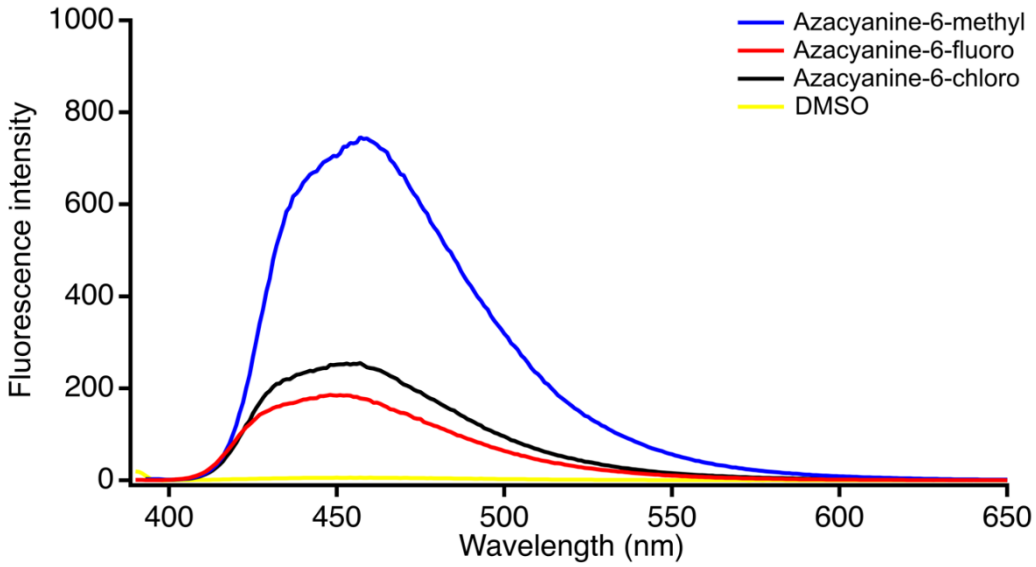

Figure 5. Fluorescence emission spectra of the synthesized Azacyanines (10.0 μM) in DMSO. The samples were excited at their maximum absorbance wavelength.

The fluorescence intensity vs. absorbance graph for the calculation of quantum yield (QY) of synthesized Azacyanines using perylene as the reference are displayed in Figure 6 and their QYs are summarized in Table 2. A digital photograph of the samples taken under UV light is given in Figure 7. Azacyanine-6-methyl has the highest, and Azacyanine-6-fluoro has the lowest fluorescence QY. This result suggests that while the electron-withdrawing groups decrease the fluorescence QY, the electron-donating group increases it.

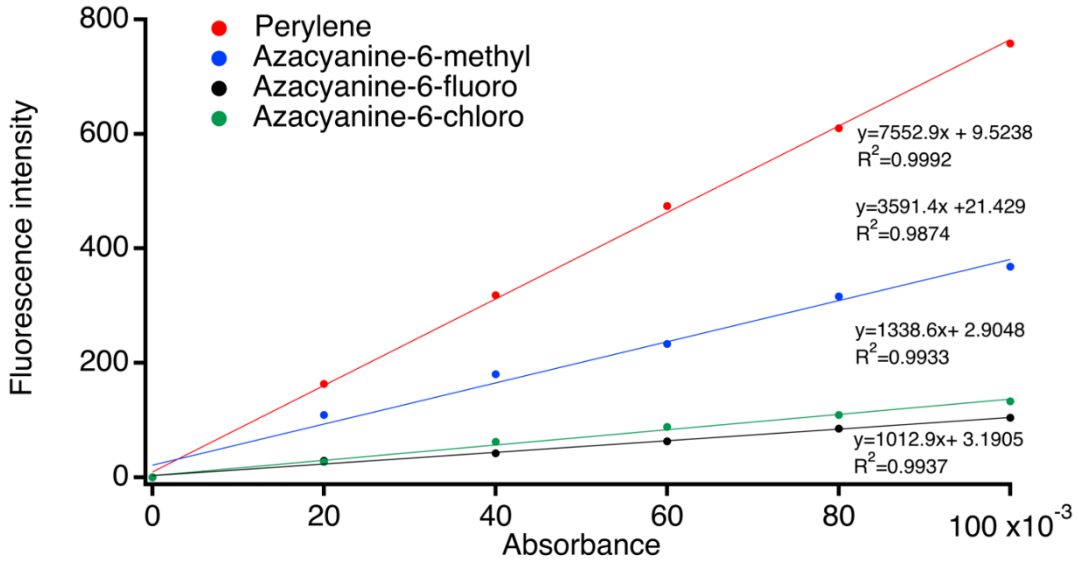

Figure 6. Fluorescence intensity vs. absorbance graph used in the calculation of QY's of the synthesized Azacyanines.

Table 2. Optical and photophysical properties of synthesized Azacyanines.

	λ_{abs} max (nm)	λ_{em} max (nm)	QY (ΦF %)[a]
Azacyanine-6-methyl	392	458	47.5
Azacyanine-6-fluoro	387	447	13.4
Azacyanine-6-chloro	390	456	17.7

[a]Measured in DMSO.

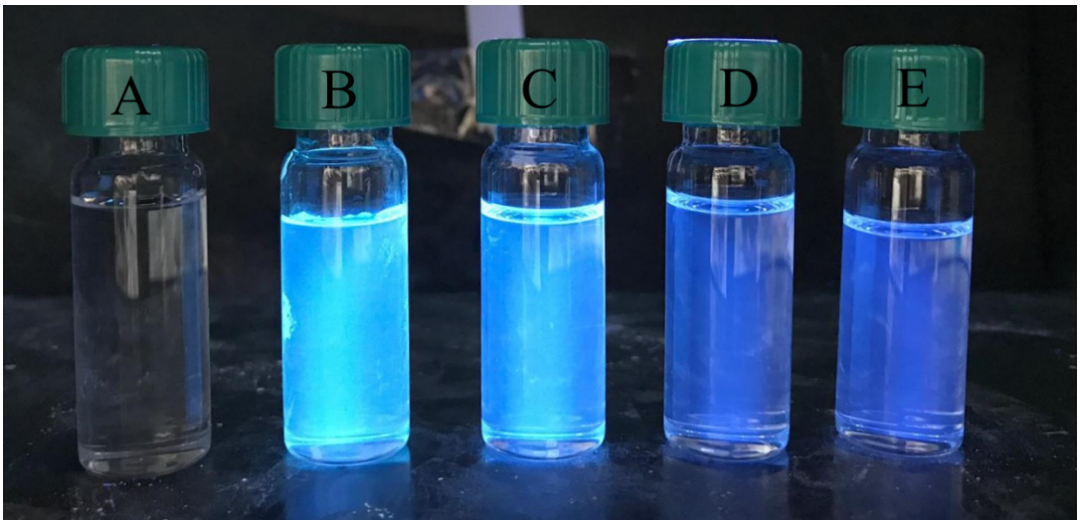

Figure 7. Digital photograph of synthesized Azacyanines in DMSO under 365 nm UV lamp. (A) DMSO, (B) Perylene, (C) Azacyanine-6-methyl, (D) Azacyanine-6-chloro and (E) Azacyanine-6-fluoro.

2.2.3 Investigating the selectivity of Azacyanines via competition dialysis

To investigate the selectivity of synthesized Azacyanines towards different nucleic acid structures, competition dialysis experiments were performed. Various nucleic acid structures were dialyzed against Azacyanine-6-methyl, Azacyanine-6-fluoro or Azacyanine-6-chloro for 24 hours. At the end of the dialysis experiment, the fluorescence intensity of samples in each dialysis cassette was measured.

In Figure 8 and Figure 9, fluorescence intensity versus wavelength of Azacyanine-6-methyl graph for first and second replicate are displayed, respectively. As can be seen from Figure 8 and Figure 9, the highest fluorescence intensity was observed for the cassettes containing Pu22, BCL-2 and C-myc. This indicates that Azacyanine-6-methyl has the highest affinity towards these nucleic acid structures among the others. The C_b values were calculated and summarized in Table 3 and Figure 10. The highest C_b values, indicating the highest affinity, are found to be 1.399, 0.925, and 0.890 for Pu22, BCL-2 and C-myc, respectively.

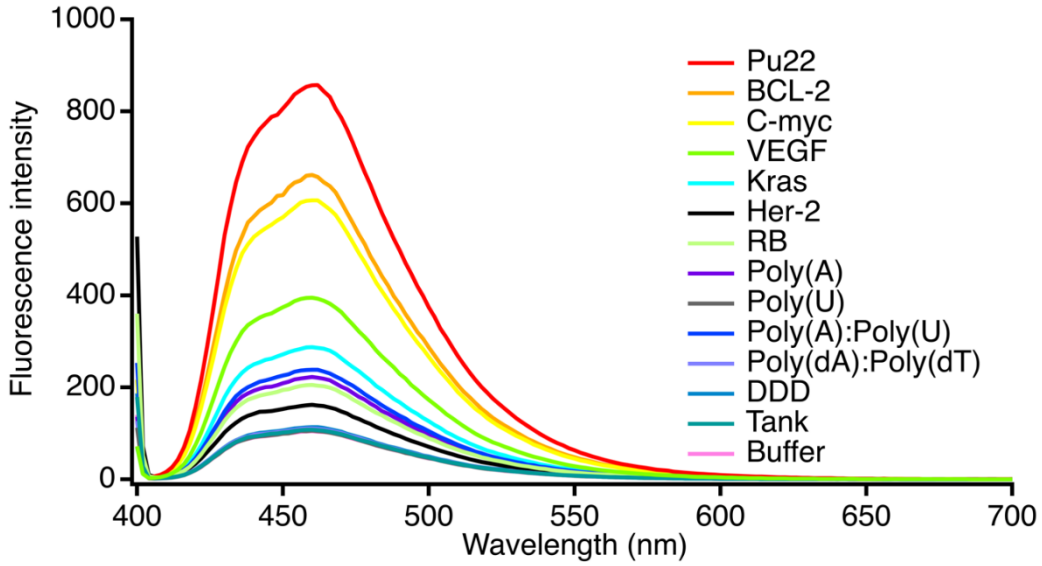

Figure 8. Fluorescence intensity vs. wavelength spectra of samples obtained from competition dialysis of Azacyanine-6-methyl (1st replicate).

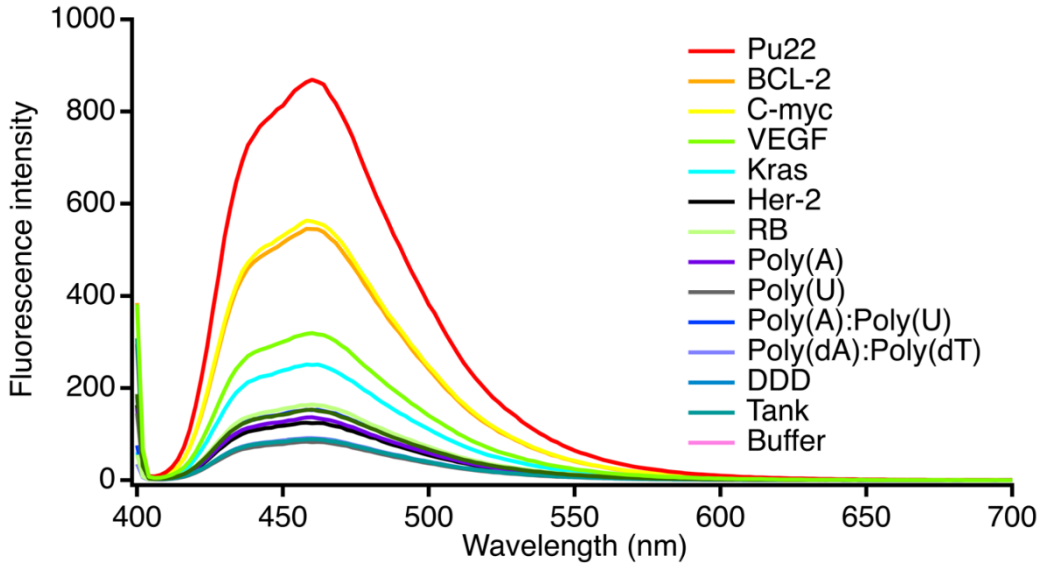

Figure 9. Fluorescence intensity vs. wavelength spectra of samples obtained from competition dialysis of Azacyanine-6-methyl (2nd replicate).

Table 3. Competition dialysis results of Azacyanine-6-methyl.

Nucleic Acid Structures	C_b			
	1st replicate	2nd replicate	Average	Standard Deviation
Pu22	1.373	1.425	1.399	0.036
BCL-2	1.017	0.834	0.925	0.130
VEGF	0.530	0.421	0.475	0.077
C-myc	0.916	0.864	0.890	0.037
Kras	0.334	0.295	0.314	0.028
Her-2	0.104	0.064	0.084	0.029
RB	0.184	0.138	0.161	0.032
Poly(A)	0.216	0.087	0.151	0.091
Poly(U)	0.002	-0.010	-0.004	0.009
DDD	0.016	0.005	0.010	0.008
Poly(A):Poly(U)	0.244	0.116	0.180	0.090
Poly(dA):Poly(dT)	0.011	0.005	0.008	0.004
Tank	0.007	0.001	0.004	0.004
Buffer	0.000	0.000	0.000	0.000

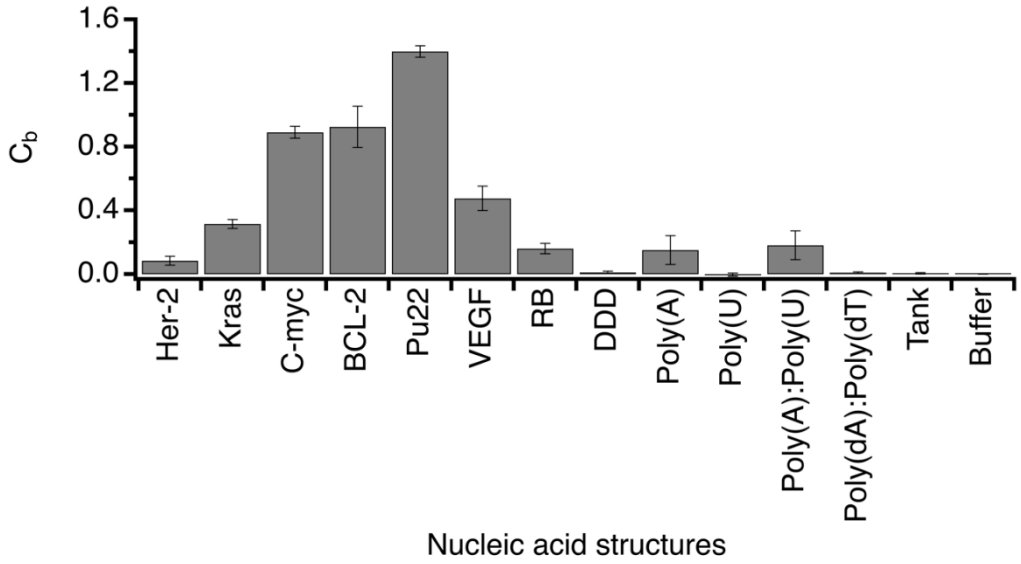

Figure 10. Average of C_b values obtained from the competition dialysis of Azacyanine-6-methyl.

Figure 11 and Figure 12 display the competition dialysis results for Azacyanine-6-fluoro. As Azacyanine-6-methyl, Azacyanine-6-fluoro has the greatest affinity towards Pu22, BCL-2 and C-myc. When compared to Azacyanine-6-methyl, C_b values obtained for Azacyanine-6-fluoro with these structures are lower. As shown in Table 4 and Figure 13, averaged C_b values for Pu22, BCL-2 and C-myc are 0.552, 0.525 and 0.393, respectively.

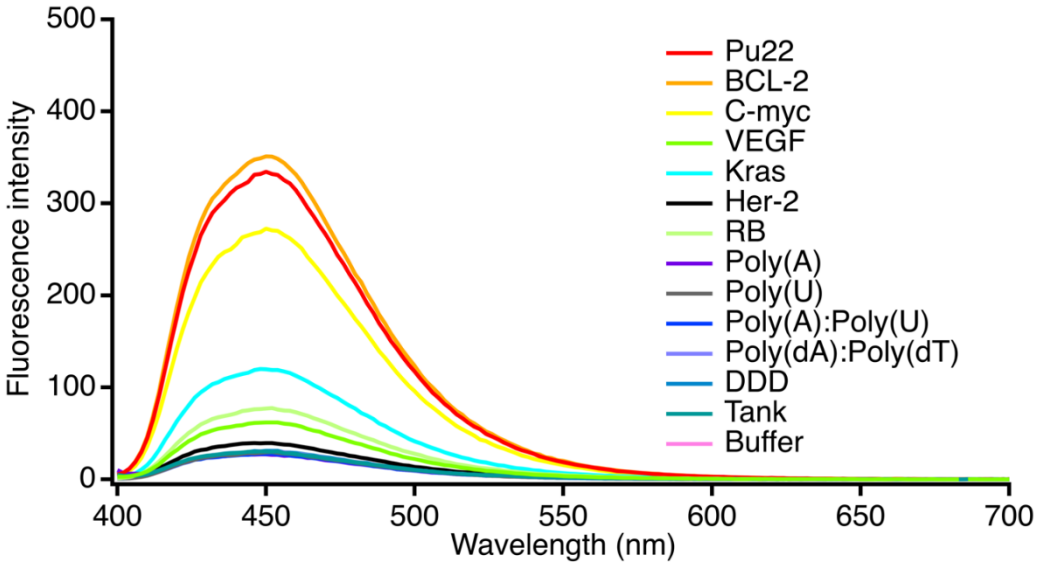

Figure 11. Fluorescence intensity vs. wavelength (nm) spectra of samples obtained from competition dialysis of Azacyanine-6-fluoro (1st replicate).

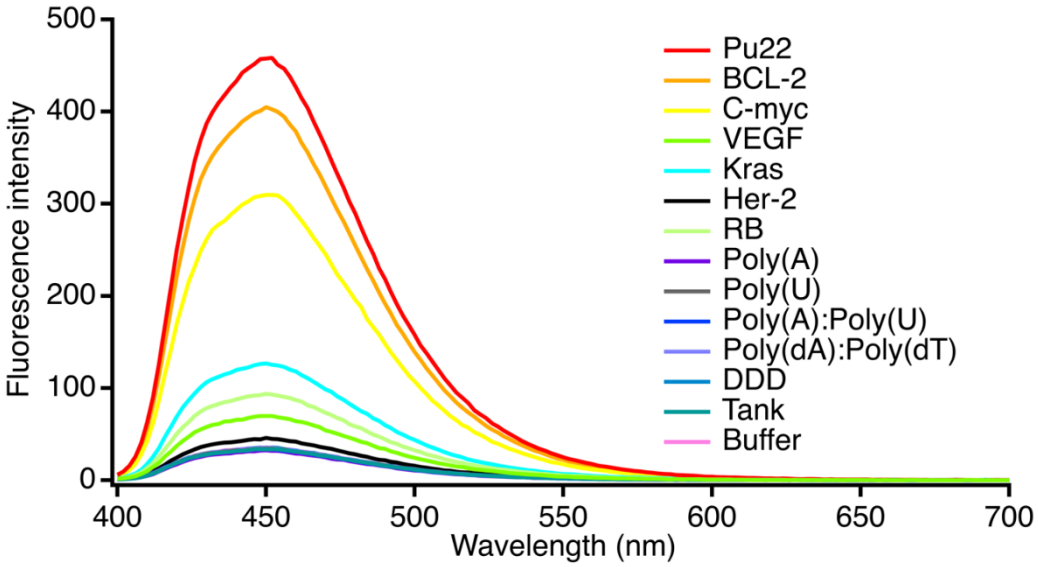

Figure 12. Fluorescence intensity vs. wavelength (nm) spectra of samples obtained from competition dialysis of Azacyanine-6-fluoro (2nd replicate).

Table 4. Competition dialysis results of Azacyanine-6-fluoro.

Nucleic Acid Structures	C_b			
	1st replicate	2nd replicate	Average	Standard Deviation
Pu22	0.463	0.641	0.552	0.126
BCL-2	0.488	0.562	0.525	0.052
VEGF	0.048	0.052	0.050	0.002
C-myc	0.368	0.417	0.393	0.034
Kras	0.136	0.138	0.137	0.001
Her-2	0.014	0.016	0.015	0.001
RB	0.071	0.088	0.080	0.012
Poly(A)	-0.004	-0.005	-0.004	0.001
Poly(U)	-0.001	-0.002	-0.001	0.000
DDD	0.001	-0.001	0.000	0.002
Poly(A):Poly(U)	-0.004	-0.002	-0.003	0.001
Poly(dA):Poly(dT)	0.000	0.000	0.000	0.000
Tank	0.000	-0.003	-0.001	0.002
Buffer	0.000	0.000	0.000	0.000

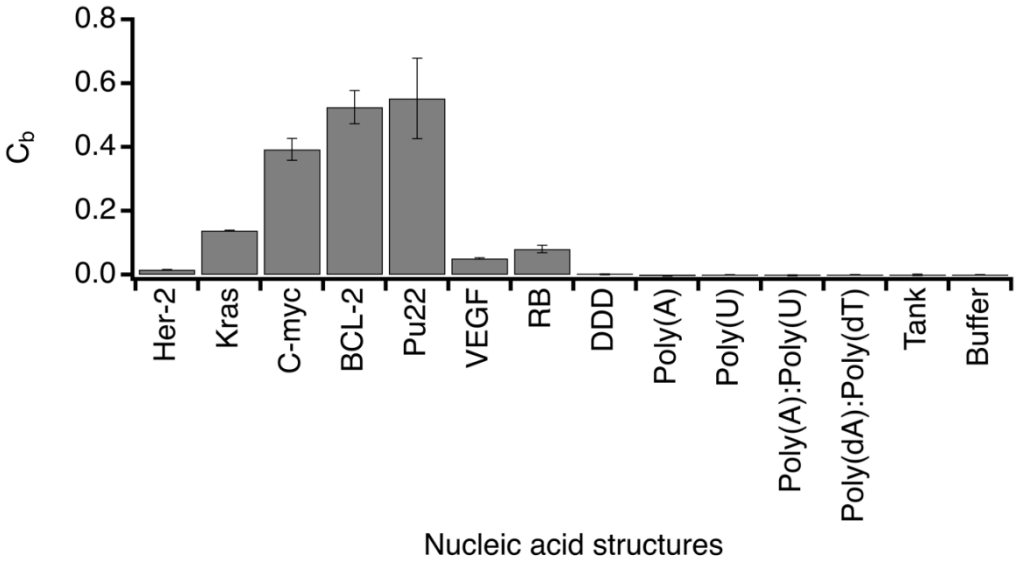

Figure 13. Average of C_b values obtained from the competition dialysis of Azacyanine-6-fluoro.

Figure 14 and Figure 15 display the fluorescence intensity versus wavelength graphs obtained from the competition dialysis of nucleic acid structures towards Azacyanine-6-chloro. Compared to Azacyanine-6-methyl and Azacyanine-6-fluoro, the relative affinity of Azacyanine-6-chloro towards VEGF was greater than its affinity to C-myc. The highest fluorescence intensity was observed for Pu22, BCL-2 and VEGF, respectively. The calculated C_b values are summarized in Table 5 and shown in Figure 16. Average C_b values were calculated as 1.238, 1.044 and 0.790 for Pu22, BCL-2 and VEGF, respectively.

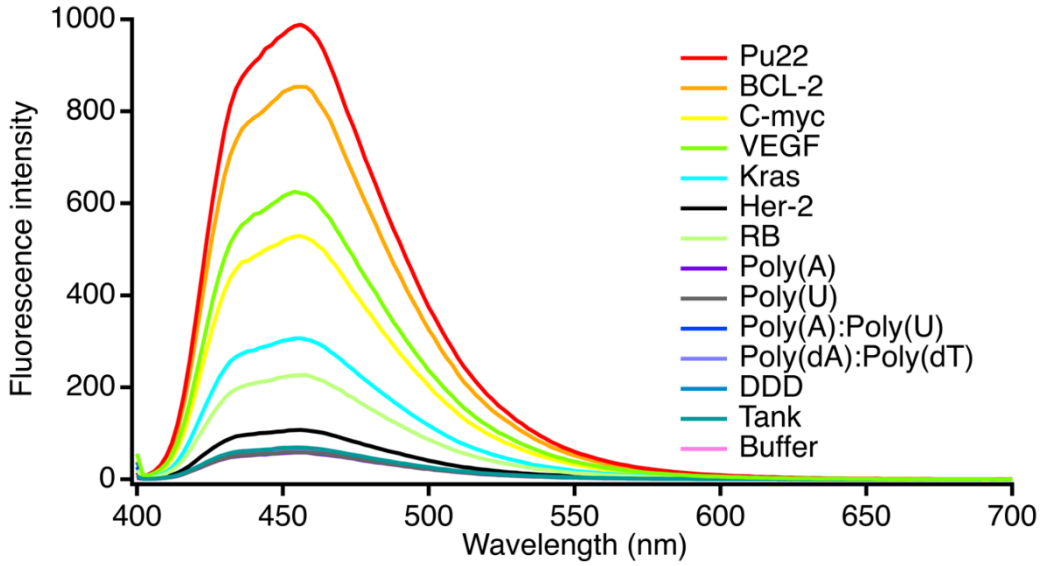

Figure 14. Fluorescence intensity vs. wavelength (nm) spectra of samples obtained from competition dialysis of Azacyanine-6-chloro (1st replicate).

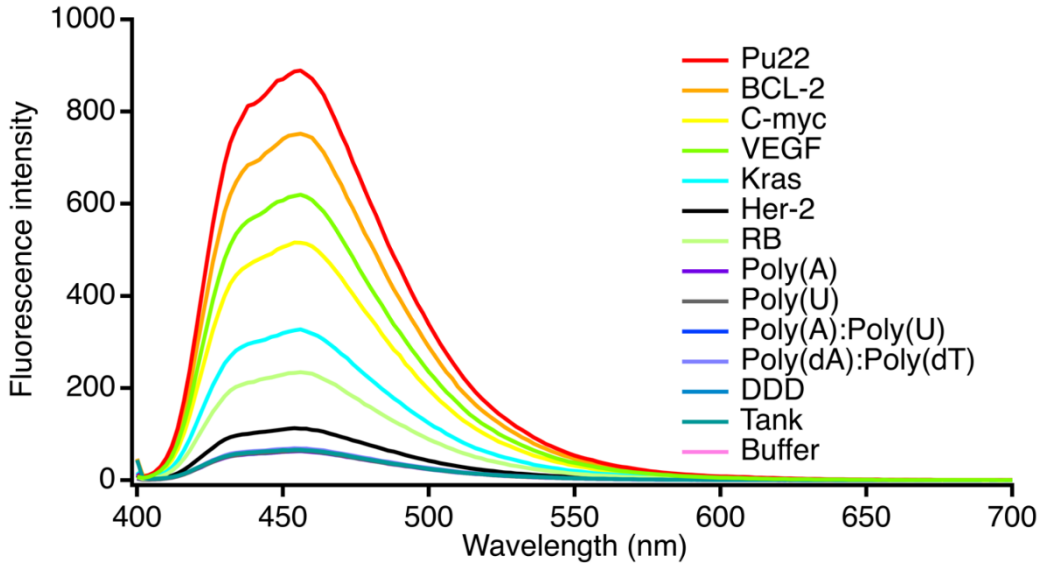

Figure 15. Fluorescence intensity vs. wavelength (nm) spectra of samples obtained from competition dialysis of Azacyanine-6-chloro (2nd replicate).

Table 5. Competition dialysis results of Azacyanine-6-chloro.

Nucleic Acid Structures	C_b			
	1st replicate	2nd replicate	Average	Standard Deviation
Pu22	1.224	1.252	1.238	0.020
BCL-2	1.045	1.043	1.044	0.001
VEGF	0.739	0.842	0.790	0.073
C-myc	0.615	0.683	0.649	0.048
Kras	0.320	0.397	0.359	0.055
Her-2	0.055	0.070	0.063	0.010
RB	0.213	0.256	0.235	0.030
Poly(A)	-0.010	-0.004	-0.007	0.004
Poly(U)	-0.009	-0.003	-0.006	0.004
DDD	-0.002	-0.004	-0.003	0.002
Poly(A):Poly(U)	-0.004	-0.003	-0.004	0.001
Poly(dA):Poly(dT)	-0.002	0.004	0.001	0.004
Tank	0.005	0.000	0.002	0.003
Buffer	0.000	0.000	0.000	0.000

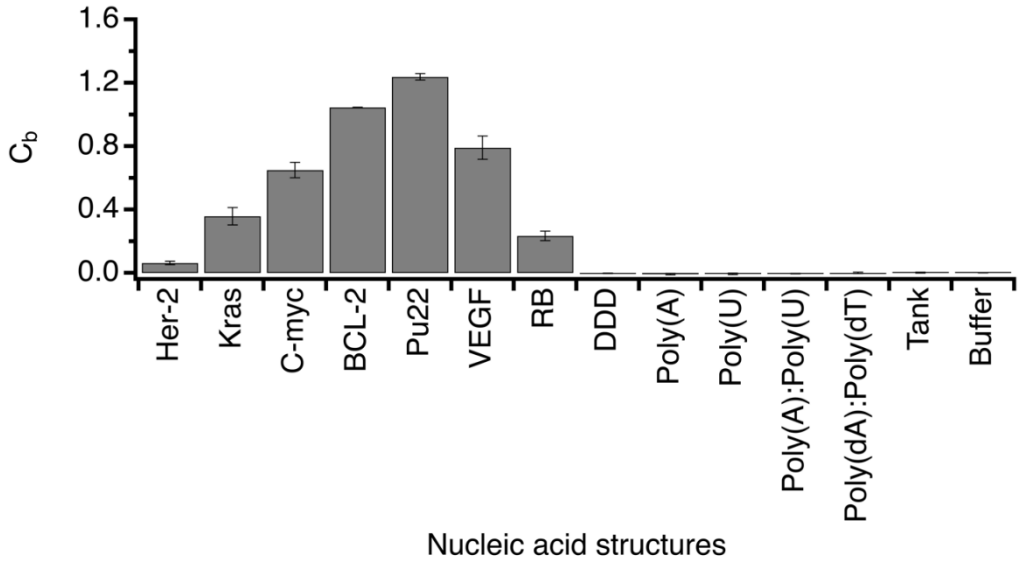

Figure 16. Average of C_b values obtained from the competition dialysis of Azacyanine-6-chloro.

Competition dialysis experiments results indicate the preferential binding of all three Azacyanines to G-quadruplex structures. Our results clearly point to the selective binding of Azacyanine-6-methyl, Azacyanine-6-fluoro and Azacyanine-6-chloro to G4 nucleic acid structures, especially to Pu22. Compared to other G4 structures, their affinity to Kras, Her-2 and RB are lower. Yet, their affinities to these structures were still higher than their affinity to double-stranded DNA, single and double-stranded RNA structures. The obtained C_b values for these nucleic acids were relatively low compared to C_b values obtained for G4 structures.

2.2.4 Investigating interactions of Azacyanines via UV-vis, Fluorescence and Circular Dichroism Spectroscopy

UV-vis spectroscopy is a widely used method for determination of interactions between DNA and small molecules. Generally, the binding of small molecules to DNA results in a change in the absorption spectra of either DNA, small molecule or both. That change in absorption indicates the presence of interactions between the small molecule and DNA. Circular Dichroism (CD) spectroscopy is another

commonly used technique for determining the secondary structure of nucleic acids and their interactions with small molecules or other biomolecules [107]. To see if the presence of Azacyanines caused any structural changes in the G4 structure, CD spectra of samples were measured.

According to competition dialysis experiments, Azacyanine-6-methyl, Azacyanine-6-fluoro and Azacyanine-6-chloro have relatively high affinity towards Pu22. So, samples in a 1:1 (Pu22:Azacyanine) concentration ratio were prepared, and their UV-vis, fluorescence and CD spectra were collected (Figure 17,18 and 19). At around 387 nm, the absorbance of Azacyanine-6-fluoro and Azacyanine-6-fluoro:Pu22 sample was nearly identical, with only a slight bathochromic shift. In that region, the absorbance of Azacyanine-6-chloro:Pu22 sample is observed to be slightly higher than the absorbance of Azacyanine-6-chloro and again, a slight bathochromic shift is observed. For Azacyanine-6-methyl, a slight bathochromic shift is also observed, and at 392 nm. The absorbance of Azacyanine-6-methyl is observed to be slightly higher than the absorbance of Azacyanine-6-methyl: Pu22 sample. Previously, similar affects were observed upon binding of Azacyanines to Tel24 and PolyA [56,57].

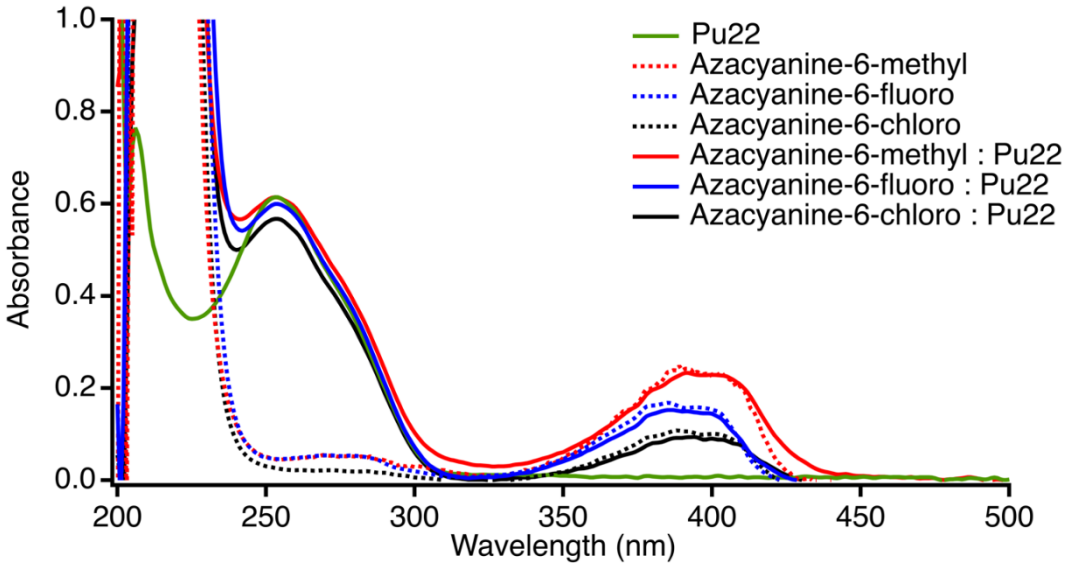

Figure 17. UV-vis spectra of synthesized Azacyanines and Pu22. The concentration of all the samples is 10.0 μM. Azacyanine: Pu22 samples prepared in 1:1 ratio.

Even though the slight changes in the absorption spectra might indicate the binding of Azacyanines to Pu22 nucleic acid structure, we aimed to further investigate the interactions between Pu22 and synthesized Azacyanines using UV-vis thermal denaturation experiments. However, Azacyanines were found to be decomposing at temperatures above 50 ºC.

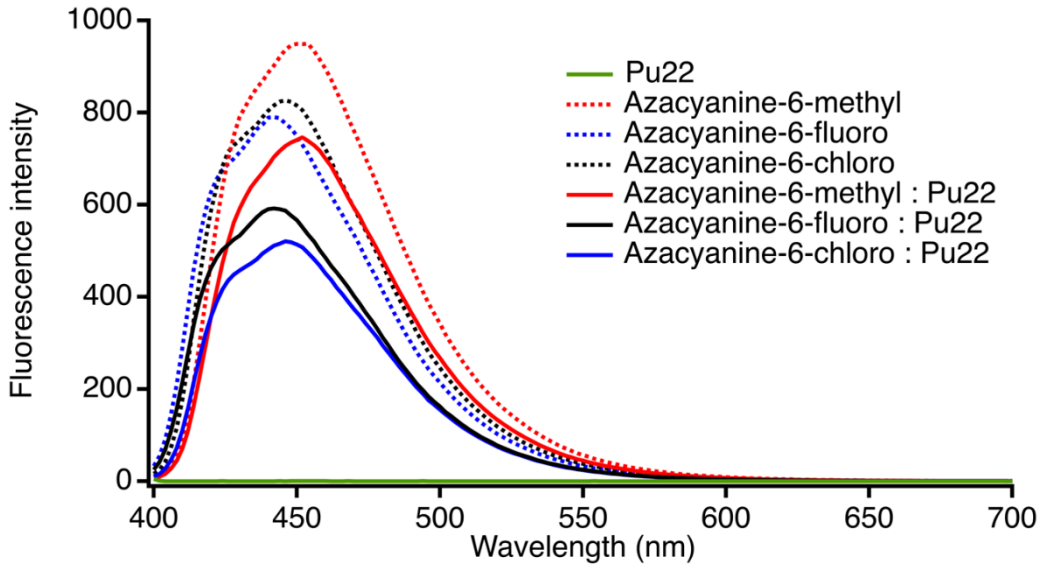

Figure 18. Fluorescence spectra of synthesized Azacyanines and Pu22. The concentration of all the samples is 10.0 µM. Azacyanine: Pu22 samples prepared in 1:1 ratio.

Fluorescence spectra of the samples (Figure 18) indicates that the fluorescence intensity of Azacyanines were decreased in the presence of Pu22 confirming the presence of interactions between Pu22 and Azacyanines.

The CD spectra of Pu22 in the presence and absence of Azacyanines were also collected. Azacyanines are achiral molecules and they do not give any CD bands. Due to the asymmetric backbone, chiral nucleic acids give rise to CD bands [108]. Characteristics of CD spectra depend on the sequence and helical structure of nucleic acids [107]. Parallel G-quadruplexes have a characteristic positive peak around 260 nm and a negative peak at around 240 nm. In addition, antiparallel G-quadruplexes have a positive peak around 290 nm. [109]. Hybrid type of G4 structures have a positive peak around 290 nm with a shoulder peak at 260 nm and at around 240 nm

negative band is observed [110–112]. Figure 19 shows that Pu22 has a characteristic negative band around 240 nm and positive peaks around 260 and 290 nm. This indicates that Pu22 has a hybrid structure. The addition of Azacyanine-6-fluoro and Azacyanine-6-chloro to Pu22 samples slightly increase the intensity of the CD peak at around 240 nm. The addition of Azacyanine-6-methyl to Pu22 sample increased the intensity of the peak at around 240 nm more than Azacyanine-6-fluoro or Azacyanine-6-chloro.This result might be indicating that there is a slight interaction between Pu22 and Azacyanines. In addition, this result in an agreement with our competition dialysis that the Azacyanine-6-methyl has higher affinity toward Pu22 compared to other molecules.

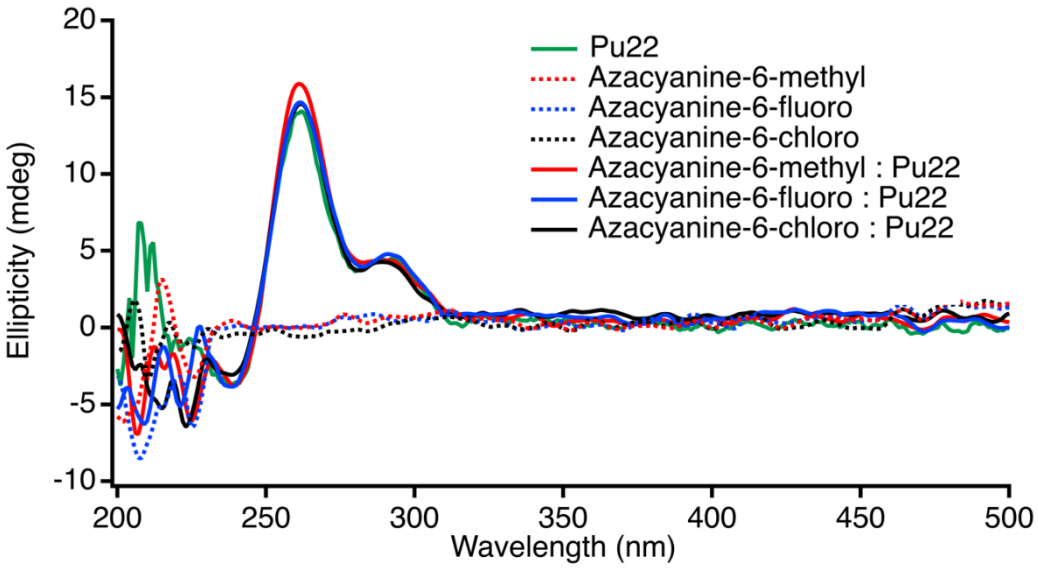

Figure 19. CD spectra of synthesized Azacyanines and Pu22. The concentration of Pu22 in all the samples is 10.0 μM. Azacyanine: Pu22 samples prepared in 1:1 ratio.

CHAPTER 3

DEVELOPMENT OF FLUORESCENCE PLATFORM BASED ON G-QUADRUPLEX AND THIOFLAVIN T INTERACTIONS FOR THE DETECTION OF HYDROXYCHLOROQUINE

3.1 Materials and methods

3.1.1 Chemicals and instrumentation

Thioflavin T (ThT, $C_{17}H_{19}ClN_2S$), human serum, potassium chloride (KCl), dipotassium hydrogen phosphate (K_2HPO_4), potassium dihydrogen phosphate (KH_2PO_4), sodium chloride (NaCl), methanol (≥99.8%), 2,2′-biquinoline ($C_{18}H_{12}N_2$) and human serum were obtained from Sigma-Aldrich (St. Louis, USA). Ethanol (≥99.9%), calcium chloride ($CaCl_2$), urea (H_4N_2O) and 8-hydroxyquinoline (C_9H_7NO) were purchased from Merck (Darmstadt, Germany). Quinoline (C_9H_7N) was purchased from Acros Organics (Geel, Belgium). Thiourea (CH_4N_2S) was purchased from Carlo Erba Reagents (Milan, Italy). Acetylsalicylic acid ($C_8H_8O_4$) was purchased from Fischer Scientific (Waltham, USA). Drugs used in selectivity studies, including Hydroxychloroquine sulfate (HCQ, $C_{18}H_{28}ClN_3O_5S$), Azithromycin ($C_{38}H_{72}N_2O_{12}$), Lopinavir ($C_{37}H_{48}N_4O_5$), Ritonavir ($C_{37}H_{48}N_6O_5S_2$), Favipiravir ($C_5H_4FN_3O_2$), Ivermectin ($C_{47}H_{72}O_{14}$), were obtained from World Medicine (İstanbul, Turkey). Tel24 G4 used in this study was supplied by Integrated DNA Technologies (IDT; Leuven, Belgium). Human urine samples were obtained from METU Medical Center. All the solvents were of analytical grade and used without further purification. Millipore water (Milli-Q, 18.2 MΩ cm^{-1}) was used to prepare the samples and buffer solutions.

Fluorescence emission spectra were collected using a Cary Eclipse fluorescence spectrophotometer (Santa Clara, CA, USA) using 10 mm quartz cells (3.5 mL, 111-

QS, Hellma). A Cary spectrophotometer (Santa Clara, CA, USA) equipped with a Peltier-type temperature control system was used to record the absorption spectra of the samples using a 10 mm quartz cell.

3.1.2 Sample preparation

ThT and HCQ (1500.0 μM and 30.0 μM respectively) stock solutions were prepared in Millipore water, and their concentrations were calculated using UV-vis spectroscopy (ε_{412}=31,600 M^{-1} cm^{-1} and ε_{329}=17,000 M^{-1} cm^{-1}, respectively).

Stock solutions of ligands (30.0 μM) used in selectivity studies were prepared in ethanol except for ivermectin, urea and thiourea. Urea and thiourea stock solutions were prepared in Millipore water, whereas ivermectin stock solution was prepared in methanol.

Tel24 G4 used in this study was prepared in 25 mM K-Phosphate buffer containing 70 mM KCl (pH = 7.0). Preparation of K-Phosphate buffer and KCl is given in Appendix C. Prepared samples were annealed as reported in section 1.4. The concentration of the Tel24 was calculated using UV–vis absorbance and the molar extinction coefficient listed in Appendix B.

3.1.3 Procedure for fluorometric detection of HCQ

For the fluorometric detection of HCQ, ThT and Tel24 were mixed into water (final concentrations 0.6 μM and 0.8 μM, respectively) to a total volume of 2500 μL. The mixture was vortex-mixed and let sit for 5 minutes. The fluorescence intensity of the sample was measured after the waiting period of 5 minutes. Subsequently, different volumes of HCQ (30.0 μM) were added to the ThT-Tel24 mixture and vortex-mixed and let sit for 5 minutes before the fluorescence measurements. The parameters for the fluorescence measurements were: Emission spectra collected from 430 to 700

nm, excitation wavelength 425 nm, excitation and emission slits: 5.0 nm and 5.0 nm, operation at 765 V and scan rate 12,000 nm/min.

The response time of the probe was monitored in 60 minutes time interval after the addition of HCQ (final concentration 3.20 μM). The selectivity of the proposed fluorescent probe towards different ligands was investigated via recording the emission spectra of the probe at 30.0 μM concentration of the ligand. And, to determine the sensitivity of the proposed probe, fluorescence titration experiments were performed (HCQ concentration: 0.24 μM -5.17 μM).

All the experiments were performed at room temperature in triplicate. The average value of the calibration plots [plots of F_0/F versus concentration of HCQ] was used to evaluate the quantitative characteristics of the probe. The comparison of the fluorescence intensity at 486 nm (F_0/F; F_0: the fluorescence intensity in the absence of the added analyte; F: the fluorescence intensity in the presence of different concentrations of the added HCQ) was used to assess the optimization, selectivity and sensitivity of the probe.

3.1.4 Sample preparation for real sample analysis

To investigate the applicability of the proposed fluorescent probe, human urine samples obtained from healthy volunteers were used. All samples were filtered through 0.45 μM filters and centrifuged at 7000 rpm for 20 minutes. After that, HCQ (final concentrations: between 0.70 μM and 5.20 μM) was spiked into urine samples. The samples were diluted 50 times with water before the fluorescence measurements.

To further investigate the applicability of the probe in various matrices, a human serum sample was also spiked with three different concentrations of HCQ. For each sample, 50.0 μL serum was mixed with a known concentration of HCQ. Proteins were precipitated by adding 100.0 μL MeOH followed by centrifugation at 6000 rcf for 5 minutes. The supernatant obtained was diluted 150 times with water before the fluorescence measurements.

3.1.5 UV-vis thermal denaturation experiments

3.0 μM Tel24 samples were prepared and annealed as described previously for UV–vis thermal denaturation experiments. To prepare, 1:0:0, 0:1:0, 0:0:1, 1:1:0, 1:0:1, 1:0:5, 0:1:1, 0:1:5, 1:1:1, 1:1:5 (Tel24:ThT:HCQ) equimolar ratio samples, appropriate amounts of ThT and HCQ were added to annealed Tel24 samples. All the samples were mixed and centrifuged. The UV–vis thermal denaturation experiments were performed by varying the temperature between 15 °C and 95 °C with 2 °C/min increments.

3.1.6 Circular Dichroism studies

Samples prepared previously for UV-vis thermal denaturation studies were used in CD studies. All the CD spectra were collected between 200-550 nm at 15 ºC at 100nm/min scanning speed with 1.00 nm bandwidth.

3.2 Results and discussions

3.2.1 Fluorescence detection of HCQ

A fluorescence detection platform for HCQ was developed usingTel24 G4 structure and ThT.

ThT is a light probe that is known to be interacting selectively with G4 structures [76]. Figure 20 shows the fluorescence response of the probe upon addition of each sensing element. Tel24, ThT and HCQ have no fluorescence when alone in solution. Mixing Tel24 with ThT causes a significant fluorescence enhancement (blue line). After the addition of HCQ to the Tel24 + ThT mixture, the fluorescence was quenched (black line). Increasing the HCQ concentration further enhances the quenching (black dashed line). Figure 21 demonstrates the proposed sensing mechanism of the probe.

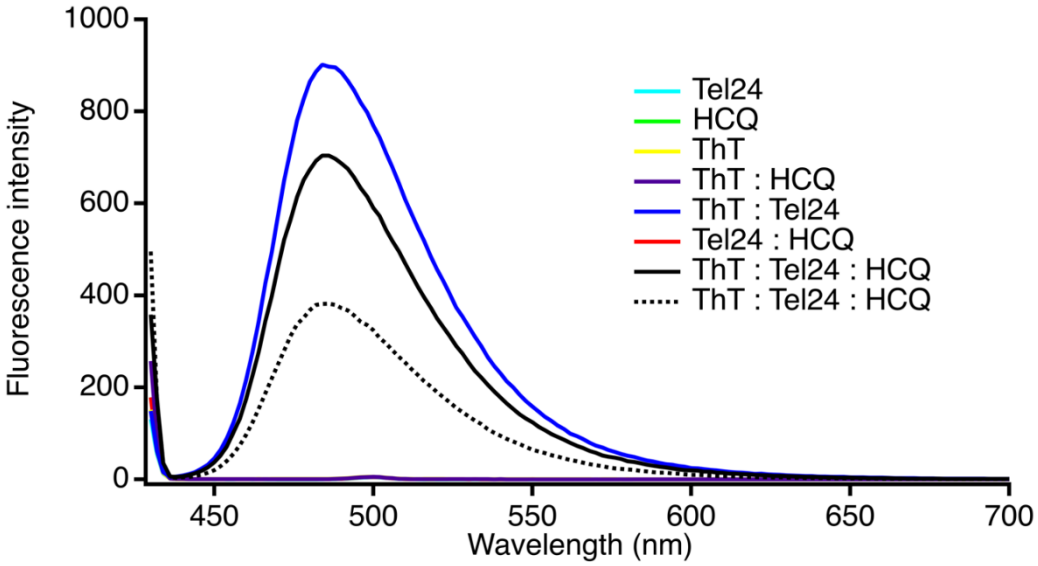

Figure 20. Fluorescence intensity vs. wavelength (nm) graph of each sensing element of the probe. Tel24: 0.80 µM, ThT: 0.60 µM, HCQ: 0.70 µM. Only in the ThT : Tel24 : HCQ sample, HCQ concentration was 3.20 µM (black dashed line) instead of 0.70 µM.

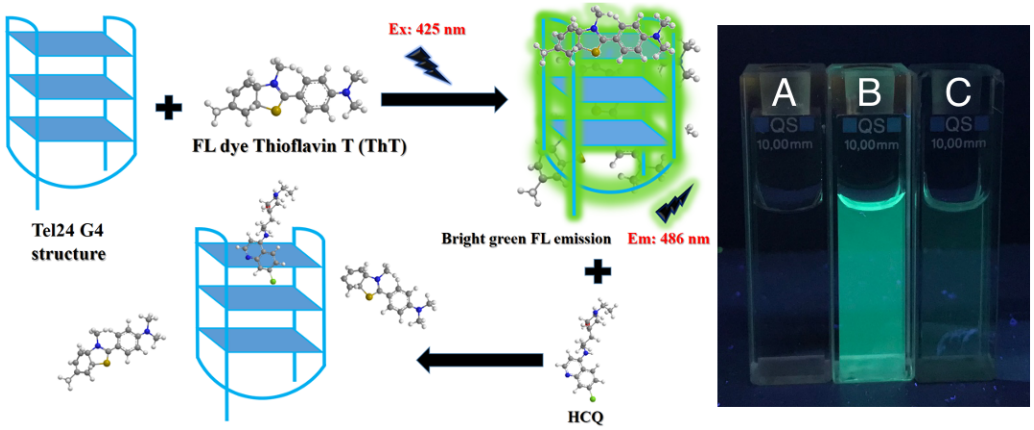

Figure 21. The proposed sensing mechanism for the detection of HCQ and digital photograph of (A) Tel24 (B) Tel24 + ThT and (C) Tel24 + ThT + HCQ under 365 nm UV lamp.

As mentioned, ThT selectively interacts with G4 structures. To investigate the effect of different G4 structures, Tel24, C-myc, BCL-2 and Kras G4 structures were investigated. In figure 22, the fluorescence response of the probe with different G4 structures in the presence and absence of the HCQ is shown. As can be seen, Tel24 has enhanced the fluorescence of ThT the most compared to other G4s, and HCQ

quenched the fluorescence the most in the presence of Tel24. Hence, Tel24 was selected as the nucleic acid platform for the fluorescence detection of HCQ.

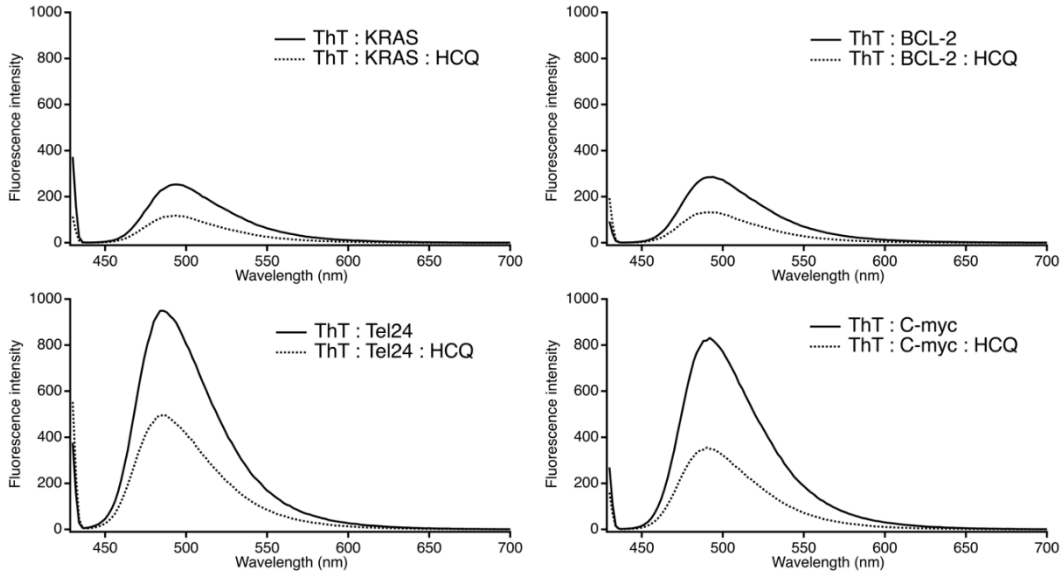

Figure 22. Fluorescence intensity vs. wavelength (nm) graph of G4s+ThT in the absence and in the presence of HCQ (3.20 µM).

3.2.2 Optimization and characterization of the detection platform

3.2.2.1 Optimization of the concentration for Tel24 and ThT

In order to obtain a highly responsive system, samples with different concentration ratios of G4:ThT were prepared and tested for their ability to respond to a specific amount of HCQ. Figure 23 shows the effect of Tel 24 concentration and ThT in the presence and absence of HCQ. As a result of these studies, 0.80 µM Tel24:0.60 µM ThT concentration ratio was selected as the platform to be used in further studies due to the relatively high initial increase in fluorescence upon addition of Tel24 to ThT, followed by the relatively good quenching of the fluorescence upon addition of HCQ.

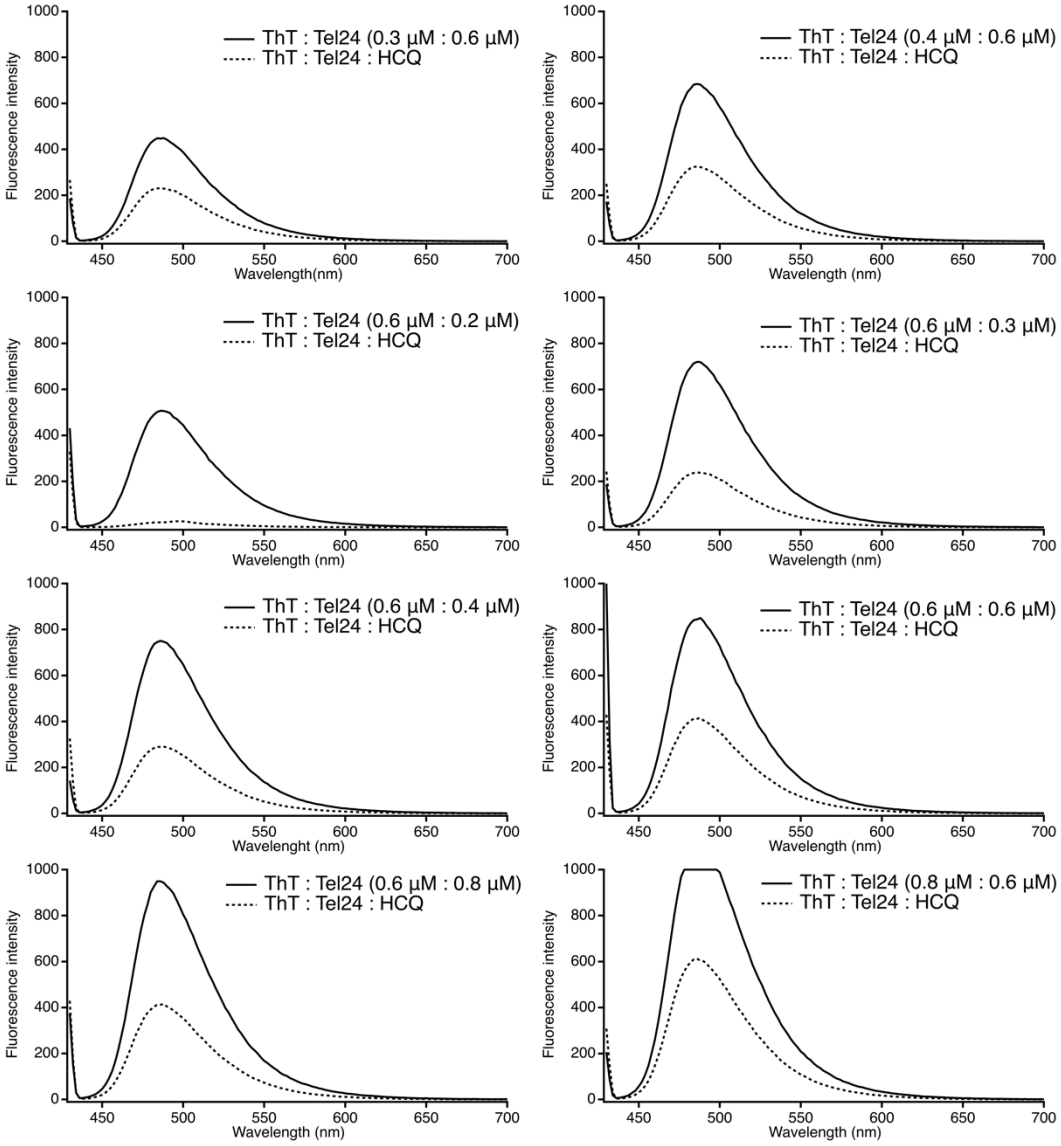

Figure 23. Fluorescence intensity vs. wavelength (nm) graph of Tel24 + ThT and responses after addition of HCQ (3.20 μM).

3.2.2.2 Response time of the probe

The response time of the probe to detect HCQ was measured in a 1-hour time interval. Figure 24 shows the fluorescence intensity vs. wavelength (nm) graph, and Figure 25 shows the F_0/F vs. time (min.) graph. As can be observed from both figures 24 and 25, the probe responded to HCQ in less than 5 minutes and the fluorescence

intensity didn't change afterwards within time. Consequently, 5 minutes was selected as the time interval to be used in further studies.

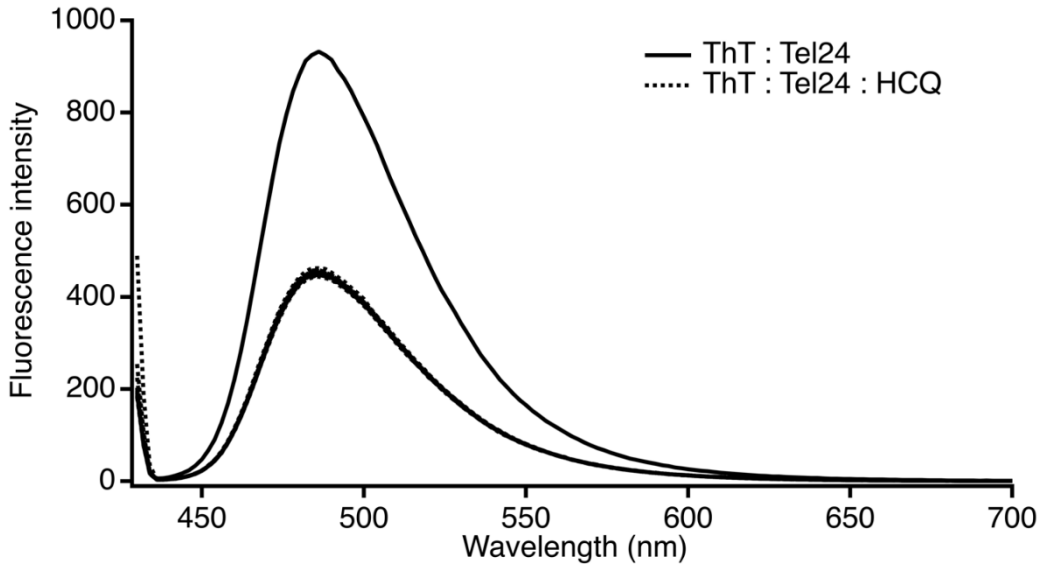

Figure 24. Fluorescence intensity vs. wavelength (nm) graph to determine the fluorescence response upon addition of HCQ to Tel24 + ThT mixture. The final concentration of HCQ is 3.20 μM.

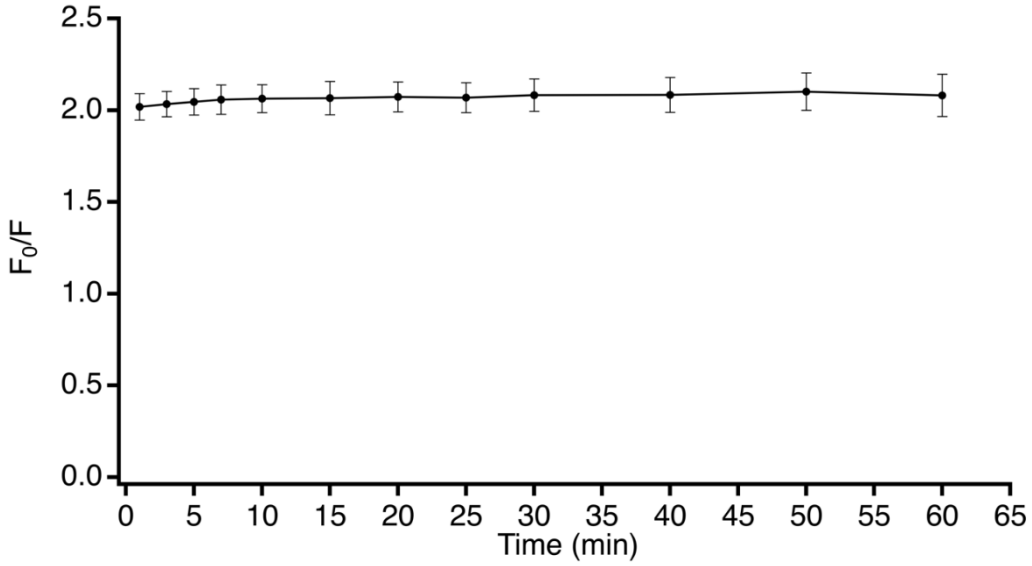

Figure 25. F_0/F vs. time (min.) graph of fluorescence response upon addition of HCQ to Tel24 + ThT mixture.

3.2.2.3 UV-vis, CD spectroscopy and thermal denaturation studies

Our detection platform was further investigated via UV-vis spectroscopy and UV-vis thermal denaturation studies. UV-vis spectroscopy is a widely used method for determining the interactions between DNA and small molecules. Moreover, thermal denaturation studies are generally used to investigate the effect of small molecules on DNA stability. If a small molecule stabilizes the DNA structure, the thermal denaturation temperature of that structure increases, meaning that it becomes more difficult to denature that DNA structure in the presence of the small molecule. Here, our aim was to determine the interactions between Tel24, ThT and HCQ and to investigate the effect of HCQ and ThT on Tel24 stability.

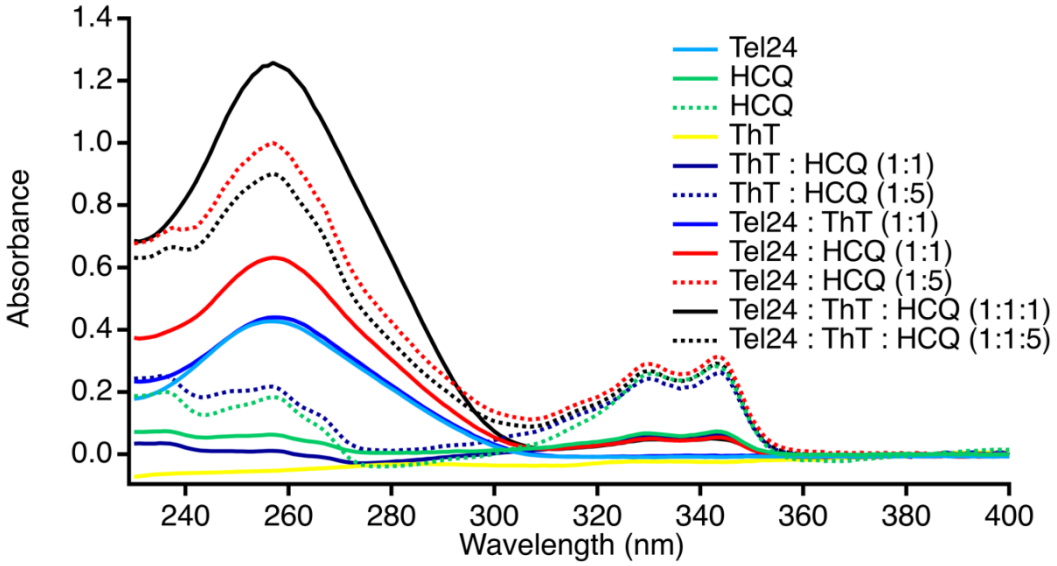

Figure 26. UV-vis absorption spectra of samples containing Tel24 (3.0 µM), ThT (3.0 µM) and/or HCQ (3.0 µM or 15.0 µM; dashed lines indicate the samples containing 15.0 µM HCQ and solid lines indicate the samples containing 3.0 µM HCQ).

When UV-vis spectra were analyzed, no significant change was observed in the spectrum of HCQ in the longer wavelength region in the presence of Tel24 or ThT. The observed changes in the spectrum were slight, plausibly only indicating the nonspecific interactions.

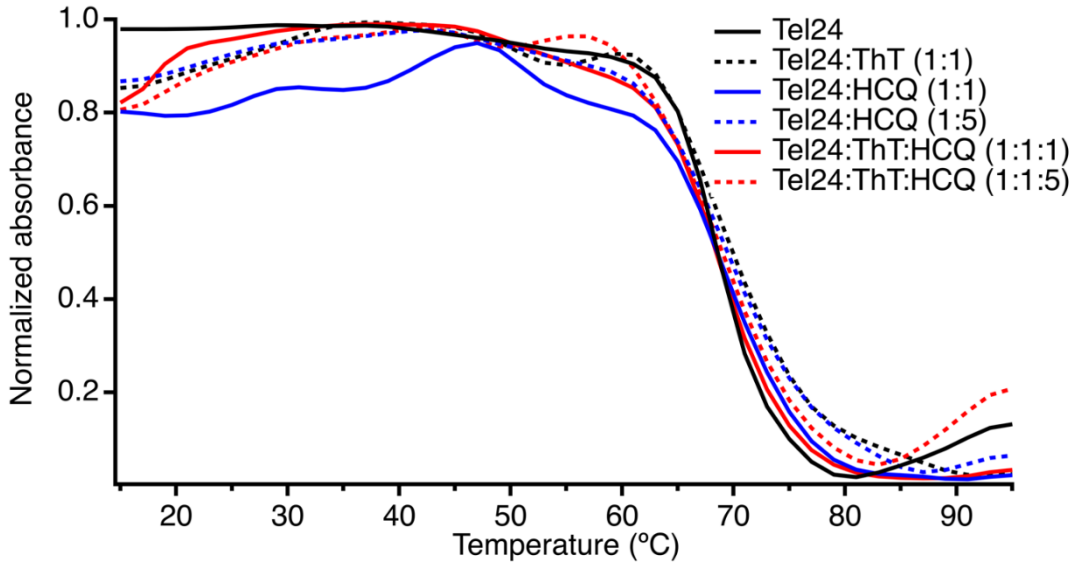

Figure 27. UV-vis thermal denaturation profiles.

Thermal denatures profiles for Tel24 in the presence and absence of ThT and/or HCQ were also obtained (Figure 27) by monitoring the change in UV-vis absorbance at 295 nm. The UV-vis absorbance spectra for each sample at 15 °C and graphs 95 °C are given in Appendix E. During the UV-vis thermal denaturation studies, increasing the temperature from 15 °C to 90 °C resulted in the unfolding of Tel24 G4 structure as indicated by the change in absorbance at 295 nm. It is common to monitor the structural changes in the G4s by monitoring the change in absorbance at 295 nm [113]. As shown in figure 27, ThT and HCQ have only a slight effect on the melting temperature of Tel24. Tel 24 has a melting temperature of 67 ºC. The addition of ThT and HCQ shift the melting curve slightly to the right, increasing the thermal denaturation temperature to 69 ºC for Tel24 + ThT and Tel24 + ThT +HCQ. One should not neglect the fact that such a change may not be significant and be in the experimental error range.

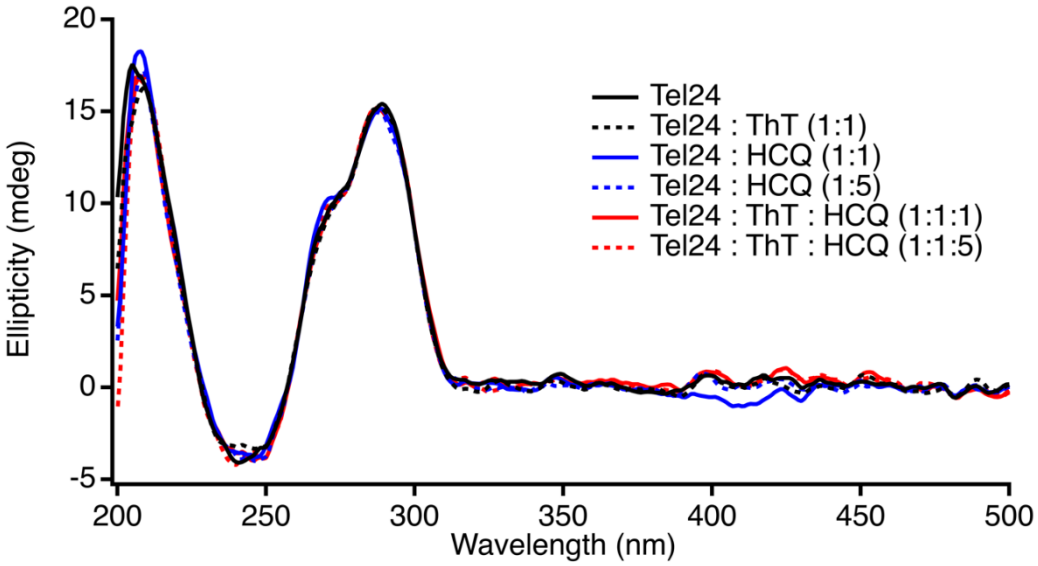

Figure 28. CD spectra of sensing elements.

Finally, CD spectra were also collected for further characterization of Tel24, Tht and HCQ interactions (Figure 28). Tel24 G4 structure has a negative band around 240 nm and a positive peak around 290 nm with a shoulder around 270 nm. ThT and HCQ do not cause any conformational change upon interacting with Tel24, the obtained spectra were almost identical. These results reassure that G4 structure does not affected from ThT and HCQ. Overall, even though there were slight changes in the UV-vis spectra and thermal denaturation temperatures, the presence of interactions between Tel24, ThT and HCQ were not apparent from UV-vis and CD experiments.

3.2.3 Selectivity studies

Next, the selectivity of the probe to HCQ was investigated. The selectivity studies included drugs (Azithromycin, Lopinavir, Ritonavir, Ivermectin, Favipiravir, Asetylsalicylic acid), ions (Na^+, K^+, Ca^{2+}), molecules found in urine (urea, creatinine) and quinoline derivatives (quinoline, biquinoline, 8-hydroxyquinoline). To screen selectivity, equal concentrations of each molecule were added to Tel24 + ThT mixture. F_0/F obtained for each ligand is displayed in Figure 29. The most

significant response of the probe was obtained for HCQ. A mixture of all drugs, including also HCQ, showed a response very similar to HCQ sample. The probe did not respond to the mixture of drugs without HCQ. These results indicate that our probe is effective in use for screening HCQ.

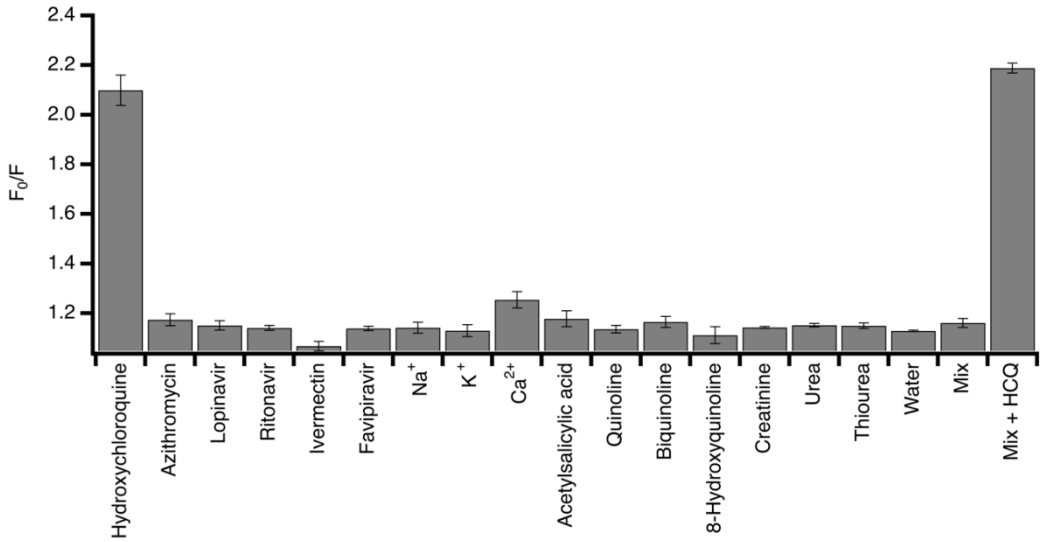

Figure 29. F_0/F vs. ligands graph for the selectivity studies. The final concentration of each ligand is 3.20 µM.

3.2.4 Sensitivity studies

Next, the sensitivity of the probe to HCQ was explored. The sensitivity studies were performed by titrating the Tel24 + ThT solution with HCQ. Upon gradual addition of HCQ, a decrease in fluorescence was observed, as can be seen in Figure 30. Figure 31 displays F_0/F vs. [HCQ], where F_0 represents the fluorescence intensity in the absence of HCQ and F represents the fluorescence intensity when HCQ was added to the system at 486 nm. The calibration plot was constructed between 0.24 and 5.17 µM HCQ concentration. As shown in Figure 31, the linearity equation was found to be $F_0/F = 0.5777C + 0.7941$ (R^2=0.9971). In addition, the LOD value of the probe was calculated to be 0.116 µM using the relation $LOD = 3.3 \times (S_b/a)$ where "S_b" is the standard error of the intercept and "a" is the slope of the calibration curve.

Overall, these results indicate the effectiveness of the probe for the quantitative analysis of HCQ.

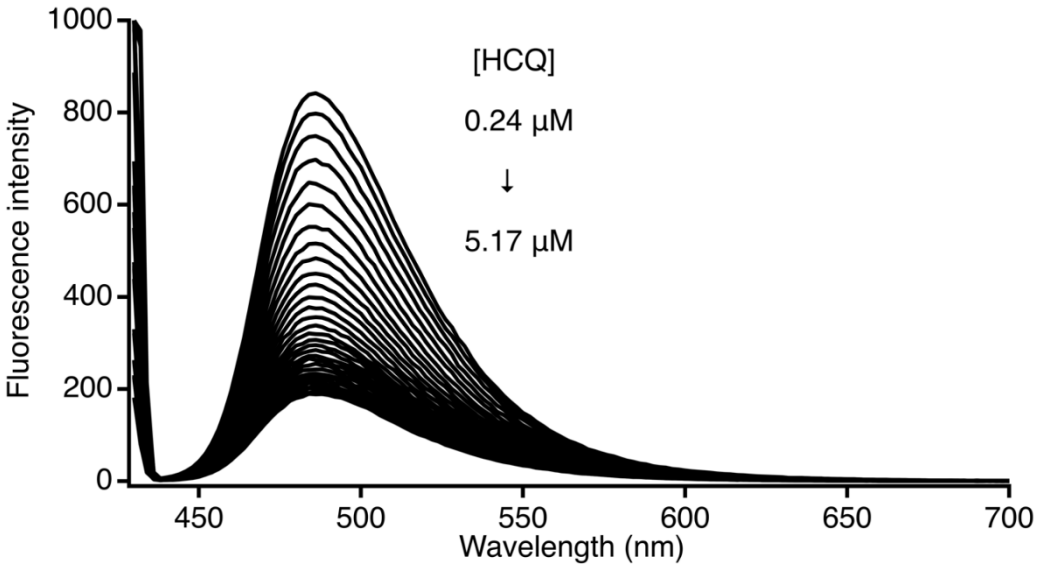

Figure 30. Fluorescence titration profile of the proposed probe with increasing concentration of HCQ.

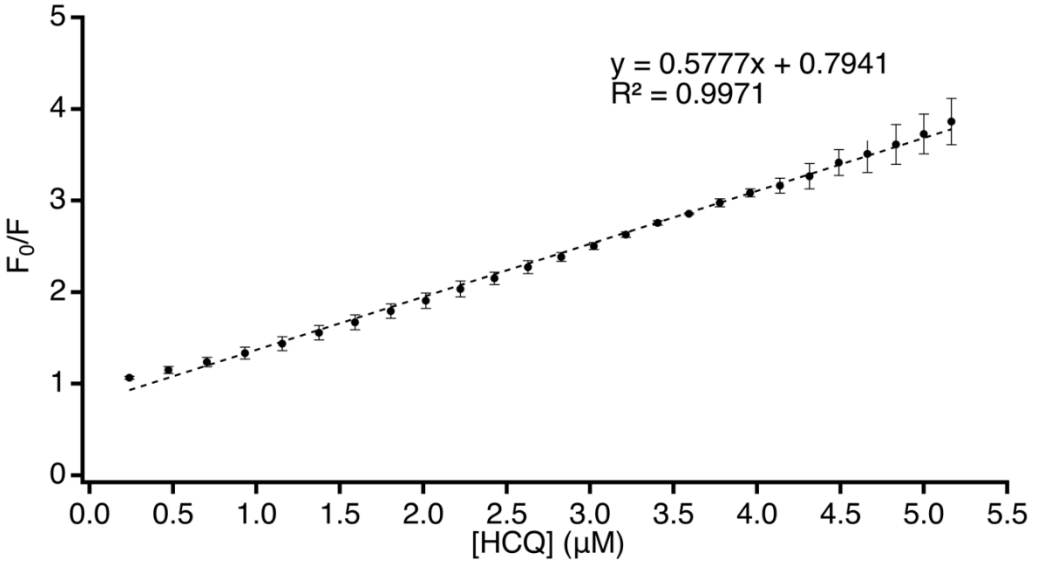

Figure 31. The linear range of the F_0/F at 486 nm vs. [HCQ] (µM) with linear regression fit equation.

3.2.5 Real sample studies

Since the proposed probe was found to be selective and sensitive towards HCQ, we predicted it to be useful for the detection of HCQ also in various matrices, including human urine and serum samples. The applicability and feasibility of the proposed probe in real samples were evaluated by spiking the samples with HCQ. The results are summarized in Table 6. The obtained average recoveries for HCQ were in the range of 75.43 to 110.2 % for urine samples and 62.58 to 83.78 % for human serum samples, demonstrating the suitability of the probe for the detection of HCQ in various matrices. As summarized in Table 6, relative standard deviation (RSD) % values were all below 10%.

Table 6. Analytical results for the determination of HCQ in real samples using the proposed probe.

Sample	Spiked concentration (µM; n = 3[a])	Mean found concentration (µM)	RSD (%)	Recovery (%)[b]
Urine Sample 1	0.70	0.77	1.84	110.20
	2.83	2.24	3.08	79.11
	5.17	3.90	1.54	75.43
Urine Sample 2	0.70	0.76	1.08	108.39
	2.83	2.51	1.17	88.70
	5.17	4.24	1.25	82.07
Urine Sample 3	0.70	0.61	2.04	86.91
	2.83	2.28	6.06	80.70
	5.17	4.09	2.68	79.19
Serum Sample	0.70	0.59	0.93	83.75
	2.83	1.77	0.59	62.58
	5.17	3.39	0.85	65.61

[a] Number of replicates

[b] Recovery (%) = 100 x found value / nominal value.

CHAPTER 4

THESIS CONCLUSION

4.1 Synthesis of Azacyanines and assestment of their selectivity towards different nucleic acıd structures

This study aimed to synthesize new Azacyanine derivatives which potentially be chemotherapeutic agents as DNA binding small molecules. Azacyanine-6-methyl, Azacyanine-6-fluoro and Azacyanine-6-chloro were synthesized through a simple one-step method with yield of 45%, 34% and 60% respectively. They have all the maximum emissions between 447 nm and 458 nm and their quantum yields were calculated as 47.5,13.4 and 17.7, respectively. To investigate the selectivity of synthesized Azacyanines towards different nucleic acid structures, competition dialysis experiments were performed and competition dialysis experiments results indicate the preferential binding of all three Azacyanines to G-quadruplex structures especially to Pu22. UV-vis and CD studies indicate the presence of interactions especially between Pu22 and Azacyanine-6-methyl. These results in an agreement with our competition dialysis that the Azacyanine-6-floro and Azacyanine-6-chloro have lower affinity toward Pu22 compared to Azacyanine-6-methyl.

4.2 Development of fluorescence platform based on G-quadruplex and thioflavin t interactions for the detection of hydroxychloroquıne

A fluorescent detection method for Hydroxychloroquine (HCQ) based on the interactions between Tel24 G4 structure and Thioflavin T was developed within the scope of this study. Tel24, ThT and HCQ have no fluorescence when alone in solution. Mixing Tel24 with ThT causes a significant fluorescence enhancement and increasing the concentration of HCQ lowers the fluorescence intensity. Tel24 was

selected due to the higher enhancement of the fluorescence of ThT compared to other G4s, and HCQ quenched the fluorescence the most in the presence of Tel24. The probe responded to HCQ in less than 5 minutes and the fluorescence intensity did not change afterwards within time. To determine the interactions between Tel24, ThT and HCQ and to investigate the effect of HCQ and ThT on Tel24 stability UV-vis, CD and fluorescence studies were performed. The observed changes in the spectra were slight, plausibly only indicating the nonspecific interactions and these results reassure that G4 structure does not affected from ThT and HCQ. Even though there were slight changes in the UV-vis spectra and thermal denaturation temperatures, the presence of interactions between Tel24, ThT and HCQ were not apparent from UV-vis and CD experiments. The probe did not respond to noticeablyto the mixture of drugs without HCQ. These results indicate that our probe was effective in use for HCQ screening. LOD value of the probe was calculated to be 0.116 μM. Overall, these results indicate the effectiveness of the probe for the quantitative analysis of HCQ. The applicability and feasibility of the proposed probe in real samples were evaluated by spiking the urine and human serum samples with HCQ. The obtained average recoveries for HCQ were in the range of 75.43 to 110.2 % for urine samples and 62.58 to 83.78 % for human serum samples, demonstrating the suitability of the probe for the detection of HCQ in human serum and urine.

Overall, the studies performed within the contex of this thesis demonstrate the versability of the interactions of G4 nucleic acid structures with small molecules.

REFERENCES

[1] J. Šponer, A. Mládek, J.E. Šponer, D. Svozil, M. Zgarbová, P. Banáš, P. Jurečka, M. Otyepka, The DNA and RNA sugar–phosphate backbone emerges as the key player. An overview of quantum-chemical, structural biology and simulation studies, Physical Chemistry Chemical Physics. 14 (2012) 15257–15277.

[2] G. Ghosal, K. Muniyappa, Hoogsteen base-pairing revisited: resolving a role in normal biological processes and human diseases, Biochemical and Biophysical Research Communications. 343 (2006) 1–7.

[3] A. Travers, G. Muskhelishvili, DNA structure and function, The FEBS Journal. 282 (2015) 2279–2295.

[4] S. Neidle, Human telomeric G-quadruplex: The current status of telomeric G-quadruplexes as therapeutic targets in human cancer, The FEBS Journal. 277 (2010) 1118–1125.

[5] M.W. Germann, H.J. Vogel, R.T. Pon, J.H. van de Sande, Characterization of a parallel stranded DNA hairpin, Biochemistry. 28 (1989) 6220–6228.

[6] M.I. Wallace, L. Ying, S. Balasubramanian, D. Klenerman, FRET fluctuation spectroscopy: exploring the conformational dynamics of a DNA hairpin loop, The Journal of Physical Chemistry B. 104 (2000) 11551–11555.

[7] S. Rhee, Z. Han, K. Liu, H.T. Miles, D.R. Davies, Structure of a Triple Helical DNA with a Triplex− Duplex Junction, Biochemistry. 38 (1999) 16810–16815.

[8] A. Jain, G. Wang, K.M. Vasquez, DNA triple helices: biological consequences and therapeutic potential, Biochimie. 90 (2008) 1117–1130.

[9] H.J. Lipps, D. Rhodes, G-quadruplex structures: in vivo evidence and function, Trends in Cell Biology. 19 (2009) 414–422.

[10] C.T. McMurray, DNA secondary structure: a common and causative factor for expansion in human disease, Proceedings of the National Academy of Sciences. 96 (1999) 1823–1825.

[11] J.L. Huppert, S. Balasubramanian, G-quadruplexes in promoters throughout the human genome, Nucleic Acids Research. 35 (2007) 406–413.

[12] D. Rhodes, H.J. Lipps, G-quadruplexes and their regulatory roles in biology, Nucleic Acids Research. 43 (2015) 8627–8637.

[13] W.S. Klug, M.R. Cummings, C.A. Spencer, M.A. Palladino, S.M. Ward, Concepts of genetics, Pearson, 2009.

[14] N.C. Garbett, P.A. Ragazzon, J.B. Chaires, Circular dichroism to determine binding mode and affinity of ligand–DNA interactions, Nature Protocols. 2 (2007) 3166–3172.

[15] S. Neidle, S. Balasubramanian, Quadruplex nucleic acids, Royal Society of Chemistry, 2006.

[16] J.G. Fernández, D.A. Rodríguez, M. Valenzuela, C. Calderon, U. Urzúa, D. Munroe, C. Rosas, D. Lemus, N. Díaz, M.C. Wright, Survivin expression promotes VEGF-induced tumor angiogenesis via PI3K/Akt enhanced β-catenin/Tcf-Lef dependent transcription, Molecular Cancer. 13 (2014) 1–15.

[17] T. Li, J. Hu, F. Gao, X. Du, Y. Chen, Q. Wu, Transcription factors regulate GPR91-mediated expression of VEGF in hypoxia-induced retinopathy, Scientific Reports. 7 (2017) 1–16.

[18] A.M. Granato, O. Nanni, F. Falcini, S. Folli, G. Mosconi, F. de Paola, L. Medri, D. Amadori, A. Volpi, Basic fibroblast growth factor and vascular endothelial growth factor serum levels in breast cancer patients and healthy women: useful as diagnostic tools, Breast Cancer Research. 6 (2003) 1–8.

[19] S. Ławicki, G.E. Będkowska, M. Szmitkowski, VEGF, M-CSF and CA 15-3 as a new tumor marker panel in breast malignancies: a multivariate analysis with ROC curve, Growth Factors. 31 (2013) 98–105.

[20] H.-M. Kim, Genome instability induced by triplex forming mirror repeats in Saccharomyces cerevisiae, Georgia Institute of Technology, 2009.

[21] Y. Chen, D. Yang, Sequence, stability, and structure of G-quadruplexes and their interactions with drugs, Current Protocols in Nucleic Acid Chemistry. 50 (2012) 15–17.

[22] B. Pucci, M. Kasten, A. Giordano, Cell cycle and apoptosis, Neoplasia. 2 (2000) 291–299.

[23] M.L. Bochman, K. Paeschke, V.A. Zakian, DNA secondary structures: stability and function of G-quadruplex structures, Nature Reviews Genetics. 13 (2012) 770–780.

[24] K.W. Yip, J.C. Reed, Bcl-2 family proteins and cancer, Oncogene. 27 (2008) 6398–6406.

[25] D. Henderson, L.H. Hurley, Molecular struggle for transcriptional control, Nature Medicine. 1 (1995) 525–527.

[26] M. Aleksić, V. Kapetanović, An overview of the optical and electrochemical methods for detection of DNA-drug interactions, Acta Chimica Slovenica. 61 (2014) 555–573.

[27] S.U. Rehman, T. Sarwar, M.A. Husain, H.M. Ishqi, M. Tabish, Studying non-covalent drug–DNA interactions, Archives of Biochemistry and Biophysics. 576 (2015) 49–60.

[28] J. Sheng, J. Gan, Z. Huang, Structure-based DNA-targeting strategies with small molecule ligands for drug discovery, Medicinal Research Reviews. 33 (2013) 1119–1173.

[29] H.-K. Liu, P.J. Sadler, Metal complexes as DNA intercalators, Accounts of Chemical Research. 44 (2011) 349–359.

[30] V.G.S. Box, The intercalation of DNA double helices with doxorubicin and nagalomycin, Journal of Molecular Graphics and Modelling. 26 (2007) 14–19.

[31] S.M. Nelson, L.R. Ferguson, W.A. Denny, Non-covalent ligand/DNA interactions: minor groove binding agents, Mutation Research/Fundamental and Molecular Mechanisms of Mutagenesis. 623 (2007) 24–40.

[32] N.N. Degtyareva, B.D. Wallace, A.R. Bryant, K.M. Loo, J.T. Petty, Hydration changes accompanying the binding of minor groove ligands with DNA, Biophysical Journal. 92 (2007) 959–965.

[33] S. Neidle, DNA minor-groove recognition by small molecules, Natural Product Reports. 18 (2001) 291–309.

[34] N. Kosiol, S. Juranek, P. Brossart, A. Heine, K. Paeschke, G-quadruplexes: A promising target for cancer therapy, Molecular Cancer. 20 (2021) 1–18.

[35] A. Siddiqui-Jain, C.L. Grand, D.J. Bearss, L.H. Hurley, Direct evidence for a G-quadruplex in a promoter region and its targeting with a small molecule to repress c-MYC transcription, Proceedings of the National Academy of Sciences. 99 (2002) 11593–11598.

[36] X. Cui, H. Chen, Q. Zhang, M. Xu, G. Yuan, J. Zhou, Exploration of the Structure and Recognition of a G-quadruplex in the her2 Proto-oncogene Promoter and Its Transcriptional Regulation, Scientific Reports. 9 (2019) 1–12.

[37] D.J. Slamon, G.M. Clark, S.G. Wong, W.J. Levin, A. Ullrich, W.L. McGuire, Human breast cancer: correlation of relapse and survival with amplification of the HER-2/neu oncogene, Science. 235 (1987) 177–182.

[38] Y. Dai, Y. Zhang, W. Liao, W. Wang, L. Wu, G-quadruplex specific thioflavin T-based label-free fluorescence aptasensor for rapid detection of tetracycline, Spectrochimica Acta Part A: Molecular and Biomolecular Spectroscopy. 238 (2020) 118406.

[39] S. Cogoi, L.E. Xodo, G-quadruplex formation within the promoter of the KRAS proto-oncogene and its effect on transcription, Nucleic Acids Research. 34 (2006) 2536–2549.

[40] D.M. Miller, S.D. Thomas, A. Islam, D. Muench, K. Sedoris, c-Myc and cancer metabolism, Clinical Cancer Research. 18 (2012) 5546–5553.

[41] D. Sun, W.-J. Liu, K. Guo, J.J. Rusche, S. Ebbinghaus, V. Gokhale, L.H. Hurley, The proximal promoter region of the human vascular endothelial growth factor gene has a G-quadruplex structure that can be targeted by G-quadruplex–interactive agents, Molecular Cancer Therapeutics. 7 (2008) 880–889.

[42] Y. Yao, B. Xu, Y. Zhang, CX-3543 promotes cell apoptosis through Downregulation of CCAT1 in Colon Cancer cells, BioMed Research International. 2018 (2018).

[43] F.X. Han, R.T. Wheelhouse, L.H. Hurley, Interactions of TMPyP4 and TMPyP2 with quadruplex DNA. Structural basis for the differential effects on telomerase inhibition, Journal of the American Chemical Society. 121 (1999) 3561–3570.

[44] M.-Y. Kim, M. Gleason-Guzman, E. Izbicka, D. Nishioka, L.H. Hurley, The different biological effects of telomestatin and TMPyP4 can be attributed to their selectivity for interaction with intramolecular or intermolecular G-quadruplex structures, Cancer Research. 63 (2003) 3247–3256.

[45] Y.-J. Lu, T.-M. Ou, J.-H. Tan, J.-Q. Hou, W.-Y. Shao, D. Peng, N. Sun, X.-D. Wang, W.-B. Wu, X.-Z. Bu, 5-N-methylated quindoline derivatives as telomeric g-quadruplex stabilizing ligands: effects of 5-N positive charge on

quadruplex binding affinity and cell proliferation, Journal of Medicinal Chemistry. 51 (2008) 6381–6392.

[46] T.-M. Ou, Y.-J. Lu, C. Zhang, Z.-S. Huang, X.-D. Wang, J.-H. Tan, Y. Chen, D.-L. Ma, K.-Y. Wong, J.C.-O. Tang, Stabilization of G-quadruplex DNA and down-regulation of oncogene c-myc by quindoline derivatives, Journal of Medicinal Chemistry. 50 (2007) 1465–1474.

[47] M.-Y. Kim, H. Vankayalapati, K. Shin-Ya, K. Wierzba, L.H. Hurley, Telomestatin, a potent telomerase inhibitor that interacts quite specifically with the human telomeric intramolecular G-quadruplex, Journal of the American Chemical Society. 124 (2002) 2098–2099.

[48] D. SUNa, L.H. HURLEY, The Mechanism of Action of Telomestatin, a G-Quadruplex-Interactive Compound, Sequence-Specific DNA Binding Agents. (2007) 207.

[49] M. Demeunynck, Antitumour acridines, Expert Opinion on Therapeutic Patents. 14 (2004) 55–70.

[50] A.M. Burger, F. Dai, C.M. Schultes, A.P. Reszka, M.J. Moore, J.A. Double, S. Neidle, The G-quadruplex-interactive molecule BRACO-19 inhibits tumor growth, consistent with telomere targeting and interference with telomerase function, Cancer Research. 65 (2005) 1489–1496.

[51] F. Berardinelli, M. Tanori, D. Muoio, M. Buccarelli, A. di Masi, S. Leone, L. Ricci-Vitiani, R. Pallini, M. Mancuso, A. Antoccia, G-quadruplex ligand RHPS4 radiosensitizes glioblastoma xenograft in vivo through a differential targeting of bulky differentiated-and stem-cancer cells, Journal of Experimental & Clinical Cancer Research. 38 (2019) 1–17.

[52] K.S. Huang, M.J. Haddadin, M.M. Olmstead, M.J. Kurth, Synthesis and reactions of some heterocyclic azacyanines1, The Journal of Organic Chemistry. 66 (2001) 1310–1315.

[53] M.J. Haddadin, M.J. Kurth, M.M. Olmstead, One-step synthesis of new heterocyclic azacyanines, Tetrahedron Letters. 41 (2000) 5613–5616.

[54] M. Javet, C. Müller, A. Roulin, C. Pasquíer, Colorants comprising cationic azacyanine dyes, (2008).

[55] Y. Kurose, T. Miyazawa, H. Kubo, N. Uchida, S. Furomoto, K. Satake, H. Shoda, Y. Aizawa, Y. Dan-Oh, M. Toki, Optical recording medium and azacyanine dye, (2010).

[56] Ö.P. Çetinkol, N. v Hud, Molecular recognition of poly (A) by small ligands: an alternative method of analysis reveals nanomolar, cooperative and shape-selective binding, Nucleic Acids Research. 37 (2009) 611–621.

[57] Ö. Persil Çetinkol, A.E. Engelhart, R.K. Nanjunda, W.D. Wilson, N. v Hud, Submicromolar, Selective G-Quadruplex Ligands from One Pot: Thermodynamic and Structural Studies of Human Telomeric DNA Binding by Azacyanines, ChemBioChem. 9 (2008) 1889–1892.

[58] S. Tutuncu, S. Guloglu, A. Kucukakdag, O.P. Cetinkol, Selective high binding affinity of azacyanines to polyd (a) polyd (t)· polyd (t) triplex: the effect of chain length and branching on stabilization, selectivity and affinity, ChemistrySelect. 3 (2018) 12878–12887.

[59] A.K. Doğu, Ö.P. Çetinkol, Targeting human telomeric DNA with azacyanines, Turkish Journal of Chemistry. 43 (2019) 1040–1051.

[60] E. Bilgen, M. Forough, Ö.P. Çetinkol, A conjugated gold nanoparticle-azacyanine off-on-off fluorescence probe for sensitive and selective detection of G-quadruplexes, Talanta. 217 (2020) 121076.

[61] L. Guo, D. Nie, C. Qiu, Q. Zheng, H. Wu, P. Ye, Y. Hao, F. Fu, G. Chen, A G-quadruplex based label-free fluorescent biosensor for lead ion, Biosensors and Bioelectronics. 35 (2012) 123–127.

[62] Y.-P. Xing, C. Liu, X.-H. Zhou, H.-C. Shi, Label-free detection of kanamycin based on a G-quadruplex DNA aptamer-based fluorescent intercalator displacement assay, Scientific Reports. 5 (2015) 1–8.

[63] J. Ren, H. Qin, J. Wang, N.W. Luedtke, E. Wang, J. Wang, Label-free detection of nucleic acids by turn-on and turn-off G-quadruplex-mediated fluorescence, Analytical and Bioanalytical Chemistry. 399 (2011) 2763–2770.

[64] T. Li, S. Dong, E. Wang, Label-free colorimetric detection of aqueous mercury ion (Hg2+) using Hg2+-modulated G-quadruplex-based DNAzymes, Analytical Chemistry. 81 (2009) 2144–2149.

[65] X.-H. Zhou, D.-M. Kong, H.-X. Shen, Ag+ and cysteine quantitation based on G-quadruplex− hemin DNAzymes disruption by Ag+, Analytical Chemistry. 82 (2010) 789–793.

[66] H. Qin, J. Ren, J. Wang, E. Wang, G-quadruplex facilitated turn-off fluorescent chemosensor for selective detection of cupric ion, Chemical Communications. 46 (2010) 7385–7387.

[67] L. Lan, R.-L. Wang, L. Liu, L. Cheng, A label-free colorimetric detection of microRNA via G-quadruplex-based signal quenching strategy, Analytica Chimica Acta. 1079 (2019) 207–211.

[68] J. Dong, X. Cui, Y. Deng, Z. Tang, Amplified detection of nucleic acid by G-quadruplex based hybridization chain reaction, Biosensors and Bioelectronics. 38 (2012) 258–263.

[69] H. Yang, Q. Wu, D. Su, Y. Wang, L. Li, X. Zhang, A label-free and turn-on fluorescence strategy for kanamycin detection based on the NMM/G-quadruplex Structure, Analytical Sciences. 33 (2017) 133–135.

[70] H. Yang, H. Cui, L. Wang, L. Yan, Y. Qian, X.E. Zheng, W. Wei, J. Zhao, A label-free G-quadruplex DNA-based fluorescence method for highly

sensitive, direct detection of cisplatin, Sensors and Actuators B: Chemical. 202 (2014) 714–720.

[71] Y. Dai, Y. Zhang, W. Liao, W. Wang, L. Wu, G-quadruplex specific thioflavin T-based label-free fluorescence aptasensor for rapid detection of tetracycline, Spectrochimica Acta Part A: Molecular and Biomolecular Spectroscopy. 238 (2020) 118406.

[72] R. Khurana, C. Coleman, C. Ionescu-Zanetti, S.A. Carter, V. Krishna, R.K. Grover, R. Roy, S. Singh, Mechanism of thioflavin T binding to amyloid fibrils, Journal of Structural Biology. 151 (2005) 229–238.

[73] M.R.H. Krebs, E.H.C. Bromley, A.M. Donald, The binding of thioflavin-T to amyloid fibrils: localisation and implications, Journal of Structural Biology. 149 (2005) 30–37.

[74] J. Mohanty, N. Barooah, V. Dhamodharan, S. Harikrishna, P.I. Pradeepkumar, A.C. Bhasikuttan, Thioflavin T as an efficient inducer and selective fluorescent sensor for the human telomeric G-quadruplex DNA, Journal of the American Chemical Society. 135 (2013) 367–376.

[75] X.F. Zhang, H.M. Xu, L. Han, N.B. Li, H.Q. Luo, A Thioflavin T-induced G-Quadruplex fluorescent biosensor for target DNA detection, Analytical Sciences. 34 (2018) 149–153.

[76] S. Xu, Q. Li, J. Xiang, Q. Yang, H. Sun, A. Guan, L. Wang, Y. Liu, L. Yu, Y. Shi, Thioflavin T as an efficient fluorescence sensor for selective recognition of RNA G-quadruplexes, Scientific Reports. 6 (2016) 1–9.

[77] S. Verma, S.A. Ghuge, V. Ravichandiran, N. Ranjan, Spectroscopic studies of thioflavin-T binding to c-myc G-quadruplex DNA, Spectrochimica Acta Part A: Molecular and Biomolecular Spectroscopy. 212 (2019) 388–395.

[78] V. Gabelica, R. Maeda, T. Fujimoto, H. Yaku, T. Murashima, N. Sugimoto, D. Miyoshi, Multiple and cooperative binding of fluorescence light-up probe

thioflavin T with human telomere DNA G-quadruplex, Biochemistry. 52 (2013) 5620–5628.

[79] A.R. Surrey, H.F. Hammer, The Preparation of 7-Chloro-4-(4-(N-ethyl-N-β-hydroxyethylamino)-1-methylbutylamino)-quinoline and Related Compounds, Journal of the American Chemical Society. 72 (1950) 1814–1815.

[80] E.W. McChesney, Animal toxicity and pharmacokinetics of hydroxychloroquine sulfate, The American Journal of Medicine. 75 (1983) 11–18.

[81] M.T. Hoekenga, The treatment of malaria with hydroxychloroquine, The American Journal of Tropical Medicine and Hygiene. 4 (1955) 221–223.

[82] J. Han, X. Li, X. Luo, J. He, X. Huang, Q. Zhou, Y. Han, H. Jie, J. Zhuang, Y. Li, The mechanisms of hydroxychloroquine in rheumatoid arthritis treatment: Inhibition of dendritic cell functions via Toll like receptor 9 signaling, Biomedicine & Pharmacotherapy. 132 (2020) 110848.

[83] M.E. Suarez-Almazor, E. Belseck, B. Shea, J. Homik, G.A. Wells, P. Tugwell, Antimalarials for treating rheumatoid arthritis, Cochrane Database of Systematic Reviews. (2000).

[84] C. Tang, T. Godfrey, R. Stawell, M. Nikpour, Hydroxychloroquine in lupus: emerging evidence supporting multiple beneficial effects, Internal Medicine Journal. 42 (2012) 968–978.

[85] C. Ponticelli, G. Moroni, Hydroxychloroquine in systemic lupus erythematosus (SLE), Expert Opinion on Drug Safety. 16 (2017) 411–419.

[86] N. Sinha, G. Balayla, Hydroxychloroquine and covid-19, Postgraduate Medical Journal. 96 (2020) 550–555.

[87] Z. Chen, J. Hu, Z. Zhang, S. Jiang, S. Han, D. Yan, R. Zhuang, B. Hu, Z. Zhang, Efficacy of hydroxychloroquine in patients with COVID-19: results of a randomized clinical trial, Medrxiv. (2020).

[88] Coronavirus (COVID-19) Update: FDA Revokes Emergency Use Authorization for Chloroquine and Hydroxychloroquine, (2020).

[89] Y.-C. Lin, J.-F. Lin, S.-I. Wen, S.-C. Yang, T.-F. Tsai, H.-E. Chen, K.-Y. Chou, I. Thomas, S. Hwang, Chloroquine and hydroxychloroquine inhibit bladder cancer cell growth by targeting basal autophagy and enhancing apoptosis, The Kaohsiung Journal of Medical Sciences. 33 (2017) 215–223.

[90] D.J. Browning, Pharmacology of chloroquine and hydroxychloroquine, in: Hydroxychloroquine and Chloroquine Retinopathy, Springer, 2014.

[91] F. Wolfe, M.F. Marmor, Rates and predictors of hydroxychloroquine retinal toxicity in patients with rheumatoid arthritis and systemic lupus erythematosus, Arthritis Care & Research. 62 (2010) 775–784.

[92] I.H. Yusuf, S. Sharma, R. Luqmani, S.M. Downes, Hydroxychloroquine retinopathy, Eye. 31 (2017) 828–845.

[93] M.D. Sumpter, L.S. Tatro, W. v Stoecker, R.K. Rader, Evidence for risk of cardiomyopathy with hydroxychloroquine, Lupus. 21 (2012) 1594–1596.

[94] D. Dabić, S. Babić, I. Škorić, The role of photodegradation in the environmental fate of hydroxychloroquine, Chemosphere. 230 (2019) 268–277.

[95] M.L.P.M. Arguelho, J.F. Andrade, N.R. Stradiotto, Electrochemical study of hydroxychloroquine and its determination in plaquenil by differential pulse voltammetry, Journal of Pharmaceutical and Biomedical Analysis. 32 (2003) 269–275.

[96] P.B. Deroco, F.C. Vicentini, G.G. Oliveira, R.C. Rocha-Filho, O. Fatibello-Filho, Square-wave voltammetric determination of hydroxychloroquine in

pharmaceutical and synthetic urine samples using a cathodically pretreated boron-doped diamond electrode, Journal of Electroanalytical Chemistry. 719 (2014) 19–23.

[97] L.R.M. Ferraz, F.L.A. Santos, P.A. Ferreira, R.T.L. Maia-Junior, T.A. Rosa, S.P.M. Costa, C.M. Melo, L.A. Rolim, P.J. Rolim-Neto, Quality by design in the development and validation of analytical method by ultraviolet-visible spectrophotometry for quantification of hydroxychloroquine sulfate, International Journal of Pharmaceutical Sciences and Research. 5 (2014) 4666.

[98] L.-Z. Wang, R.Y.-L. Ong, T.-M. Chin, W.-L. Thuya, S.-C. Wan, A.L.-A. Wong, S.-Y. Chan, P.C. Ho, B.-C. Goh, Method development and validation for rapid quantification of hydroxychloroquine in human blood using liquid chromatography–tandem mass spectrometry, Journal of Pharmaceutical and Biomedical Analysis. 61 (2012) 86–92.

[99] G. Noé, Z. Amoura, D. Combarel, L. Lori, N. Tissot, A. Seycha, C. Funck-Brentano, N. Zahr, Development and Validation of a Fast Ultra-High Performance Liquid Chromatography–Fluorescent Method for the Quantification of Hydroxychloroquine and Its Metabolites in Patients With Lupus, Therapeutic Drug Monitoring. 41 (2019) 476–482.

[100] A.T.R. Williams, S.A. Winfield, J.N. Miller, Relative fluorescence quantum yields using a computer-controlled luminescence spectrometer, Analyst. 108 (1983) 1067–1071.

[101] P. Ragazzon, J.B. Chaires, Use of competition dialysis in the discovery of G-quadruplex selective ligands, Methods. 43 (2007) 313–323.

[102] K. Dogan, A. Gulkaya, M. Forough, O. Persil Çetinkol, Novel Fluorescent Azacyanine Compounds: Improved Synthesis and Optical Properties, ACS Omega. 5 (2020) 22874–22882.

[103] D. Patra, N.N. Malaeb, M.J. Haddadin, M.J. Kurth, Influence of substituent and solvent on the radiative process of singlet excited states of novel cyclic azacyanine derivatives, Journal of Fluorescence. 22 (2012) 707–717.

[104] G.S. Remya, C.H. Suresh, Quantification and classification of substituent effects in organic chemistry: A theoretical molecular electrostatic potential study, Physical Chemistry Chemical Physics. 18 (2016) 20615–20626.

[105] J. Clayden, N. Greeves, S. Warren, P. Wothers, Organic chemistry, (2001).

[106] C. Coluccini, P.T. Anusha, H.-Y.T. Chen, S.-L. Liao, Y.K. Ko, A. Yabushita, C.W. Luo, Y.M. Ng, Y.L. Khung, Tuning of the electro-optical properties of tetraphenylcyclopentadienone via substitution of oxygen with sterically-hindered electron withdrawing groups, Scientific Reports. 9 (2019) 1–14.

[107] V.A. Bloomfield, D.M. Crothers, I. Tinoco Jr, Electronic and vibrational spectroscopy, Nucleic Acids, Structures, Properties, and Functions. (1999) 165–221.

[108] M. Vorlíčková, I. Kejnovská, K. Bednářová, D. Renčiuk, J. Kypr, Circular dichroism spectroscopy of DNA: from duplexes to quadruplexes, Chirality. 24 (2012) 691–698.

[109] B. Zhou, Y. Geng, C. Liu, H. Miao, Y. Ren, N. Xu, X. Shi, Y. You, T. Lee, G. Zhu, Characterizations of distinct parallel and antiparallel G-quadruplexes formed by two-repeat ALS and FTD related GGGGCC sequence, Scientific Reports. 8 (2018) 1–7.

[110] B. Zhou, Y. Geng, C. Liu, H. Miao, Y. Ren, N. Xu, X. Shi, Y. You, T. Lee, G. Zhu, Characterizations of distinct parallel and antiparallel G-quadruplexes formed by two-repeat ALS and FTD related GGGGCC sequence, Scientific Reports. 8 (2018) 1–7.

[111] R. del Villar-Guerra, J.O. Trent, J.B. Chaires, G-quadruplex secondary structure obtained from circular dichroism spectroscopy, Angewandte Chemie. 130 (2018) 7289–7293.

[112] J. Carvalho, J.A. Queiroz, C. Cruz, Circular dichroism of G-Quadruplex: A laboratory experiment for the study of topology and ligand binding, Journal of Chemical Education. 94 (2017) 1547–1551.

[113] Y. Zhang, J. Chen, H. Ju, J. Zhou, Thermal denaturation profile: A straightforward signature to characterize parallel G-quadruplexes, Biochimie. 157 (2019) 22–25.

APPENDICES

A. ^{1}H and ^{13}C NMR spectra, HRMS and Elemental Analysis results of synthesized Azacyanines

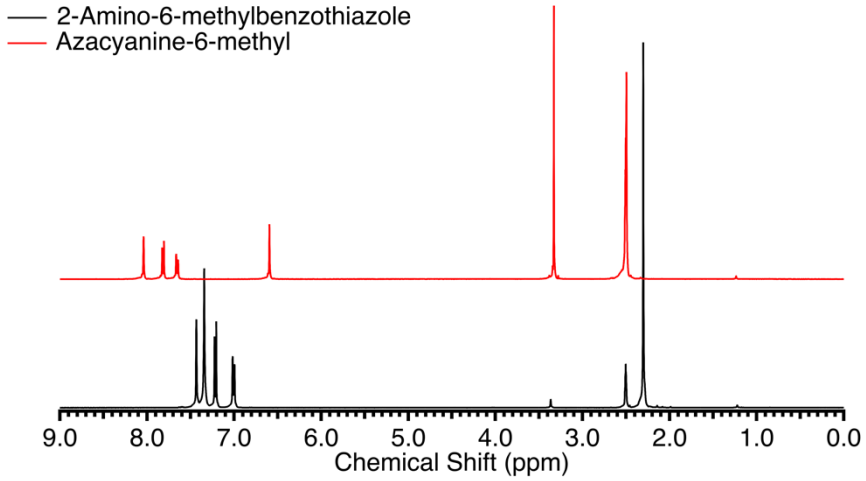

Figure 32. ^{1}H NMR Spectrum of Azacyanine-6-methyl and its starting material.

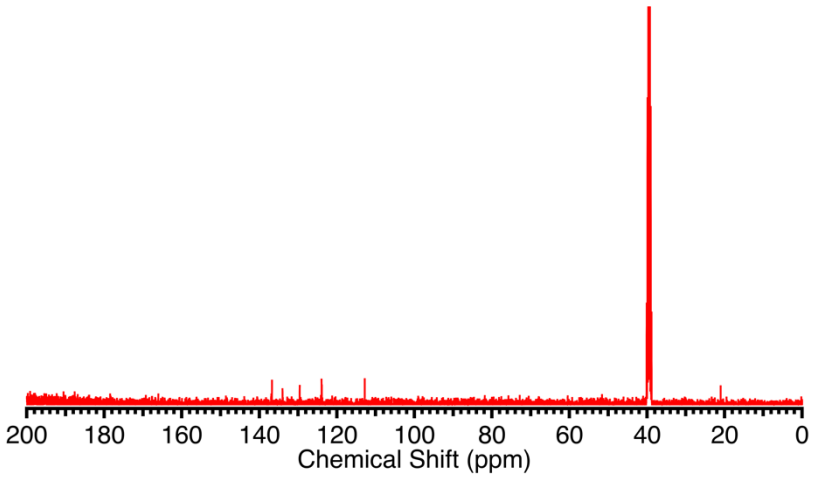

Figure 33. ^{13}C NMR Spectrum of Azacyanine-6-methyl.

Pale-yellow solid compound formed; ^{1}H NMR (400 MHz, DMSO-d6): δ 2.50 (s, 6H), δ 6.59 (s, 2H), δ 7.67, 7.66, 7.65, 7.64 (dd, 2H), 7.83, 7.81 (d, 2H), 8.04 (s, 2H); ^{13}C NMR (125 MHz, DMSO-d6): δ 20.9, 38.8, 39.1, 39.3, 39.5, 39.7, 39.9, 40.1, 112.7, 112.9, 123.9, 124.0, 129.6, 134.0, 136.7; HRMS (m/z): calculated for [M +

H]+, 324.629; found, 324.618; elemental analysis experimental: calculated for $C_{17}H_{14}N_3S_2I$: C, 45.24%, H, 3.13%, N, 9.31%, S, 14.21%. Found: C, 44.52%; H, 3.32%; N, 9.52%; S, 14.18%.

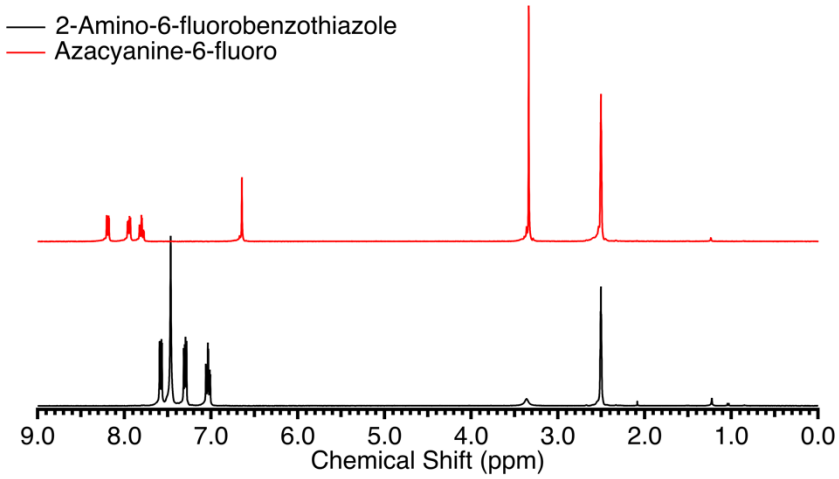

Figure 34. ^{1}H NMR Spectrum of Azacyanine-6-fluoro and its starting material.

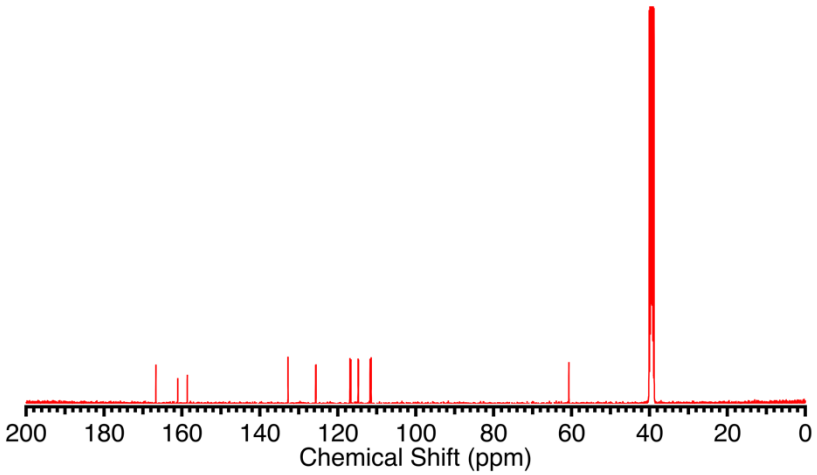

Figure 35. ^{13}C NMR Spectrum of Azacyanine-6-fluoro.

A creamy yellow solid compound was synthesized; ^{1}H NMR (400 MHz, DMSO-d6): δ 6.65 (s, 2H), δ 7.83, 7.82, 7.80, 7.80, 7.78, 7.75 (dt, 2H), δ 7.96, 7.95, 7.94, 7.93 (m, 2H), δ 8.20, 8.20, 8.18, 8.18 (dd, 2H); ^{13}C NMR (125 MHz, DMSO-d6): δ: 60.9, 111.4, 111.7, 114.7, 114.8, 116.6, 116.9, 125.6, 125.7, 133.0, 158.7, 161.1,

166.7; HRMS (m/z): calculated for [M + H]+, 332.0115; found, 332.0128; elemental analysis experimental: calculated for $C_{15}H_8N_3F_2S_2I$: C, 39.23%; H, 1.76%; N, 9.15%; S, 13.96%. Found: C, 39.11%; H, 1.97%; N, 9.05%; S, 14.08%.

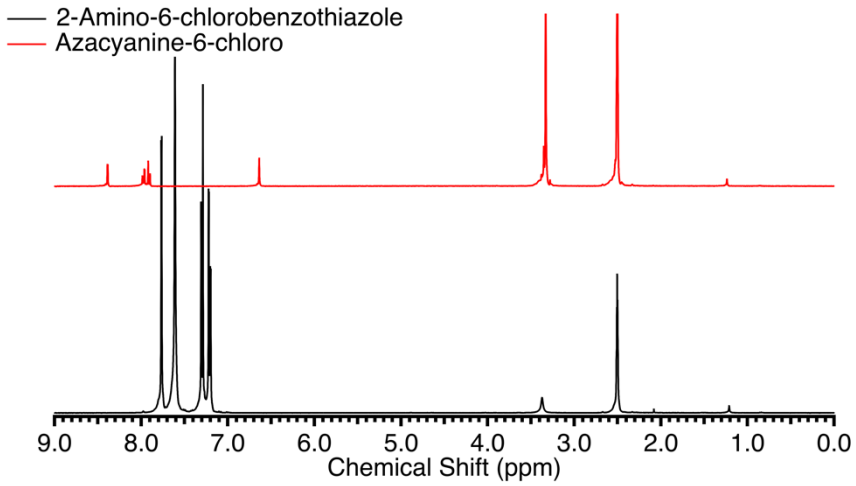

Figure 36. ^{1}H NMR Spectrum of Azacyanine-6-chloro and its starting material.

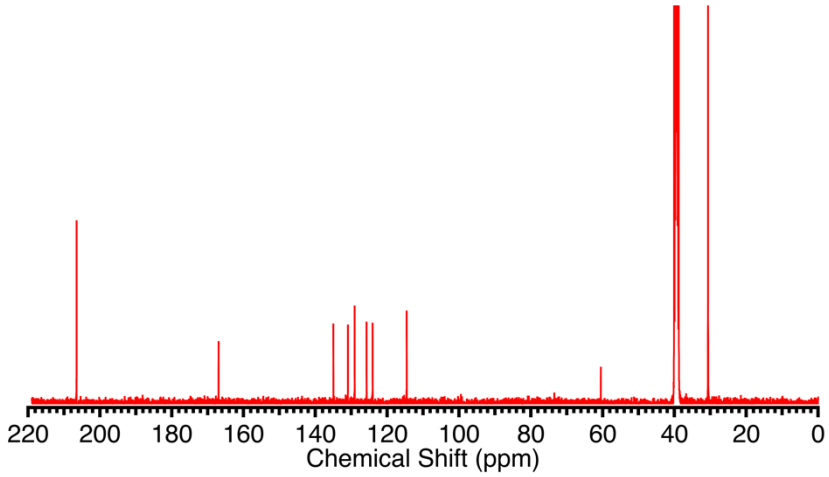

Figure 37. ^{13}C NMR Spectrum of Azacyanine-6-chloro.

A yellowish-brown solid compound was synthesized; ^{1}H NMR (400 MHz, DMSO-d6): δ 6.64 (s, 2H), δ 7.92, 7.90 (d, 2H), δ 7.99, 7.98, 7.65, 7.64 (dd, 2H), δ 7.39, 8.39 (d, 2H); ^{13}C NMR (125 MHz, DMSO-d6): δ 60.5, 114.6, 124.1, 125.7, 129.1, 130.9, 135.0, 166.9; HRMS (m/z): calculated for $[M + H]^{+}$, 363.953; found, 363.954;

elemental analysis experimental: calculated for $C_{15}H_8N_3Cl_2S_2I$: C, 36.60%; H, 1.64%; N, 8.54%; S, 13.03%. Found: C, 35.74%; H, 1.82%; N, 9.49%; S, 12.71%. Yield: 60%.

B. List of nucleic acid sequences used in this study and their extinction coefficients used in concentration calculations

Table 7. List of nucleic acid sequences used in this study.

Nucleic acids	**Sequences**
Her-2	5’ -AGG AGA AGG AGG AGG TGG AGG AGG AGG GC- 3’
Kras	5’ -GGG AAG AGG GAA GAG GGG GAG G- 3’
C-myc	5’ -TGG GGA GGG TGG GGA GGG TGG GGA AGG- 3’
BCL-2	5’ -AGG GGC GGG CGC GGG AGG AAG GGG GCG GGA GCG GGG C - 3’
Pu22	5’ -CGG GGC GGG CCG GGG GCG GGG T- 3’
Tel24	5’ -TTG GGT TAG GGT TAG GGT TAG GGA- 3’
VEGF	5’ -GGG CGG GCC GGG GGC GGG GTC CCG GCG GGG CGG GAG 3’
RB	5’ -CGG GGG GTT TTG GGC GGC- 3’
DDD	5’ -CGC GAA TTC GCG- 3’

Table 8. List of nucleic acids used in this study and their extinction coefficient values used in concentration calculations.

Nucleic acids	**λ (nm)**	**ε ($M^{-1}cm^{-1}$)**	**Monomeric Unit**	**Company**
Her-2	260	42985	Quartet	IDT
Kras	260	24646	Quartet	IDT
C-myc	260	45309	Quartet	IDT
BCL-2	260	41591	Quartet	IDT
Tel24	260	73000	Quartet	IDT
VEGF	260	35778	Quartet	IDT
RB	260	9407	Quartet	IDT
Pu22	260	205000	Strand	IDT
DDD	260	110700	Strand	IDT
Poly(A)	258	9800	Nucleotide	Sigma Aldrich
Poly(U)	260	9350	Nucleotide	Sigma Aldrich
Poly(dA):Poly(dT)	260	12000	Base pair	Sigma Aldrich

C. Preparation of buffer and stock solutions

BPES buffer preparation:

5X BPES buffer preparation:

5X BPES buffer contains 10.0 mM NaH_2PO_4, 5.00 mM Na_2EDTA, 30.0 mM Na_2HPO_4, and 925.0 mM NaCl solutions. In order to prepare these solutions 400.0 mM, NaH_2PO_4, 100.0 mM, Na_2EDTA, 600.0 mM Na_2HPO_4 and 2.0 M NaCl stock solutions were prepared.

2.0 M 0.5 L NaCl stock solution preparation:

$$M = \frac{\mathrm{n}}{\mathrm{V}} \quad \mathrm{n} = \frac{\mathrm{M}}{\mathrm{V}}$$

$$2.000\ \mathrm{M} = \mathrm{n}\frac{(\mathrm{mol})}{0.5000\ \mathrm{L}} \quad \mathrm{n} = 1.000\ \mathrm{mol} \quad \mathrm{Mw(NaCl)} = 58.44\ \mathrm{g/mol}$$

$$\mathrm{n} = \frac{\mathrm{m(g)}}{\mathrm{Mw}} \quad 1.000\ \mathrm{mol} = \frac{\mathrm{m(g)}}{58.44\frac{\mathrm{g}}{\mathrm{mol}}}$$

$$\mathrm{m} = 1.000\ \mathrm{mol} * 58.44\frac{\mathrm{g}}{\mathrm{mol}} = \ 58.44\ \mathrm{g}$$

To prepare 2.000 M NaCl stock solution, 58.44 g of NaCl was dissolved in 0.5000 L of Millipore water.

400.0 mM 0.1000 L, NaH_2PO_4 stock solution preparation:

$$M = \frac{\mathrm{n}}{\mathrm{V}} \quad \mathrm{n} = \frac{\mathrm{M}}{\mathrm{V}}$$

$$0.4000\ \mathrm{M} = \mathrm{n}\frac{(\mathrm{mol})}{0.1000\ \mathrm{L}} \quad \mathrm{n} = 0.0400\ \mathrm{mol}$$

$$\mathrm{Mw}(\mathrm{NaH_2P}O_4) = 119.98\ \mathrm{g/mol}$$

$$\mathrm{n} = \frac{\mathrm{m(g)}}{\mathrm{Mw}} \qquad 0.04\ \mathrm{mol} = \frac{\mathrm{m(g)}}{119.98 \frac{\mathrm{g}}{\mathrm{mol}}}$$

$$\mathrm{m} = 0.0400\ \mathrm{mol} * 119.98 \frac{\mathrm{g}}{\mathrm{mol}} = \ 4.80\ \mathrm{g}$$

To prepare 400.0 mM NaH_2PO_4 stock solution, 4.80 g of NaH_2PO_4 was dissolved in 0.1000 L of Millipore water.

100 mM 0.1 L, Na_2EDTA stock solution preparation:

$$M = \frac{\mathrm{n}}{\mathrm{V}} \qquad \mathrm{n} = \frac{\mathrm{M}}{\mathrm{V}}$$

$$0.100\ \mathrm{M} = \mathrm{n} \frac{(\mathrm{mol})}{0.100\ \mathrm{L}} \qquad \mathrm{n} = 0.0100\ \mathrm{mol} \quad \mathrm{Mw}(\mathrm{Na_2EDTA})$$

$$= 372.24\ \mathrm{g/mol}$$

$$\mathrm{n} = \frac{\mathrm{m(g)}}{\mathrm{Mw}}$$

$$0.0100\ \mathrm{mol} = \frac{\mathrm{m(g)}}{372.24\ \mathrm{g/mol}} \qquad \mathrm{m} = 0.0100\ \mathrm{mol} * 372.24 \frac{\mathrm{g}}{\mathrm{mol}} = \ 3.72\ \mathrm{g}$$

To prepare 100.0 mM Na_2EDTA stock solution, 3.72 g of Na_2EDTA was dissolved in 0.100 L of Millipore water.

600.0 mM 0.100 L, Na_2HPO_4 stock solution preparation:

$$M = \frac{\mathrm{n}}{\mathrm{V}} \qquad \mathrm{n} = \frac{\mathrm{M}}{\mathrm{V}}$$

$$0.600\ \mathrm{M} = \mathrm{n} \frac{(\mathrm{mol})}{0.100\ \mathrm{L}}$$

$$\mathrm{n} = 0.0600\ \mathrm{mol} \quad \mathrm{Mw}(Na_2HPO_4) = 141.96\ \mathrm{g/mol}$$

$$\mathrm{n} = \frac{\mathrm{m(g)}}{\mathrm{Mw}}$$

$$0.0600\ \mathrm{mol} = \frac{\mathrm{m(g)}}{141.96\ \mathrm{g/mol}} \qquad \mathrm{m} = 0.0600\ \mathrm{mol} * 141.96 \frac{\mathrm{g}}{\mathrm{mol}} = \ 8.51\ \mathrm{g}$$

To prepare 600.0 mM Na_2HPO_4 stock solution, 8.51 g of Na_2HPO_4 was dissolved in 0.100 L of Millipore water.

Concentrations of the above solutions were arranged by using the following equation:

$$M_1 * V_1 = M_2 * V_2$$

10.0 mM NaH_2PO_4 :

$$6.00x10^{-1}M * V_1 = 1.00x10^{-2}\ M * 5.00x10^{-1}L \quad V_1 = 12.5\ mL$$

5.0 mM Na_2EDTA:

$$1.00x10^{-1}\ M * V_1 = 5.00x10^{-3}\ M * 5.00x10^{-1}\ L \quad V_1 = 25.0\ mL$$

30.0 mM Na_2HPO_4:

$$4.00x10^{-1}\ M * V_1 = 3.00x10^{-2}\ M * 5.00x10^{-1}\ L \quad V_1 = 37.5\ mL$$

925 mM NaCl:

$$2.00\ M * V_1 = 9.25x10^{-1}M * 5.00x10^{-1}\ L \quad V_1 = 231.25\ mL$$

To prepare 5X BPES buffer, 12.5 mL NaH_2PO_4, 25.0 mL Na_2EDTA, 37.5 mL Na_2HPO_4 and 231.25 mL NaCl solutions were mixed, and the volume of the buffer solution was completed to 0.500 L by using Millipore water. The pH of the buffer solution was adjusted to 7.0 with NaOH solution.

1X BPES buffer preparation:

5X BPES buffer was diluted to prepare 1x BPES buffer.

$$M_1 * V_1 = M_2 * V_2$$

$$5x * V_1 = 1x * 1.000L \quad V_1 = 200.\ mL$$

200 mL of 5X BPES buffer was diluted to 1.00 L by Millipore water to obtain 1X BPES buffer.

%10 (w/v) SDS solution preparation for competition dialysis experiments:

10.0 g SDS was weighed and dissolved in 80.0 mL of Millipore water, then the total volume was completed to 100.0 mL using Millipore water.

Potassium Phosphate Buffer Preparation:

100.0 mM K-Phosphate buffer contains 620.0 mM KH_2PO_4 and 390.0 mM K_2HPO_4 solutions, and these solutions were prepared using 1.000M KH_2PO_4 and 1.000 M K_2HPO_4 stock solutions.

1.000M, 0.500 L KH_2PO_4 stock preparation:

$$M = \frac{\mathrm{n}}{\mathrm{V}} \quad \mathrm{n} = \frac{\mathrm{M}}{\mathrm{V}}$$

$$1.000\ \mathrm{M} = \mathrm{n}\frac{(\mathrm{mol})}{0.5000\ \mathrm{L}} \quad \mathrm{n} = 0.5000\ \mathrm{mol} \quad \mathrm{Mw}(KH_2PO_4)$$

$$= 136.09\ \mathrm{g/mol}$$

$$\mathrm{n} = \frac{\mathrm{m(g)}}{\mathrm{Mw}} \qquad 0.5000\ \mathrm{mol} = \frac{\mathrm{m(g)}}{136.09\ \mathrm{g/mol}} \quad \mathrm{m}$$

$$= 0.5000\ \mathrm{mol} * 136.09\ \mathrm{g/mol} = \ 68.05\mathrm{g}$$

To prepare 1.00 M KH_2PO_4 stock solution, 68.05 g of KH_2PO_4 dissolved in 0.500 L of Millipore water.

$$M_1 * V_1 = M_2 * V_2 \qquad 1.00\ M * V_1 = 0.620M * 1L \quad V_1 = 61.5\ mL$$

1.000 M, 0.5000 L K_2HPO_4 stock preparation:

$$M = \frac{\mathrm{n}}{\mathrm{V}} \quad \mathrm{n} = \frac{\mathrm{M}}{\mathrm{V}}$$

$$1.000\mathrm{M} = \mathrm{n}\frac{(\mathrm{mol})}{0.5\ \mathrm{L}} \quad \mathrm{n} = 0.5000\ \mathrm{mol}$$

$$\mathrm{Mw}(K_2\mathrm{HPO}_4) = 174.18\ \mathrm{g/mol}$$

$$\mathrm{n} = \frac{\mathrm{m(g)}}{\mathrm{Mw}}$$

$$0.5000\ \mathrm{mol} = \frac{\mathrm{m(g)}}{174.18\frac{\mathrm{g}}{\mathrm{mol}}}$$

$$\mathrm{m} = 0.5000\ \mathrm{mol} * 174.18\mathrm{g/mol} = \ 87.09\mathrm{g}$$

To prepare 1.00 M K_2HPO_4 solution, 87.09 g of K_2HPO_4 dissolved in 0.500 L of Millipore water.

Concentrations of the stock solutions were arranged as follows;

KH_2PO_4 solution:

$$M_1 * V_1 = M_2 * V_2 \qquad 1.000M * V_1 = 0.6200M * 1L \quad V_1 = 61.5\ mL$$

K_2HPO_4 solution:

$$M_1 * V_1 = M_2 * V_2 \qquad 1.000M * V_1 = 0.3900M * 1L \quad V_1 = 38.5\ mL$$

61.50 mL of KH_2PO_4 and 38.50 mL of K_2HPO_4 solutions were mixed. Then, the volume of the buffer solution was completed to 1.000 L by Millipore water, and the pH of the buffer solution was adjusted to 7.0 by using NaOH.

500.0 mM KCl solution preparation for thermal denaturation

$$M = \frac{\mathrm{n}}{\mathrm{V}} \quad \mathrm{n} = \frac{\mathrm{M}}{\mathrm{V}}$$

$$0.5000\mathrm{M} = \mathrm{n}\frac{(\mathrm{mol})}{0.1\ \mathrm{L}} \quad \mathrm{n} = 0.050\ \mathrm{mol} \quad \mathrm{Mw(KCl)} = 74.55\ \mathrm{g/mol}$$

$$\mathrm{n} = \frac{\mathrm{m(g)}}{\mathrm{Mw}} \quad 0.0500\ \mathrm{mol} = \frac{\mathrm{m(g)}}{74.55\frac{\mathrm{g}}{\mathrm{mol}}}$$

$$\mathrm{m} = 0.0500\ \mathrm{mol} * \frac{74.55\mathrm{g}}{\mathrm{mol}} = 3.73\mathrm{g}$$

3.73 g of KCl dissolved in 0.100 L of Millipore water to prepare 500.0 mM KCl solution.

D. Calibration curves used to evalulate for the results of competition dialysis experiments

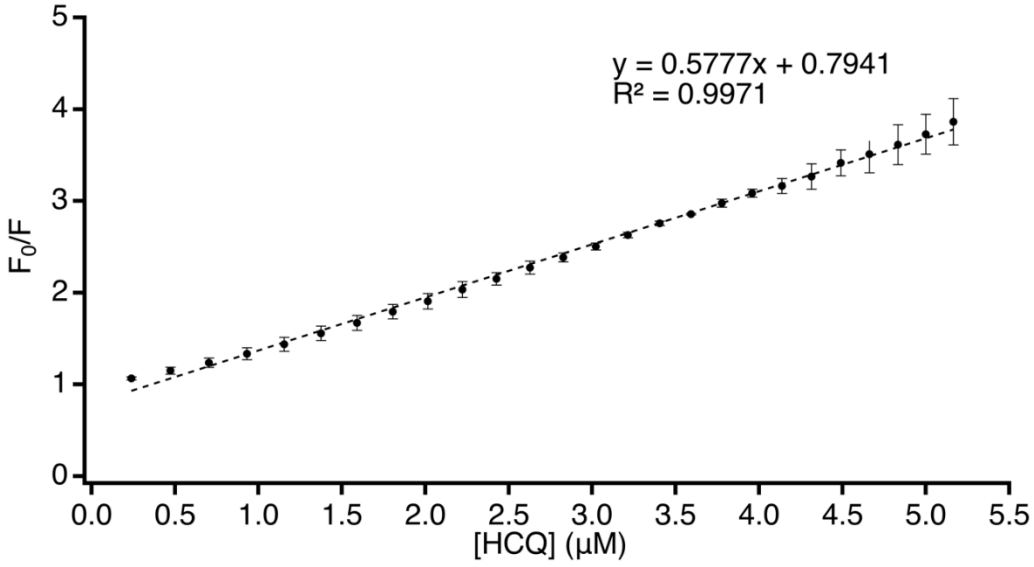

Figure 38. Azacyanine-6-methyl calibration curve constructed for the competition dialysis assay.

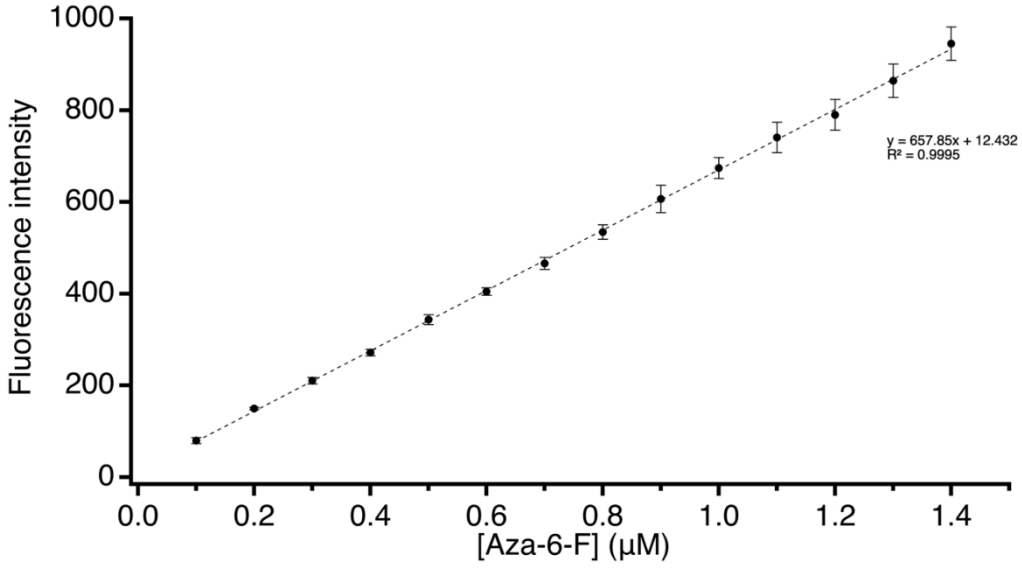

Figure 39. Azacyanine-6-fluoro calibration curve constructed for the competition dialysis assay.

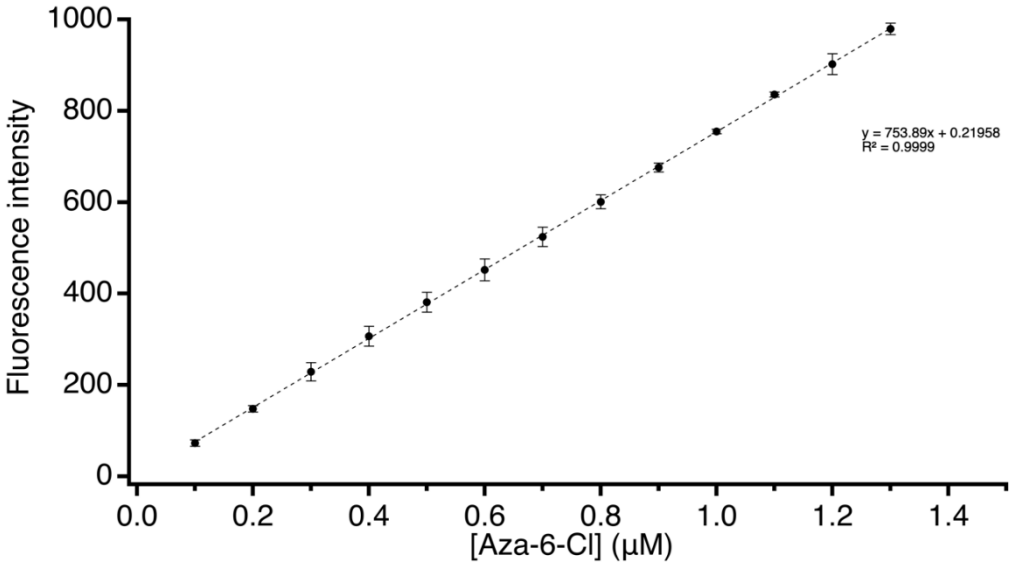

Figure 40. Azacyanine-6-chloro calibration curve constructed for the competition dialysis assay.

E. UV-vis thermal denaturation profiles

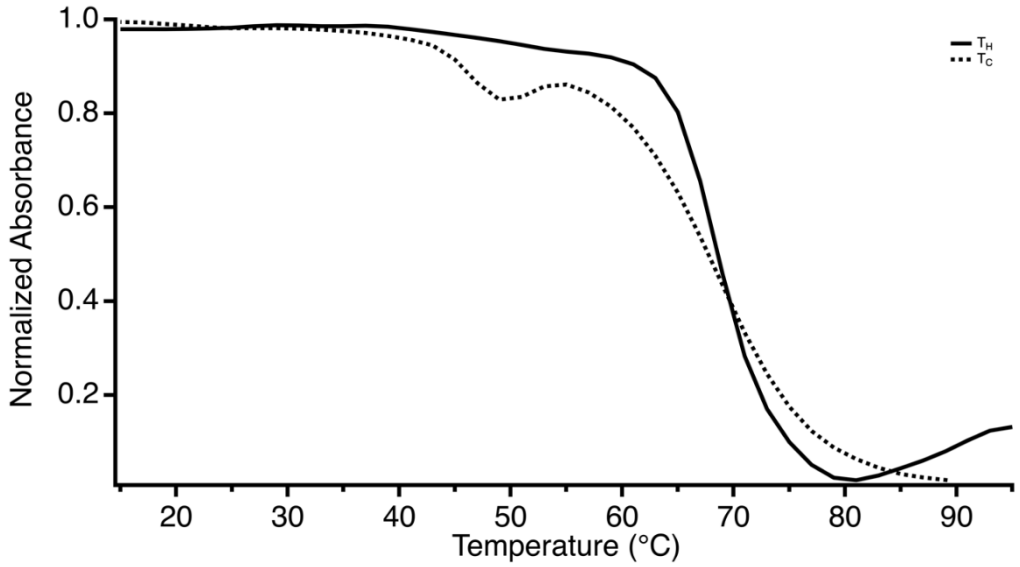

Figure 41. Thermal denaturation profiles for Tel24 obtained by monitoring UV-vis absorbance at 295 nm. T_H represents the heating profile and T_C represents the cooling profile.

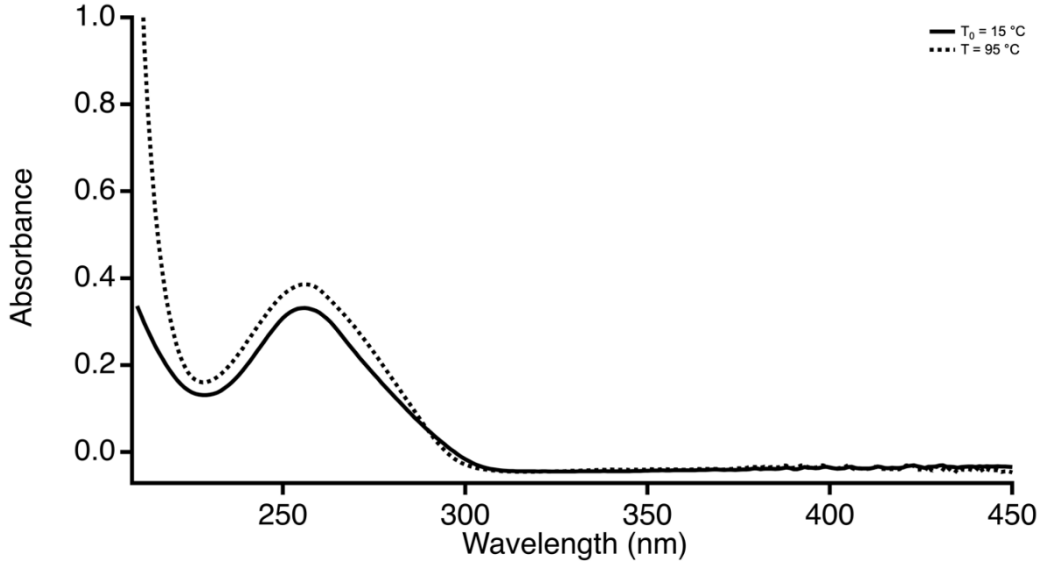

Figure 42. UV-vis absorption spectra of Tel24 obtained during thermal denaturation experiments.

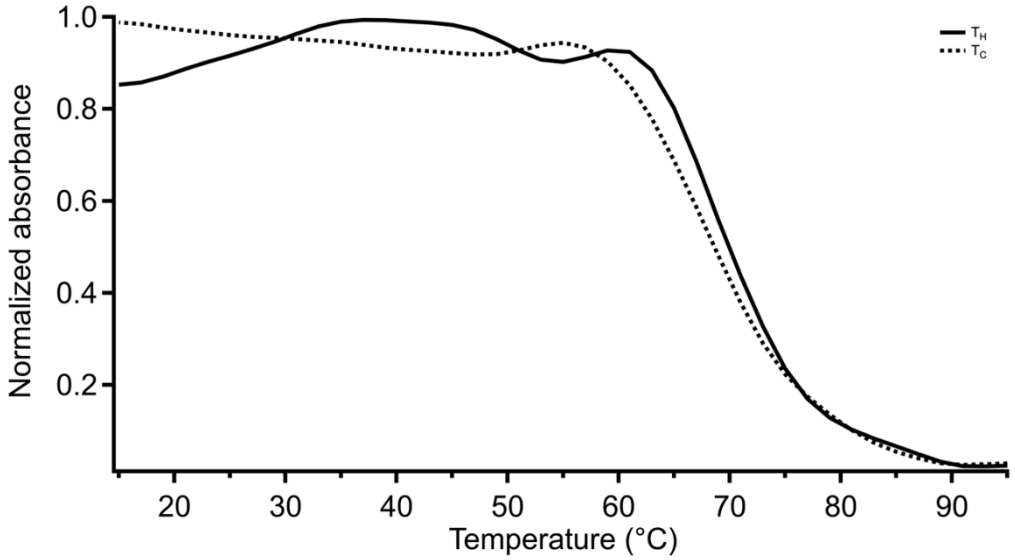

Figure 43.Thermal denaturation profiles for 1:1 Tel24:ThT sample obtained by monitoring UV-vis absorbance at 295 nm. T_H represents the heating profile and T_C represents the cooling profile.

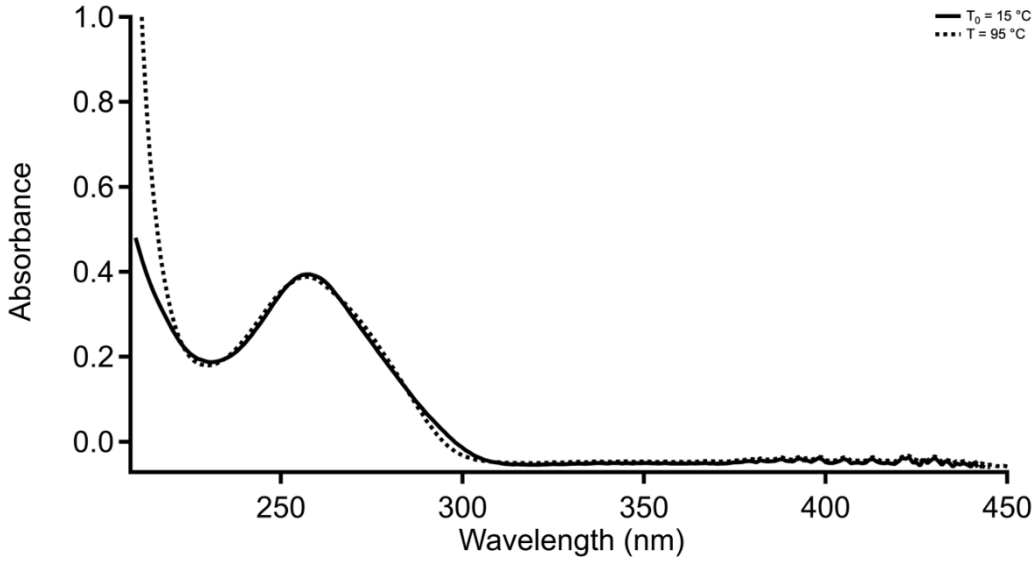

Figure 44. UV-vis absorption spectra of 1:1 Tel24:ThT sample obtained during thermal denaturation experiments.

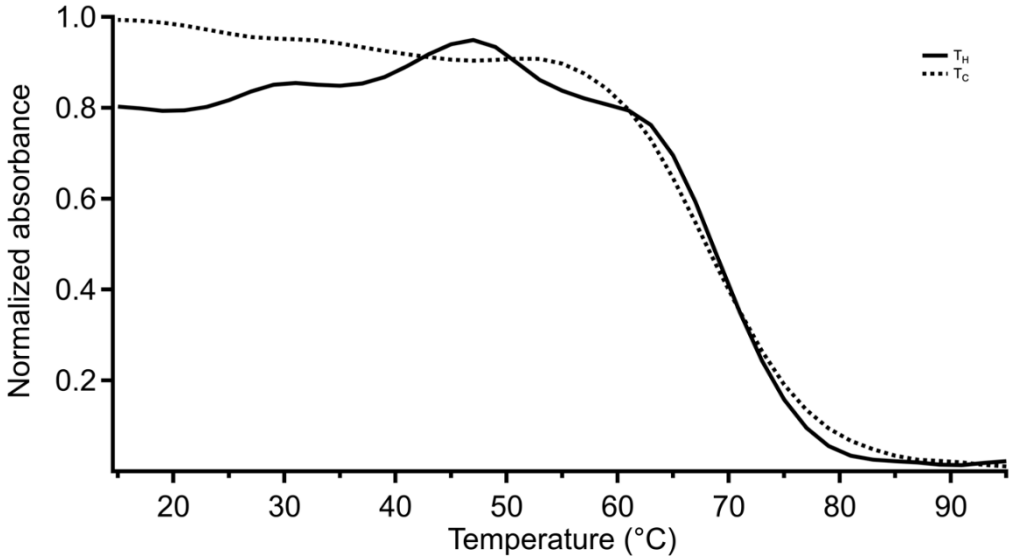

Figure 45. Thermal denaturation profiles for 1:1 Tel24:HCQ sample obtained by monitoring UV-vis absorbance at 295 nm. T_H represents the heating profile and T_C represents the cooling profile.

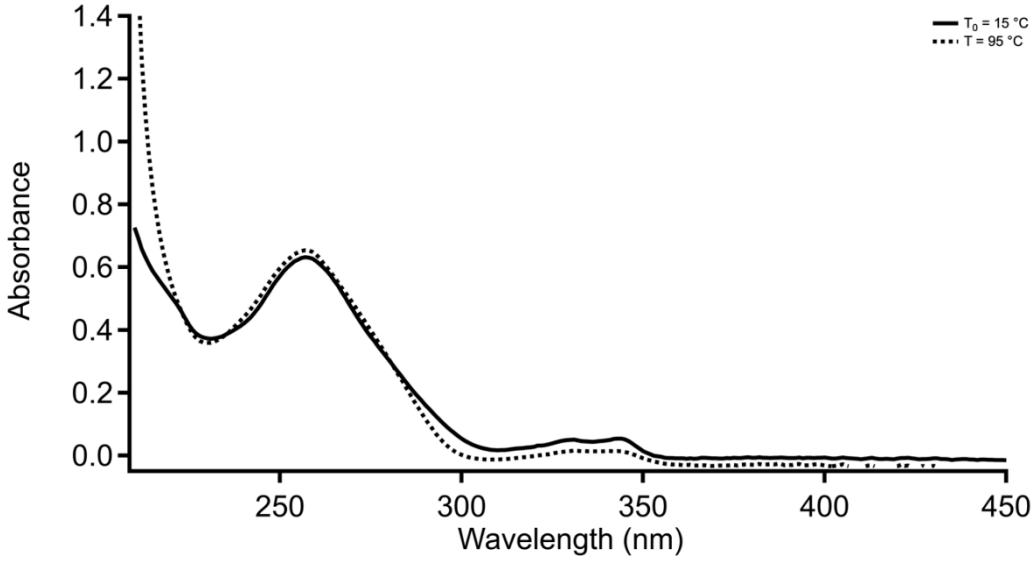

Figure 46. UV-vis absorption spectra of 1:1 Tel24:HCQ sample obtained during thermal denaturation experiments.

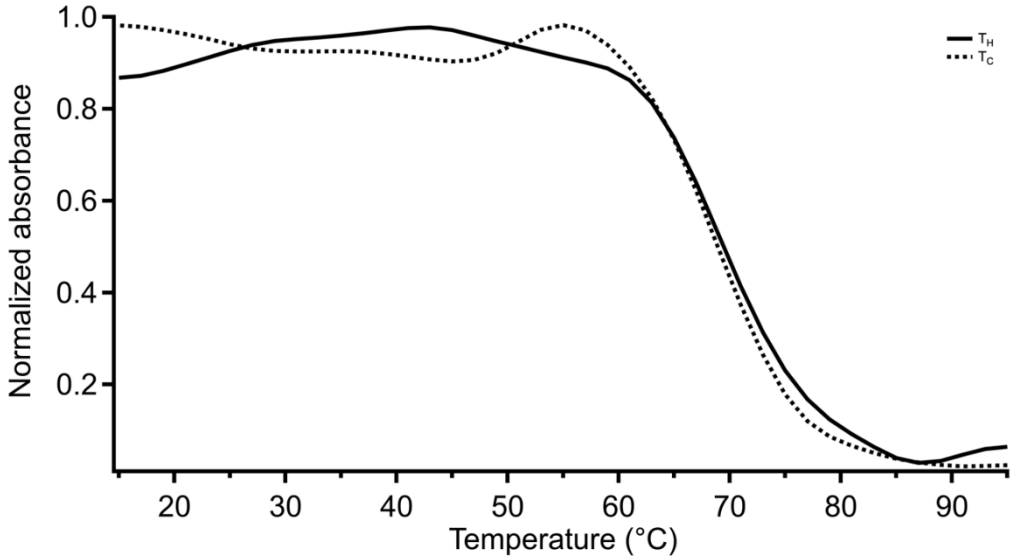

Figure 47. Thermal denaturation profiles for 1:5 Tel24:HCQ sample obtained by monitoring UV-vis absorbance at 295 nm. T_H represents the heating profile and T_C represents the cooling profile.

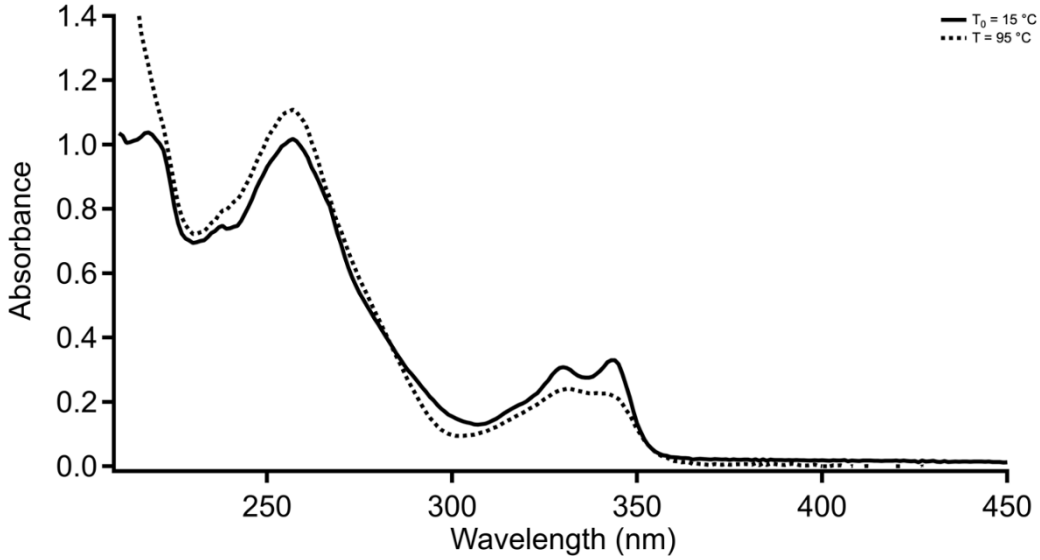

Figure 48. UV-vis absorption spectra of 1:5 Tel24: HCQ sample obtained during thermal denaturation experiments.

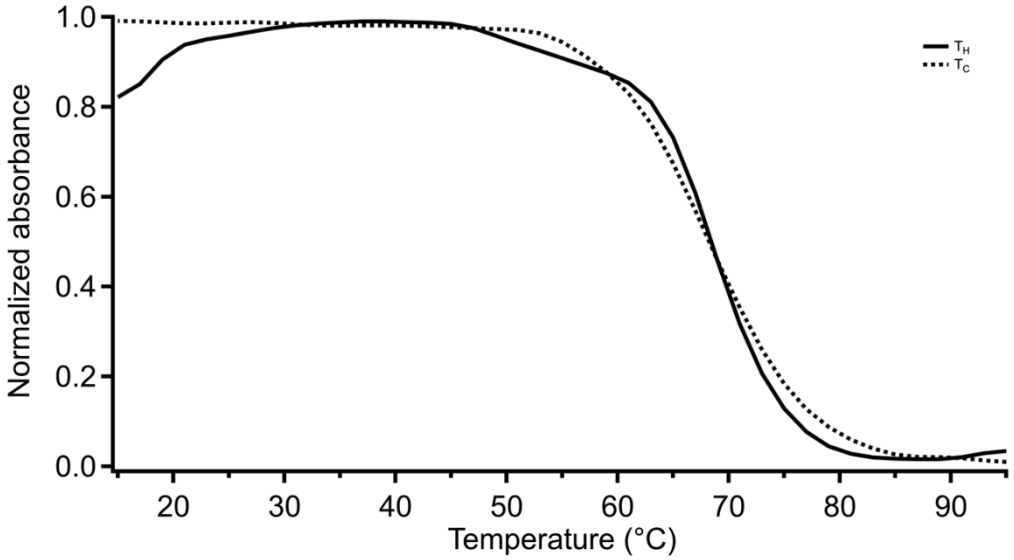

Figure 49. Thermal denaturation profile for 1:1:1 Tel24:ThT:HCQ sample obtained by monitoring UV-vis absorbance at 295 nm. T_H represents the heating profile and T_C represents the cooling profile.

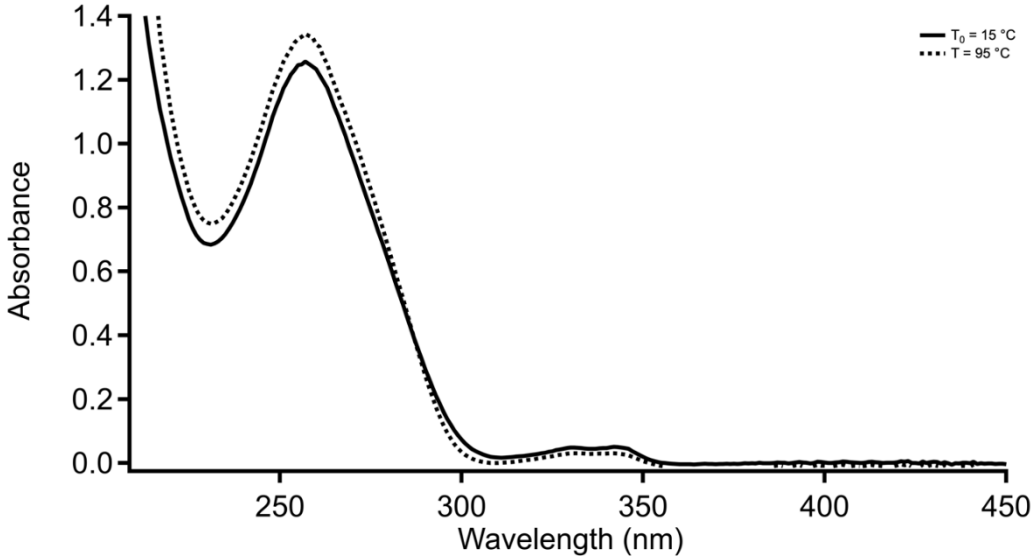

Figure 50. UV-vis absorption spectra of 1:1:1 Tel24:ThT:HCQ sample obtained during thermal denaturation experiments.

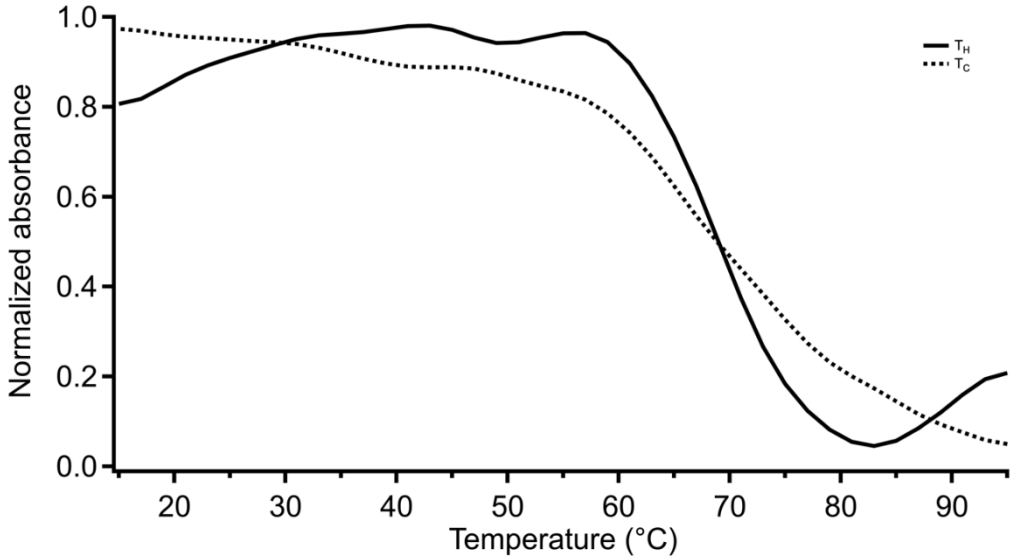

Figure 51. Thermal denaturation profile for 1:1:5 Tel24:ThT:HCQ sample obtained by monitoring UV-vis absorbance at 295 nm. T_H represents the heating profile and T_C represents the cooling profile.

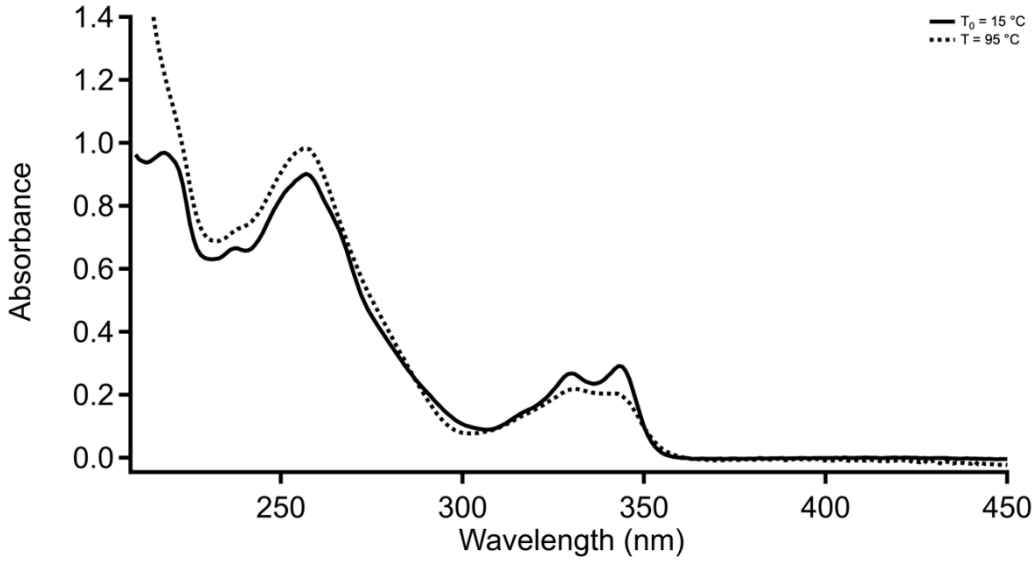

Figure 52. UV-vis absorption spectra of 1:1:5 Tel24: ThT:HCQ sample obtained during thermal denaturation experiments.